REVIEW ARTICLE

Dealloyed nanoporous materials for rechargeable lithium batteries

Xuan Wu[1,2] · Guang He[1] · Yi Ding[1]

Abstract

Dealloying has been recognized as a universal strategy to fabricate various functional electrode materials with open networks, nanoscale ligaments, tunable pore sizes and rich surface chemistry, all of which are very attractive characteristics for rechargeable lithium batteries. In particular, lithium ion insertion/extraction in metal anodes is naturally associated with the alloying/dealloying mechanism. The past decade has witnessed rapid growth of this research field with enormous progress. In this review article, we first summarize the recent development and microstructural regulation of dealloyed materials. Next, we focus on the rational design of nanoporous electrodes for rechargeable lithium batteries and related structure-performance correlations. Finally, some critical issues and perspectives are presented to guide the future development directions of such promising technology for high-energy batteries.

Keywords Dealloying · Lithium batteries · Nanoporous · Rechargeable · Electrodes

1 Introduction

Dealloying, or selective leaching, is an alloy corrosion process in which less noble elements in alloy precursors are preferentially etched away to generate three-dimensional (3D) open frameworks with interconnected backbones (ligaments) and nanoscale pore channels. The constituent elements in the alloy precursors are usually of significant difference in their oxidation potentials. During the dealloying process, the residual atoms remain connected to their neighboring atoms and the pores stay open, finally creating a self-assembled spongy structure. As the dissolution proceeds, the volume fraction (porosity) of the resulting structures can typically evolve within a range of 40%–80%, as determined by the alloy parting limit and the percolation threshold [1, 2]. Homogeneous nanopore/ligament distributions are determined by the rates of dealloying and surface diffusion, and their length scales can range from a few nanometers to micrometers by rationally tuning the precursor alloys, etching parameters, and subsequent post-annealing treatments [3, 4]. Hierarchical networks with multimodal pore sizes can also be achieved through stepwise structuring of the parent-phase alloys [5].

Nanoporous metals (NPMs) are among the most studied dealloyed materials [6–11]. Compared with their bulk counterparts, they exhibit novel mechanical, physical, chemical, and biological properties arising from their unique architectures, which have been widely utilized in actuators [12–14], sensors [15–17], water splitting [18, 19], energy storage and conversion [2, 10, 20], drug loading and release [21–23], and so forth. It should be noted that there are various strategies to prepare porous metals [24], such as templating [25], anodization [26], laser etching [27, 28], combustion synthesis [29, 30], chemical reduction [31] and thermal decomposition [32]. Among them, dealloying is probably one of the most promising routes for immediate commercialization feasibility due to its very low manufacturing costs and ease of mass production. For example, Raney® nickel (Ni), which is an active hydrogenation catalyst produced by dealloying Ni-based alloys such as NiSi and NiAl in alkaline solutions, has been used in the chemical industry for nearly a century [33, 34]. In 2017, the global production of Raney Ni reportedly reached ~28000 tons with a market value of ~630 million USD, thus remaining the most important industrial

✉ Yi Ding
yding@tjut.edu.cn

[1] Tianjin Key Laboratory of Advanced Functional Porous Materials, Institute for New Energy Materials and Low-Carbon Technologies, School of Materials Science and Engineering, Tianjin University of Technology, Tianjin 300384, China

[2] State Key Laboratory of Quality Research in Chinese Medicines, Macau University of Science and Technology, Taipa, Macau, China

catalyst for hydrogenation and desulfurization reactions [35]. The key advantages of Raney® nanostructures include the abundant porosity and large specific surface area derived by etching MAl-type alloys, where M can be Ni, Cu, Ag, Co, Fe, and even the corresponding alloys. The simple treatment in alkaline solution enables very scalable production of Raney®-type metals worldwide, and the H_2 byproduct can also be collected for other applications. NPMs prepared in this manner also possess the following compositional and structural advantages [36–38]: (1) rich compositional possibilities (metals, alloys, oxides, sulfides, and semiconductors) with predetermined composition accuracy; (2) inherent 3D ligaments/channels; (3) controllable porosity and interconnectivity through the tuning of corrosion conditions and precursor compositions, or combination with post-treatments such as thermal heating. These remarkable merits endow NPMs with great potential to satisfy the structural and functional demands of a large variety of practical applications.

To date, most efforts have been dedicated to the fabrication and processing of noble NPMs. For example, dealloyed nanoporous Pt, Pd, Au, and Ag can possess unique bicontinuous structures that have demonstrated great potentials on catalytic and electrocatalytic properties [2, 8]. However, little attention had been focused on applications of NPMs in lithium ion batteries (LIBs) until non-noble materials (Si, Ge, Sn, Sb, Fe_2O_3, Mn_2O_3, and so on) emerged recently as promising anodes with higher specific capacities than the commercial graphite anodes [37]. In fact, there is an essential correlation between Li-ion extraction/insertion and the formation of porous structures in oxide/alloy electrodes [39–42]. Hu et al. [39] first noticed that nanoporosity can be formed with metal and metal oxide anodes via a template-free lithiation/delithiation process. Further studies by Chen and Sieradzki [41] revealed porous Sn with typical bicontinuous structure could be constructed by delithiation from Li–Sn alloys. The structures can be readily tuned by controlling the amount of lithium extracted from the alloys. For example, the as-obtained Sn particles with 30 at.% Li exhibited a roughened sinusoidal-like surface structure, whereas further increase in the Li content to > 75 at.% results in a typical structure as seen in nanoporous gold (NPG). Two mechanisms (percolation dissolution and solid-state diffusion) can account for the Li segregation process in this system [41]. In principle, the slight tuning of the alloy composition and particle size can remarkably affect the final porous morphologies. Thus, this versatile template-free method for the synthesis of porous architectures can essentially be applied to any solid elements that can form alloys with Li or other guest ions over a wide composition range. Several transition metals and even metal compounds with characteristic nanoporosity and large surface area have been successfully developed based on the above electrochemical insertion/extraction process [43–48]. Inspired by this finding, there

are ever-increasing relevant publications and the annual citation rate has also grown rapidly in the past decade [33, 38].

Overall, a few efforts have been devoted to reviewing research progress on dealloyed NPMs, including the structural and compositional regulations [38, 49–51], and potential applications in catalysis, supercapacitors, sensors, and optical devices [2, 10, 52–54]. Nonetheless, there is still a lack of systematic summarization of dealloyed materials for battery applications [37, 55]. In this connection, we attempt to provide an overview of the recent progress on dealloyed materials in rechargeable lithium batteries (Fig. 1). First, this work will present typical fabrication and microstructural regulations. Subsequently, this review will focus on key applications of nanoporous materials in rechargeable lithium batteries, including LIBs and lithium metal batteries (LMBs). Finally, several critical challenges and opportunities are discussed to provide insights into the future development of this research area.

2 Fabrication and microstructural regulation

The practical performance of NPMs in batteries is significantly influenced by their compositions and microstructures. Thus, the fabrication and post-treatment processes are critical for NPM electrodes. In this section, four typical dealloying routes to fabricate nanoporous materials are summarized, and the key parameters affecting pore formation and growth are discussed, including precursor design, reaction
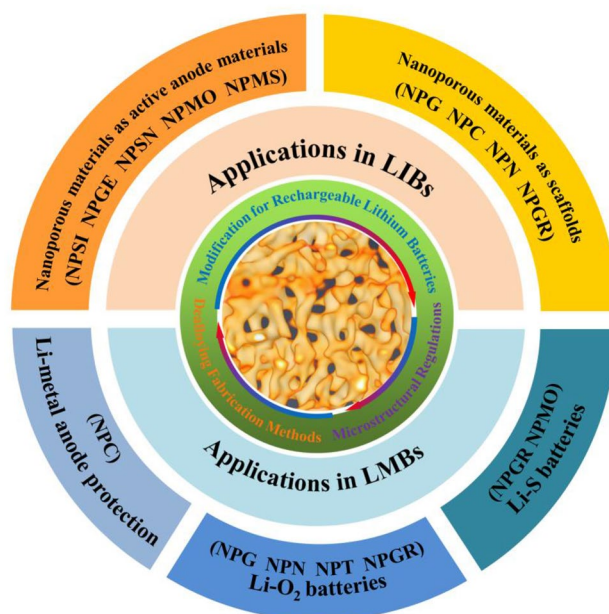

Fig. 1 Schematic of the applications of dealloyed nanoporous materials in rechargeable lithium batteries

parameter control, and post-treatment. Besides, modification strategies that can further enhance the compatibility of NPMs in rechargeable lithium batteries are presented.

2.1 Dealloying fabrication methods

Dealloying refers to a process in which one or more less stable components are selectively removed from an alloy precursor and the remaining relatively stable components evolve into a porous network [6, 56, 57]. The current mainstream routes can be classified into four categories: chemical, electrochemical, liquid metal, and vapor phase dealloying [2, 36].

Chemical and electrochemical dealloying technologies are the most employed approaches. Because the alloy components possess different standard electrochemical potentials, the less noble components are selectively etched away by an appropriate electrolyte (i.e., a strong acid/alkali solution), and the remaining components form a porous structure. This process can be driven by spontaneous chemical reactions (chemical dealloying) or an external electrical current (electrochemical dealloying) between the counter electrodes and precursor alloys. Due to the ease of operation and tunable porosity, this technique has been widely utilized to produce various NPMs, alloys, and compounds [5, 58]. A typical example is the fabrication of NPG from Au–Ag binary alloy. During chemical dealloying, Ag can be selectively removed in the concentrated HNO_3. The initial reaction occurs at the interior grain regions, in which residual Au ligaments and void networks are generated at the grain boundaries to eventually induce a 3D bicontinuous NPG composed of nanoscale ligaments [59]. Alternatively, NPG can also be generated through an electrochemical process in various electrolytes such as $HClO_4$ or KNO_3. The anodic potential leads to the electrochemical dissolution of Ag from the Au–Ag alloy with more controllable rates and thus allows the formation of more refined ligaments [59]. These two methods produce NPMs with different characteristic length scales and even microstructures. Compared with chemical dealloying, the electrochemical treatment is more controllable due to the tunable applied potential [60]. However, these two approaches are only applied to alloy systems with sufficient potential difference between the metal components, such as noble metals, stable compounds, and easily passivated transition metals. Moreover, additional costs are also inevitable due to the waste disposal process of the environmentally hazardous etchants and the recovery of the dissolved elements in the corrosion process.

Although the traditional etching process is efficient to prepare nanoporous structures, alternative approaches such as liquid metal and vapor phase dealloying have recently emerged to reduce the utilization of corrosive acids/alkalis. Furthermore, liquid metal route provides additional viability for some special systems composed of constituents that are sensitive to the environment [36, 61, 62]. In general, the liquid metal route involves the selective removal of elements by using a liquid metal melt as an extraction medium in place of the traditional electrolyte. The selected liquid metal should possess a high mixing enthalpy with one of the elements in the alloy precursor. Upon the dissolution of miscible elements, the immiscible phase simultaneously organizes and forms a nanostructure after the subsequent solidification and phase excavation steps. A good example is the fabrication of nanoporous Si (NPSI) from SiMg binary alloy using a Bi melt [63]. This material system is suitable because Mg and Bi are highly miscible at a desired temperature, and Si and Bi are non-soluble with each other. Nevertheless, liquid metal dealloying requires relatively high temperatures, and the subsequent phase etching process is still inevitable to remove the solidified metal melts.

Alternatively, physical vacuum dealloying is a relatively neat process to obtain a pure high-boiling-point phase by sublimating one or more low boiling point components in the precursor. The structural formation is the consequence of the Kirkendall effect, where the different diffusion rates of metal atoms cause the motion of the interface between two metals [64, 65]. The selected temperature for vacuum dealloying should be lower than the precursor melting point to allow for pore maintenance. For example, nanoporous Cu (NPC) can be obtained through the sublimation of Zn in brass (Cu–Zn alloys) at 500 °C under vacuum [65].

Overall, the selection of suitable methods to fabricate desired NPMs requires the comprehensive consideration of the characteristics of different fabrication methods and the feasibility to meet the requirements of the relevant applications.

2.2 Microstructural regulation

To understand the pore formation mechanisms, several important factors need to be considered for the microstructural regulation of NPMs, including the design of alloy precursors, control of etching parameters, and post-treatment procedures.

Dealloyed NPG is a well-researched prototype case. Relevant investigations based on this system suggest that the rational design of alloy precursors should comply with four basic criteria [4, 56, 60, 66, 67]. (1) The potential to dissolve the pure alloy component must be of significant difference, up to a few hundred millivolts, namely the targeted alloy should be composed of a relatively active metal and a relatively inert one. (2) The chemical composition of the inert metal must be below its parting limit, which is its maximum concentration in an alloy precursor. Otherwise, the dealloying cannot proceed throughout the whole process to obtain a desired structure. (3) The alloy must possess a homogeneous

phase distribution to avoid phase separation prior to dissolution. Ideally, the alloy precursor should be a single-phase solid solution or intermetallic phase. The dealloying of a single-phase structure can endow products with a uniform 3D morphology. A complicated two-phase or multiphase precursor is conducive to the fabrication of NPMs with multilevel and multiscale microstructures. (4) The diffusion of inert elements must be sufficiently fast at the alloy/interface, which can facilitate their surface rearrangement after the selective dissolution of the active components. Based on the above design principles, many alloy precursors have also been explored, such as Cu-based alloys [68], Al-based alloys [24], and Zn-based alloys [69].

In general, the dealloying process involves several steps and parameters [46]. Here, we primarily analyze the influence of crucial parameters on the formation process of NPMs, including solution, temperature, and applied potential. First, a dealloying solution with proper composition and concentration is important to selectively remove the less noble element. For example, dealloying of Al_2Au can be carried out in an acidic or alkaline solution and the length scale of the ligaments/channels in NPMs can be simply adjusted by selecting an appropriate solution (60–80 nm in 5 wt% HCl vs. 10–20 nm in 20 wt% NaOH) [24]. Second, the atomic diffusion rate at alloy/electrolyte interfaces strongly relies on the reaction temperature. A low-temperature treatment can significantly reduce the interfacial diffusivity of the noble element and result in an ultrafine porous network. In contrast, a high dealloying temperature would coarsen the length scale of the ligaments/channels, but simultaneously reduce cracking in the produced NPMs. Third, to drive the selective dissolution, the applied potential during electrochemical dealloying must be between the critical potential of the active element and the equilibrium corrosion potential of the inert one. A higher applied potential accelerates the dealloying process duration. Meanwhile, more cracks/defects will form in the products owing to the fast reaction rates. Thus, the potential must be optimized to balance the reaction rate and duration. In addition, dealloying steps [5, 70], atmosphere [71], and applied magnetic field [72, 73] can also modulate the microstructure/morphology of NPMs. As a result, all the relevant parameters should be reasonably considered during processing to obtain ideal NPMs.

To further regulate the morphologies, compositions, and microstructures of NPMs, post-treatment procedures, especially annealing, are frequently adopted. Specifically, the annealing of NPMs at certain temperatures maintains the initial nanoporosity but coarsens the ligaments/channels to different length scales via a self-similar process [74, 75]. Moreover, several investigations on the 3D evolution of nano-ligaments in NPG suggest that both the surface orientation and scaled surface curvature of the nano-ligaments would evolve with coarsening time [76]. Based on this

phenomenon, a unique Pt-rich surface layer coating on an alloy backbone can be obtained by combining the dealloying method with a subsequent annealing treatment. Such a structure can greatly improve the utilization of precious Pt for important catalytic reactions [77, 78]. Therefore, rational post-dealloying treatment can be used to effectively control NPM properties and facilitate their customized applications.

2.3 Modification for rechargeable lithium batteries

NPMs with 3D bicontinuous architectures and abundant nanopores greatly facilitate electrolyte permeation, reduce the Li-ion diffusion length, and accommodate large volume expansion during cycling, all of which are desirable characteristics in rechargeable lithium batteries. Nevertheless, typical dealloyed NPMs also face critical challenges in battery applications. For example, NPMs usually possess pore channels of ~ 10 nm, which are too narrow for electrolyte permeation. Moreover, these small pores usually imply a large specific surface area that would generate more solid-electrolyte interface (SEI) and lead to low Coulombic efficiency (CE) [37]. For certain materials, because the poor electrical conductivities could significantly affect their practical performance in electrodes, it is necessary to optimize the porous structures and compositions of dealloyed NPMs for different applications. In this section, three efficient strategies are summarized, including post-annealing treatment, incorporation of a carbon buffer matrix, and electrochemical deposition of active species.

As mentioned above, the pore and ligament sizes derived from direct dealloying processes are usually too small. Kunduraci [37] reported that the desired pores/ligaments should be in range of 100 nm for NPM-based alloy anodes. To resolve this problem, a quick post-annealing process can be applied to increase the ligament/channel size by increasing the surface diffusivity of the nobler elements. The annealing process only alters the corresponding length scale but maintains the topological structure of NPMs [75]. Meanwhile, the orientation distribution of the ligament surfaces during the coarsening treatment becomes more anisotropic, as evidenced by the increasing facet exposure with a lower surface energy [76]. In addition, annealing in an air atmosphere could even produce a layer of metal oxides on NPM surfaces, which can be actively involved in the subsequent redox reactions. For example, cuprous oxide (Cu_2O) is in situ generated on the surface of NPC during the annealing treatment. When tested in LIBs, thus-fabricated Cu_2O@NPC anodes show superior electrochemical performance, which is ascribed to the favorable combination of a novel structure from NPC and high specific capacity from the surface Cu_2O [79].

Depending on their electrochemical functions in LIBs, the applications of NPMs in LIBs can be classified as active anode materials (electrochemically active) or as

novel scaffolds (electrochemically inert). For electrochemically active materials, such as nanoporous Si (NPSI), Sn (NPSN), and Ge (NPGE), as well as the corresponding metal oxides (NPMO) and metal sulfides (NPMS), the alloying/conversion mechanism offers high theoretical specific capacities. For these active materials, their practical performance is mainly determined by the large volume variation and electron conduction problems during cycling. From this viewpoint, the abundant nanoporosity is beneficial to the accommodation of significant volume expansion [80–82]. Besides, carbon decorations are usually to promote electrode conductivity and further tolerate the volume influence. In most cases, commonly used carbon-coating strategies in LIBs are also generally applicable to NPMs, such as ball milling [83], chemical vapor deposition (CVD) [84, 85], hydrothermal [86], ultrasonic [87], and chemical reduction methods [88].

For NPMs without electrochemical activity such as NPG and NPC, the deposition of electrochemically active species including active metals, metal oxides, and metal sulfides onto the ligament surface of the NPMs is indispensable for ion storage. As we know, Sn could be a promising anode material for LIBs due to its high theoretical capacity (990 mAh g^{-1} for Li$_{4.4}$Sn). However, substantial volume change over 200% during the charge/discharge process greatly hinders the practical implementation of metallic Sn in LIBs [89]. Considering that NPMs possess plentiful pores and superior electrical conductivity, they can be utilized as 3D substrates, which can effectively relieve the substantial volume expansion during cycles. Indeed, a 3D NPG-supported Sn nanocrystalline thin foil was reported as an anode for rechargeable LIBs with enhanced electrochemical performance [90]. Considering the high cost of NPG, NPC with more affordable price and excellent cycling stability is a suitable alternative [91]. These investigations demonstrate the outstanding potential of NPMs as novel scaffolds to deposit various active components for rechargeable lithium batteries.

To summarize, it has been well-established that the dealloying route, microstructural regulation, and post-synthetic modification would significantly influence the resulting structures and phase constitutions of NPMs. All these factors need to be adequately taken into account during NPM preparation. The rational design of alloy precursors and careful tuning of the dealloying process can lead to desired morphologies and structures. For example, hierarchical structures with novel physicochemical properties and superior electrochemical performance for energy storage can be fabricated either by controlling the alloy precursor composition or by multiple-step dealloying and annealing [92, 93]. It is noted, however, the majority of discussions on NPMs are still limited to several relatively inert elements [8]. It is thus urgent to develop more rational dealloying methodologies for use in rechargeable lithium batteries.

3 Applications in rechargeable lithium batteries

Owing to the intrinsic correlation between the Li-ion insertion/extraction and the formation of porous electrodes, great efforts have been devoted to the applications of dealloyed materials in rechargeable lithium batteries. In principle, NPMs can be simply categorized in terms of their functions in batteries as electrodes or scaffolds. The former refers to electrochemically active metals, metal oxides, semiconductors, and their composites. They are attractive for anodes in LIBs owing to the large capacities and unique porous structures for volume variation accommodation during cycling. To date, metal anodes including Si, Ge, Sn, Sb, Bi, and commonly used metal oxides/sulfides have been successfully developed through the dealloying process. In addition, binary alloys that are difficult to prepare via regular routes can also be obtained by this technique. Actually, this is one of the key advantages of the dealloying method, where the design of complex alloy systems with desired compositions and structures is very straightforward. The other application of NPMs in batteries is to serve as scaffolds to support active ingredients, where they can be either a free-standing film/membrane or on a substrate. A well-known example is the utilization of NPG membrane in Li–O$_2$ batteries (LOBs). Indeed, metals with good flexibility can maintain the membrane continuity up to hundreds of centimeters. The abundant porosity, tunable architectures, and excellent electron conduction make such metallic membranes suitable catalyst scaffolds when applied to rechargeable lithium batteries. Furthermore, nanoporous graphene (NPGR) can be fabricated by templating preformed NPMs, and it has been recently demonstrated as a promising scaffold for LOBs and lithium–sulfur (Li–S) batteries. Here, our discussion is primarily focused on the progress of nanoporous materials in LIBs and LMBs because the aforementioned unique properties are critical to promote the practical performance of these battery systems.

3.1 Applications in LIBs

LIBs with high energy density, long cycle life, and low self-discharge properties have achieved great success in the past two decades [94–96]. However, current commercial graphite anodes have a low theoretical specific capacity of 372 mAh g^{-1}, which is not very competitive among various novel high-capacity anodes. Alternatively, alloy anodes show attractive high theoretical capacities of 2–10 times higher than that of graphite anodes. Meanwhile, the moderate operation potentials of alloy anodes offer better

safety [97, 98]. Nonetheless, the enormous electrode volume variation during cycling results in poor cell stability caused by particle pulverization. NPMs with bicontinuous porous structures and large specific surface areas can efficiently mitigate the serious volume expansion during lithiation, and the open porous structure and high electrical conductivity accelerate electrolyte percolation and electron transfer. A wide variety of dealloyed nanoporous materials have been explored in LIBs in recent years. In this section, the design principles of such electrodes and their performance in LIBs are summarized and discussed.

3.1.1 Nanoporous anodes

3.1.1.1 Nanoporous silicon (NPSI) Among various metal and alloy anodes, Si has been considered as one of the most promising candidates, owing to its high theoretical capacity (4200 mAh g^{-1}), suitable operation potential, and cost advantage [80, 99–101]. However, two fatal flaws impede its commercialization in LIBs. One is that the Li-concentration-dependent volumetric change (~300%) induces rapid capacity degradation during long-term cycling. The other is that the poor electrical conductivity (6.7×10^{-4} S cm^{-1}) and sluggish Li-ion diffusivity lead to inferior rate performance [102–104]. Thus, the primary motivation for the development of NPSI is its possibility in accommodating the severe volume expansion upon lithiation. NPSI electrodes with rational structure regulation would therefore improve cycling performance [105–107]. Considering that simply dealloyed Si electrodes are insufficient to achieve the desired battery performance [104, 108–112], in this section, we first introduce the direct application of NPSI in LIBs with favorable electrochemical performance after rational structure regulation. Then, for those NPSI electrodes with additional modifications, we attempt to summarize their feasible applications based on two efficient strategies: the optimization of battery configuration and the composition control by constructing Si composites with other buffering matrices. Finally, the synthetic approach, morphology, and electrochemical performance of the selected NPSI-based anodes are compared to better understand the correlation between their composition/structure and electrochemical properties.

By adjusting the dealloying parameters to acquire appropriate porosity and ligament dimension, the NPSI electrode itself can efficiently alleviate the adverse effects of serious volume expansion/contraction, thus exhibiting good electrochemical performance in LIBs. Based on different alloy precursors (Fe–Si and Mg–Si alloys), Tian et al. and Zhu et al. first prepared porous Si by acid-etching in HCl solution [105, 106]. Even in the absence of carbon coating, these electrodes delivered high rate capacities owing to the unique and well-organized porous structures. To further adjust the

porosity, Sohn et al. [107] developed 3D porous Si microparticles by two-step etching. The specific synthetic routes can be illustrated by Fig. 2a. First, the Si/metal-alloy composite was fabricated by melting pure Si and densely packed Al–Cu–Fe matrix. NPSI was then obtained by selectively removing the metallic matrix from the Si/Al–Cu–Fe composite in an acidic solution. After the wet alkaline etching in NaOH solution to enlarge the preexisting pores and reduce the size of the Si grains, microstructure-controlled porous Si microparticles were generated with interconnected Si networks. The specific surface area and pore volume of the 3D porous Si were also higher than those of Si alloy and one-step dealloyed Si, indicating an increase in free voids during the double chemical etching process. When applied in LIBs, the resulting 3D porous Si anode with an interconnected network exhibited initial Coulombic efficiency (ICE) of 76.5% and high Li-ion storage capacity of 1222 mAh g^{-1} at 500 mA g^{-1} over 200 cycles.

The aforementioned chemical dealloying is a simple yet efficient strategy to tune nanoporosity and grain size, but this process usually relies on strong corrosive chemicals that may cause severe environmental issues. An et al. [113] developed a novel acid/base-free method to synthesize NPSI by vacuum distillation from a commercial Mg$_2$Si alloy. Mg with its relatively low boiling point of 1107 °C would undergo sublimation and diffusion to generate voids, eventually producing the continuous NPSI skeleton (Fig. 2b). By regulating the distillation temperature and time, the NPSI with optimized pore size exhibits a greatly enhanced performance. The vacuum distillation method provides new insight into the design and fabrication of nanoporous materials, and it could possibly be extended to other complex alloy systems composed of metals with distinct melting/boiling points. The above examples reveal that NPSI can be obtained by different dealloying methods with different alloy precursors. The excellent electrochemical performance of NPSI anodes without additional optimizations is reasonably attributed to their intrinsic structure, which could alleviate the serious volume change to a large extent.

In addition to the traditional chemical dealloying and vacuum distillation dealloying technologies, Wada et al. [114] produced bulk 3D NPSI by a top-down liquid metal dealloying method. This method effectively compensates for the drawbacks of traditional approaches in the applicable elements, especially for less noble metals. The whole process is based on the metallurgical reaction between an alloy precursor solid and a liquid melt rather than the traditional corrosion in an aqueous solution. A Si–Mg precursor and Bi melt are selected owing to the miscibility of Mg–Bi and the immiscibility of Si–Bi, where Si acts as the porous structure-forming element, Mg functions as the sacrificial element, and Bi works as the dealloying melt medium. Figure 2c highlights the evolution schematic of the 3D porous

Fig. 2 Different fabrication methods for NPSI electrodes. **a** Schematic illustration and SEM images of 3D porous Si by chemical etching: Si alloy; dealloyed Si; and 3D porous Si particles. Scale bar: 150 nm. Reproduced with permission from Ref. [107]. Copyright 2018, Wiley–VCH. **b** Structural evolution of the Mg$_2$Si alloy by the vacuum distillation method. Reproduced with permission from Ref. [113]. Copyright 2018, American Chemical Society. **c** Fabrication schematic of 3D NPSI by a liquid–metal dealloying process: the initial Si–Mg precursor; upon the immersion in Bi melt; 3D NPSI after etching Bi. Reproduced with permission from Ref. [114]. Copyright 2014, American Chemical Society
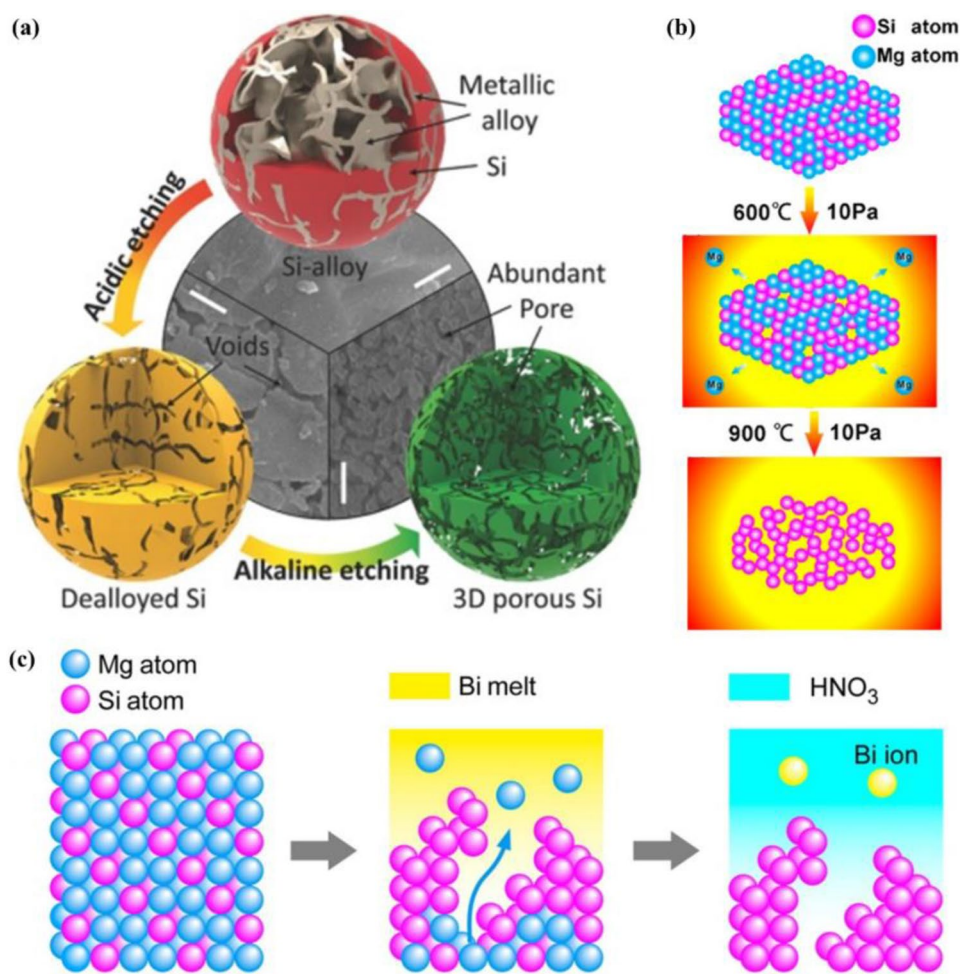
structure during dealloying, which is supported by the corresponding scanning electron microscopy (SEM) images and energy-dispersive X-ray (EDX) elemental maps. The dynamic observation of the precursor shows a typical hypereutectic structure with primary dendritic grains anchored in the eutectic matrix. Transmission electron microscopy (TEM) image shows they are composed of interconnected Si grains, which have diamond cubic structures as verified by the corresponding selected-area electron diffraction (SAED) observation. When charged/discharged with the high capacity of 2000 mAh g^{-1}, this anode suffers from severe capacity fading within a few hundred cycles. However, by restricting the lithiation capacity to 1000 mAh g^{-1} below the accommodation volume limit, the NPSI anode can demonstrate a long span life of 1500 cycles at 3.6 A g^{-1}. A similar strategy to enhance the cycling life was also reported by Saager et al. [115]. These results indicate that the abundant porosity of Si anodes could not completely avoid volume expansion under practical cycling conditions. Synchrotron X-ray nano-tomography studies have been performed to explore the lithiation/delithiation process in NPSI anodes. The Chen-Wiegart group found that cell failure could be ascribed to the

structural deformation of NPSI anodes from mesoporosity to macroporosity, accompanied by progressive volume expansion and delamination. In particular, the reduced cell life in a high-capacity cycling mode was caused by particle agglomeration [116]. Overall, the nanoporosity could mitigate the local volume expansion to a certain level, but the structural evolution eventually leads to a heterogeneous stress distribution with faster delamination. Therefore, further optimization is necessary to realize long cycling durability of NPSI electrodes.

Other strategies toward electrolytes and binders have also been proposed to promote cell cycling stability. Jiang et al. [117] obtained porous Si powder by etching Al–Si alloy in HCl solution. The intertwined Si nanobars constitute a spongy structure with homogeneously distributed pores. When applying an electrolyte containing 15% ethylene carbonate (FEC), the ICE and corresponding electrochemical cycling stability are greatly enhanced. Apart from the innovative spongy structure, FEC is beneficial for generating a thin and robust "primary SEI" on the anode surface during the initial cycle, which inhibits the breakdown and pulverization of active materials in

the electrodes [118, 119]. Another efficient technology to stabilize NPSI anodes is to develop advanced polymeric binders. Hwang et al. [120] first introduced the ecofriendly and naturally abundant agarose as an aqueous binder for NPSI anodes, which is obtained by dealloying Al–Si. The agarose binder contains functional groups, such as ether and hydroxyl groups, which could strengthen the adhesion between the Si active material and Cu current collectors, and meanwhile minimize the large volume variation during repeated charge/discharge cycles.

The construction of NPSI composites with buffering matrices is another research direction to improve cell cycling stability, and typical choices include carbons, metal oxides, and active/inactive metals. Furthermore, carbon coatings could function as a protective layer to control SEI formation on the electrode surface [121, 122]. As a result, NPSI/C composite anodes exhibit much improved electrochemical performance compared with pristine NPSI anodes. Different carbonaceous materials including reduced graphene oxide (RGO), carbon nanofibers, and graphitic carbon, have been employed to fabricate NPSI/C composites [123, 124]. As expected, the incorporation of carbons greatly enhanced the electron transfer and improved the electrochemical kinetic performance during cycling.

Si dispersion into metal matrices is regarded as another efficient strategy to tolerate volume expansion and improve electronic conductivity. Zhou et al. [125] prepared nanostructured Si spheres by etching the eutectic Al–Si. By carefully controlling the etching conditions, a ~5% Al residual is maintained in the Si crystal lattice. Moreover, Al_2O_3 deposited on the Si surface is proved to function as an efficient protection layer. These modifications can significantly enhance cycling stability owing to the suppression of the side reactions between the Si electrode and electrolyte [126–128]. Hwang et al. [128] prepared micron-scale Si/Al_2O_3 foams by a further selective thermal oxidation process (Fig. 3a). Due to the different diffusion kinetics of the chemical etchant from the surface to the core, Al_2O_3 protection layer can be homogeneously formed on the NPSI in the outer shell along with most Al_2O_3 particles located at the core. The Al content could be readily adjusted by tuning etching time, while the Al_2O_3 layer thickness could also be controlled by exposing in water vapor for certain time. The massive void spaces in the Si/Al_2O_3 foam are functionalized as buffer layers, while the superficial Al_2O_3 protective layers reduce interface side reactions.

Compared with the Al residual, Ag with its much higher electrical conductivity and negligible effects on the Li storage behavior is also a promising buffer matrix of Si-based anodes. Hao et al. [129] fabricated a micro–nano bimodal pore size distribution Si/Ag composite by etching a well-designed Si–Ag–Al ternary alloy in HCl solution (Fig. 3b). The rich porosity and incorporation of highly conductive Ag could promote the electrochemical performance of the composite electrode.

Low-cost Cu with its high electrical conductivity is also a good candidate. Nanoporous Si/Cu composites with controllable components could be easily fabricated by dealloying the Si–Cu–Al ternary alloy [130, 131], where Si nanoparticles are anchored in the Cu–Si–Cu rigid framework (Fig. 3c). After optimization, the as-prepared NPSI/$Cu_{0.83}Si_{0.17}$/Cu composites (denoted as Si_{SERE}) exhibit highly improved cycling stability and rate capability for Li storage. In order to study the impact of a porous skeleton upon the volume expansion, a nanobattery is assembled to observe the charge/discharge process by in situ TEM. As illustrated in Fig. 3d, the Si nanoparticle gradually expands during discharging, but no evident structural degradation or particle pulverization occurs after 10 min of lithiation. A high-resolution image suggests that the SEI film with a uniform thickness of ~5 nm covers the surface of the lithiated Si grain. The crystalline LiCuSi nanoparticles in the amorphous $LiSi_x$ matrix could effectively maintain the structural integrity during repeated lithiation/delithiation. Moreover, ex situ SEM/TEM shows that the Si electrode almost maintains its original morphology, even after long-term cycling. Crystal LiCuSi particles closely packed with amorphous Li_xSi are still observed in the lithiated state, and CuSi particles within the ligaments also appear in the delithiated state. These results confirm that the CuSi phase undergoes a highly reversible expansion/contraction process during cycling. Therefore, the robust framework with sufficient void space and the existence of the CuSi phase are both responsible for the stability of the composite electrode. It should be noted that most dealloying studies to date are limited to binary systems. It is expected that multicomponent precursors may offer more opportunities to further adjust the microstructures of nanoporous electrodes with desired functions.

The incorporation of conductive Li-alloyed metals into Si has also been carried out. The design of such composite anodes is based on the following considerations [132–135]: (1) the integration of highly conductive Li-alloyed metals and Si can enhance the kinetics of Li transport and improve the rate capability; (2) different active components are lithiated at different onset potentials, avoiding simultaneous expansion and facilitating the gradual release of the strain–stress; (3) one can function as a buffer matrix when Li is inserted into the other active component.

Among various alloy systems, Ge has attracted much attention owing to its high capacity (1384 mAh g^{-1} for $Li_{15}Ge_4$), favorable electronic conductivity (100 times higher than Si), and rapid Li^+ mobility (400-fold faster than that in Si) [136]. Yang et al. [137] synthesized a 3D SiGe alloy by dealloying a ternary Al–Si–Ge precursor in HCl solutions. The morphology and porosity are controllable by adjusting the sacrificial Al content in the precursor.
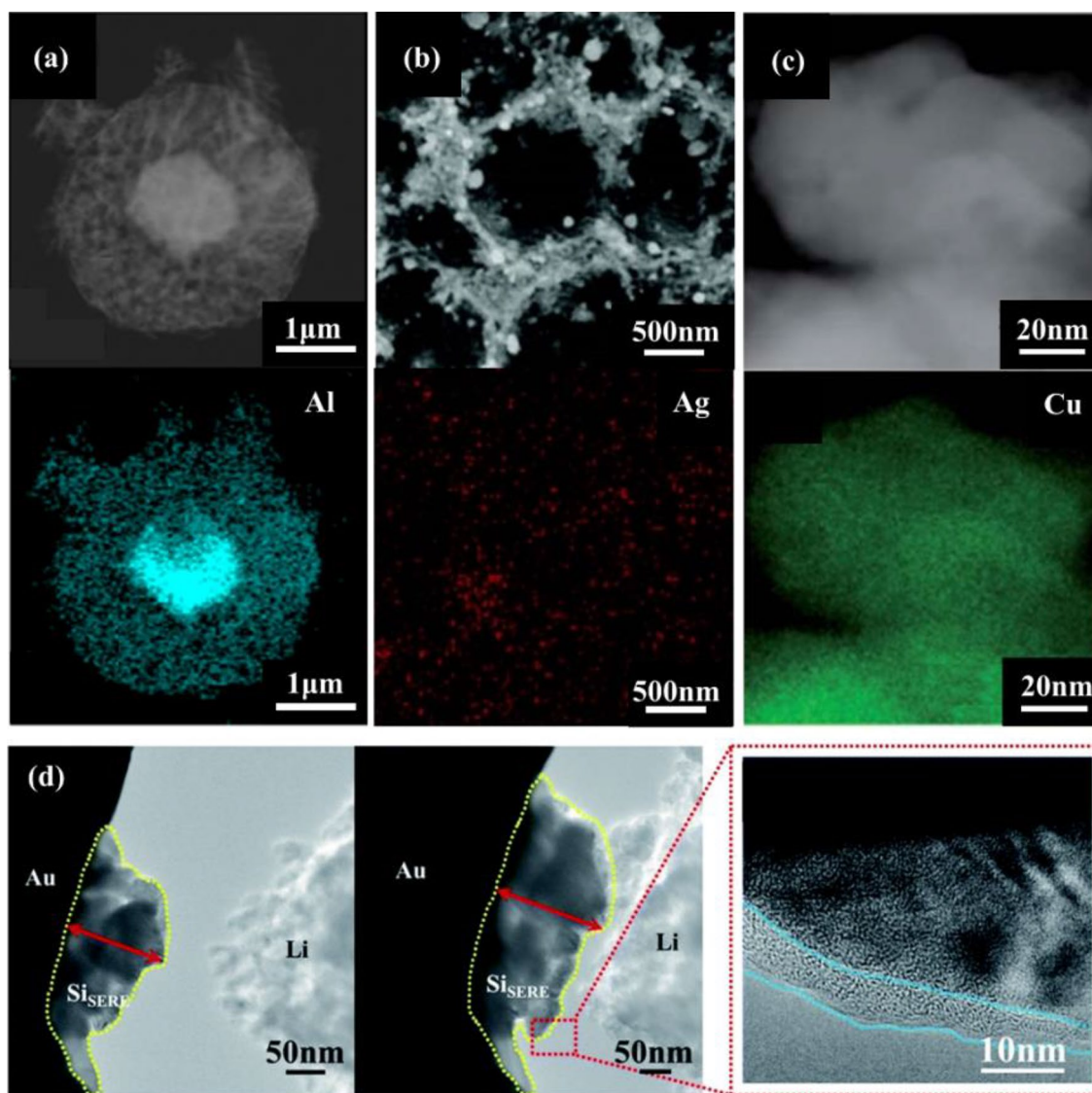
Fig. 3 Morphologies and compositions of representative metal-supported NPSI anodes. **a** Thermally oxidized Al–Si powder. Reproduced with permission from Ref. [128]. Copyright 2015, Royal Society of Chemistry. **b** Dealloyed Si/Ag composite. Reproduced with permission from Ref. [129]. Copyright 2015, Royal Society of Chemistry. **c** Si$_{SERE}$ composite. **d** In situ TEM images of Si$_{SERE}$ at the initial stage (left) and upon discharging (right); HRTEM images showing the phase boundary of the SEI film/the anode (highlighted with light blue dashed lines). Reproduced with permission from Ref. [131]. Copyright 2016, Royal Society of Chemistry

The optimized electrode has a coral-like structure with hierarchical micropores/mesopores and uniform ligaments. Benefitting from the addition of Ge into Si, the innovative porous architecture could not only efficiently accommodate the volume change but also accelerate the electron transfer and Li-ion migration kinetics. Similarly, Sn and TiO$_2$ have also been utilized as a buffer matrix to reduce the extreme volume change and enhance the lithiation/delithiation kinetics, thus boosting both the cycling stability and the CE of the dealloyed NPSI electrodes [92, 138]. Obviously, different optimization strategies can be applied simultaneously to maximize the synergistic effects on electrochemical performance. For example, the co-incorporation of carbon matrix and metal elements into NPSI has been reported by different groups [87, 139, 140].

The representative NPSI anodes in LIBs are summarized in Table 1. In general, NPSI can be fabricated by three dealloying techniques including chemical, liquid metal, and vapor phase dealloying. Meanwhile, abundant Si-based alloy systems covering binary, ternary, and even quaternary alloys have been explored for compositional and structural control. Among them, Al is the most used sacrificial element, owing to its active chemical property and low price. After etching in an acidic or alkaline solution, they readily exhibit rich

Table 1 Synthetic approach, morphology, and electrochemical performance of selected NPSI-based anodes. (Each box section includes two example studies. Left and right images correspond to the top and bottom studies in each box, respectively)
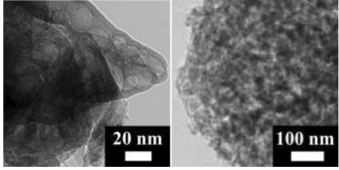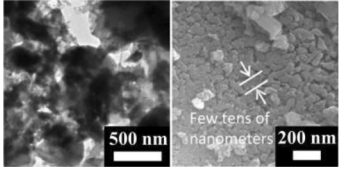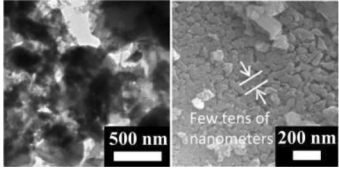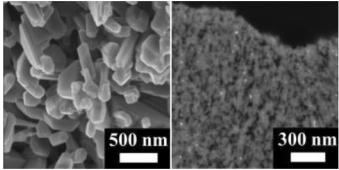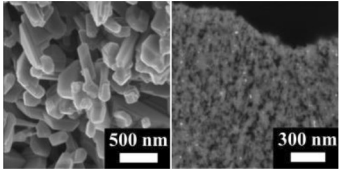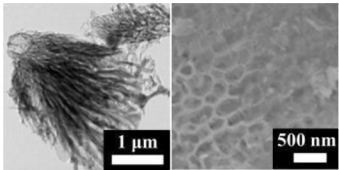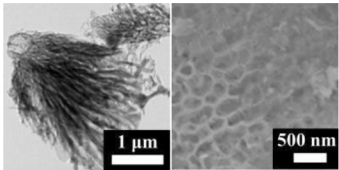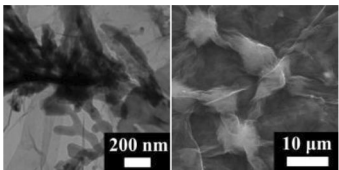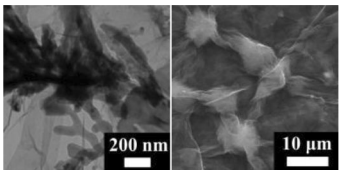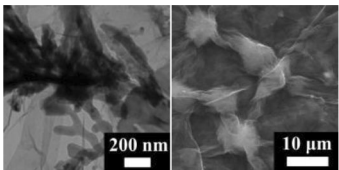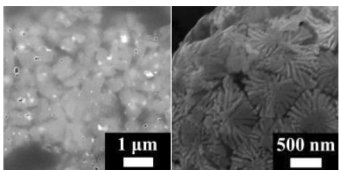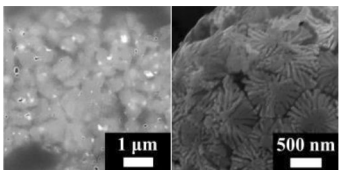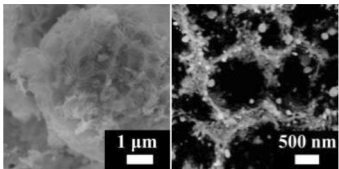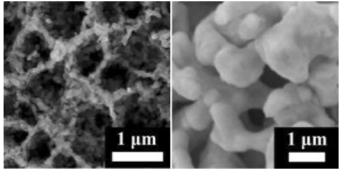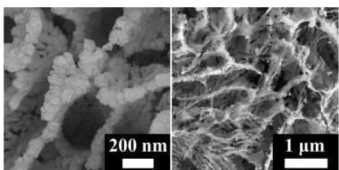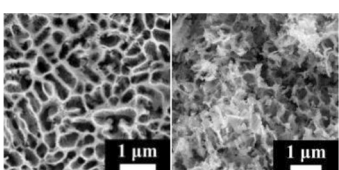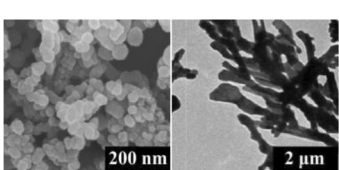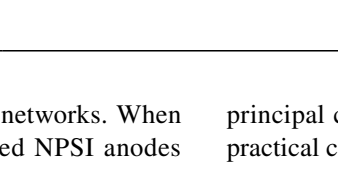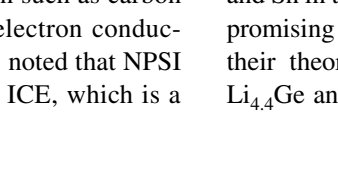
Mater.	Synthesis	Morphology	ICE	Cyclability (mAh g^{-1})	Rate (mAh g^{-1})	Ref.
Micro-sized porous Si	Fe–Si alloy in HCl and HF		88.1%	1250 at 500 mA g^{-1} after 100 cycles	558 at 5 A g^{-1}	[105]
Nanoporous Si	Mg–Si after airoxidation in HCl		88%	1200 at 1800 mA g^{-1} after 400 cycles	1000 at 36 A g^{-1}	[106]
Nanoporous Si	Mg–Si by vacuum distillation		85%	2034 at 200 mA g^{-1} after 100 cycles	855 at 5A g^{-1}	[113]
3D porous Si	Al–Cu–Fe/Si alloy in HCl and NaOH		76.5%	1222 at 500 mA g^{-1} after 200 cycles	–	[107]
3D NPSI	Mg–Si precursor in Bi melts		–	1000 at 3.6 A g^{-1} after 1500 cycles	–	[114]
Porous Si	Zn–Si layers by vacuum annealing		–	2000 at 360 mA g^{-1} after 150 cycles	–	[115]
Porous Si	Al–Si alloy in HCl solutions		60.1%	1368 at 100 mA g^{-1} after 258 cycles	–	[117]
Nanoporous Si	Al–Si alloy in HCl		68%	1400 at 100 mA g^{-1} after 60 cycles	750 at 4.2A g^{-1}	[119]
Si/RGO	Al–Si alloy in GO and HCl		75%	1942 at 100 mA g^{-1} after 100 cycles	1521 at 4 A g^{-1}	[88]
Si/graphene paper	Al–Si in HCl and graphene coating		56%	1500 at 100 mA g^{-1} after 100 cycles	400 at 2 A g^{-1}	[141]
CNF/NPSI hybrids	Al–Cu–Fe/Si alloy in HCl		82.31%	1184 at 360 mA g^{-1} after 100 cycles	–	[123]
Porous Si spheres	Al–Si in HCl under the ice bath		~75%	1150 at 200 mA g^{-1} after 60 cycles	1180 at 3.2 A g^{-1}	[125]

Table 1 (continued)

Mater.	Synthesis	Morphology	ICE	Cyclability (mAh g^{-1})	Rate (mAh g^{-1})	Ref.
NPSI/Al$_2$O$_3$ foam	Al–Si in HCl and thermal oxidation		83.1%	~750 at 720 mA g^{-1} after 300 cycles	–	[128]
Bimodal porous Si/Ag composite	Ag–Al–Si ternary alloy in HCl		79.3%	1656 at 200 mA g^{-1} after 150 cycles	960 at 1 A g^{-1}	[129]
NPSI/Cu composites	Cu–Al–Si ternary alloy in HCl		78.4%	820 at 1000 mA g^{-1} after 200 cycles	900 at 1.5 A g^{-1}	[130]
3D NPSI/CuSi/Cu	Cu–Al–Si by Sulfur-dealloying		70.5%	1186.9 at 1500 mA g^{-1} after 180 cycles	160.3 at 48 A g^{-1}	[131]
Nanoporous SiGe Alloy	Ge–Al–Si ternary alloy in HCl		75.6%	1158 at 1000 mA g^{-1} after 150 cycles	577 at 8 A g^{-1}	[137]
Macroporous Si/Sn composite	Sn–Al–Si ternary alloy in NaOH		75.0%	748.2 at 1000 mA g^{-1} after 100 cycles	620 at 4 A g^{-1}	[92]
Porous Si@TiO$_2$	Ti–Al–Si alloy in NaOH solutions		73.3%	1338.1 at 200 mA g^{-1} after 120 cycles	815 at 4 A g^{-1}	[138]
Macroporous Si/Ni/C	Ni–Al–Si in NaOH and C-coating		68.2%	1113 at 200 mA g^{-1} after 120 cycles	775.9 at 3 A g^{-1}	[87]
Micro-sized porous Si	Al–Si in HCl and carbon coating		61%	~600 at 500 mA g^{-1} after 300 cycles	200 at 10 A g^{-1}	[139]
Al/Na-doped Si nanorods@C	Al–Na–Si in HCl and C coating		87%	~700 at 1000 mA g^{-1} after 1000 cycles	420 at 4 A g^{-1}	[140]

porous morphology with interconnected networks. When evaluated in LIBs, the rationally designed NPSI anodes exhibit enhanced cycle stability with high reversible capacities (> 1000mAh g^{-1}), good rate capabilities, and high ICE (> 75%). Nonetheless, further optimization such as carbon decoration is necessary for the sake of electron conduction and volume expansion. However, it is noted that NPSI composite electrodes could result in low ICE, which is a principal challenge for the application of NPSI anodes in practical cells.

3.1.1.2 Nanoporous germanium (NPGE) and tin (NPSN) Ge and Sn in the same group as Si in the Periodic Table are also promising alternatives to commercial graphite. Although their theoretical capacities (1600 and 994 mAh g^{-1} for Li$_{4.4}$Ge and Li$_{4.4}$Sn, respectively) are lower than that of Si

(4200 mAh g^{-1}), the concomitant volume change is accordingly lower during the Li insertion/extraction process. In addition, in contrast to the anisotropic swelling and surface fracture resulting from the anisotropic lithiation in crystalline Si, crystalline Ge exhibits isotropic lithiation and swelling behaviors. More importantly, the metallic characteristics are increasingly obvious from Si, Ge, and Sn in sequence, which is beneficial for electrode conduction and electron migration. For example, the room temperature Li-diffusion rate in Ge is 400 times faster than that in Si anode [142–144]. All of these properties make Ge and Sn durable, high-capacity, and high-rate anode candidates for next-generation LIBs [145]. Nonetheless, capacity degradation is still inevitable for these anodes, owing to the drastic pulverization of bulky particles and hence the electrical isolation problem from the current collector. To solve these problems, the dealloying technique has been extended to fabricate NPGE and NPSN to control volume expansion.

Building on the experience from NPSI electrodes, NPGE has been fabricated by the vapor phase dealloying process. Such anodes deliver stable cycling for 50 cycles with a cut-off discharge capacity of 500 mAh g^{-1} [146]. Liu et al. [147] also prepared NPGE by chemical dealloying Al–Ge in HCl. The ex situ SEM and corresponding X-ray diffraction (XRD) measurements verify this evolution process. The obtained NPGE shows a high reversible capacity (1191 mAh g^{-1} after 160 cycles at 160 mA g^{-1}) and good rate capability (767 mAh g^{-1} at 1600 mA g^{-1}).

In addition, the incorporation of one or more conductive substances into NPGE is an effective method to further enhance the Li storage performance. Hao et al. [148] designed NPGE/Cu$_3$Ge composites by dealloying the Ge–Cu–Al precursor alloy, which could simultaneously acquire rich porosity and an efficient Cu$_3$Ge buffer matrix.

This composite anode exhibits improved Li storage performance compared with pure NPGE anodes in terms of both the enhanced cycling stability and rate capability. It should be noted that most investigations tend to completely remove sacrificial elements when preparing desired porous electrodes to achieve high capacities. However, recent studies reveal selective etching could result in the formation of special alloy compounds that facilitate electron/ion transfer, tolerate volumetric changes, and promote the mechanical stability of the whole electrode [149–151]. For example, a 3D nanoporous Cu–Ge–Al anode exhibits interesting temperature-dependent Li storage performance [152]. Despite the great success, the relevant studies on Ge anodes are far fewer than those on Si. It is very likely that the performance of NPGE anodes could be further improved by integrating other optimizations such as carbon coating to solve the conduction problems in the electrodes.

Sn has a relatively low theoretical capacity among the three anodes, with a theoretical volume expansion up to 260% during cycling. By selectively etching Sn-Mg binary alloy in ammonium sulfate, Cook et al. [153] prepared NPSN powders composed of clustered Sn nanocrystals. Synchrotron transmission X-ray microscopy shows that the NPSN electrode with plentiful inner space could effectively accommodate volume expansion. Specifically, areal (~20%) and volume expansion (~30%) of NPSN after lithiation is much smaller than that of dense Sn (Fig. 4a). More importantly, NPSN particles could also contract back to the original sizes upon delithiation (Fig. 4b). Compared with the rapid deteriorating performance of dense Sn, the NPSN anode exhibits better cycling stability of 200 cycles (Fig. 4c) [154], although the large strain during lithiation/delithiation may still cause pore collapse and pore size reduction [155, 156].
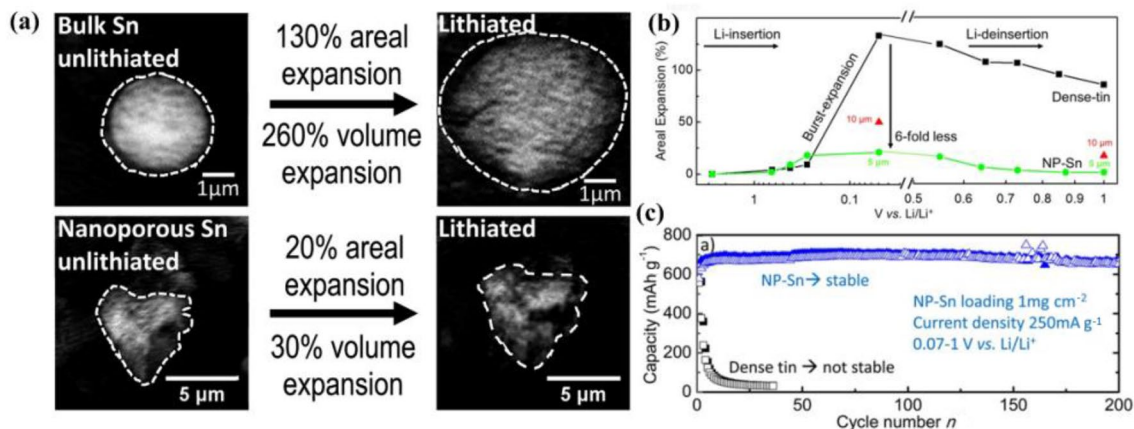

Fig. 4 **a** Transmission X-ray microscope absorption images of NPSN and dense Sn at initial and lithiated states. **b** Areal expansion of dense Sn and NPSN at different lithiation voltages. **c** Cycling performance comparison of NPSN and dense Sn at a current density of 250 mA g^{-1}. Reproduced with permission from Ref. [154]. Copyright 2017, American Chemical Society.

Thus, the incorporation of an extra matrix into Sn anodes has been proposed to generate a more ductile porous Sn–M alloy [157–159]. Liu et al. [158] reported the synthesis of a CuSn alloy by selectively etching Al from a ternary Cu–Sn–Al precursor, in which the active Sn is adhered to the conductive Cu framework. By tuning the dealloying time and media, the as-prepared nanoporous CuSn alloy displays good cycle stability (673 mAh g^{-1} after 50 cycles at 334 mA g^{-1}) and rate performance (566 mAh g^{-1} at 1670 mA g^{-1}) whereas the rigid Cu framework provides extra protection for the anodes as well as efficient electron pathways. It is noted that the inactive nature and high mass density of Cu would sacrifice the energy density of the overall electrode. Inspired by the investigations of the Li-alloyed metals as the buffer matrix [160–162], Fan et al. [86] designed a nanoporous SnO_xSb alloy by dealloying a Sn–Sb–Al ternary alloy to address this issue. The coexisting Sn and Sb elements, both as Li-active metals and frameworks, could react with Li by a two-step alloying process, which efficiently accommodate the volume expansion and electrode strain caused by lithiation/delithiation. Furthermore, tin phosphide (Sn_4P_3) with its high theoretical specific capacity (1255 mAh g^{-1}) and a lower cost has also attracted much attention as an anode for Li storage [163, 164]. It could reduce the risk of Li dendrites and enhance safety in case of overcharging owing to the higher potential than that of Li deposition [165]. For example, a porous Sn/Sn_4P_3 composite was fabricated by electrochemical dealloying of $Sn_{80}P_{20}$ alloy, followed by protective carbon coating via the pyrolysis of encapsulated dopamine, which indeed demonstrated improved overall performance upon cycling [166].

3.1.1.3 Nanoporous metal oxides (NPMO) Metal oxides have drawn considerable attention as anode materials for LIBs on account of their high theoretical capacities arising from a conversion mechanism [96, 167, 168]. Different from Li storage by intercalation or alloying chemistry, the conversion reaction involves the reversible reduction/oxidation of metal nanoparticles along with the formation/decomposition of Li_2O. Multiple-electron transfer could be involved in this process to provide exceptionally high capacities. The initial reduction by Li induces the generation of metal nanoparticles anchored into the Li_2O matrix, followed by the crystal structure destruction (amorphization of the lattice). The metal oxides are recovered during the reversible oxidation process as a consequence of Li_2O decomposition [156]. Similar to alloy anodes, particle swelling/shrinking is one of the most serious challenges for metal oxide anodes, which results in poor cycling life owing to the pulverization of the active materials [169, 170].

As mentioned above, dealloyed NPMs are efficient to regulate the volume variation of electrodes with plentiful nanopores and tunable morphology. Furthermore, the

traditional chemical/electrochemical dealloying process can also be applied for the production of nanostructured transition metal oxides. With alloys containing metals of different activities against alkaline solutions, the sacrificial atoms are selectively etched. Meanwhile, the remaining less-coordinated metal atoms are directly exposed to the OH$^-$ and oxygen-containing atmosphere. In such an alkaline environment, these active fresh metal sites would undergo spontaneous oxidation at the metal/electrolyte interface to form nanostructured metal oxides [171]. The structures of the as-obtained metal oxides can be readily controlled by selecting suitable precursor compositions and etching conditions.

Considering the versatility in fabricating various low-cost transition metals, a large variety of material systems have been studied to fabricate metal oxide anodes. It is worth noting that dealloyed metal compounds do not always evolve into the typical bicontinuous open structures upon the dissolution of alloy components, revealing that metal oxidation could significantly affect the rates of dealloying and surface diffusion. Nonetheless, the morphology and pore architectures are highly tunable in such oxide anodes to optimize favorable electrochemical performance in LIBs. For example, the compositions of NPMO can be easily controlled by retaining one or more metal species to fabricate single-element, bimetallic, or composite oxides. For oxides composed of a single-metal element, the Li storage mechanism can be described by the following reaction: $M_xO_y + 2yLi^+ + 2ye^- \leftrightarrow yLi_2O + xM$, where the capacity primarily depends on the number of electrons involved in the reaction. More electrons transferred upon the reduction/oxidation process offer higher capacities, but meanwhile the anode suffers from severer volume expansion.

The inverse spinel Fe_3O_4 exists in nature as the mineral magnetite. It is a promising anode owing to its high theoretical capacity (928 mAh g^{-1}), low cost, and environmental benignity [96]. Jia et al. [172] synthesized regular Fe_3O_4 octahedra by leaching out the Al from Al–Fe alloy ribbons consisting of α-Al(Fe) and $Al_{13}Fe_4$ phases in NaOH solutions. Galvanostatic charge–discharge cycling of the Fe_3O_4 octahedra in half cells with Li exhibited deteriorating electrochemical performance, which could be attributed to the intrinsic inferior electronic conductivity and the serious volume swelling during the conversion reaction process.

By introducing a conductive buffer matrix, such as Ag or Cu [173, 174], the capacity of the Fe_3O_4/Cu electrode can increase to 512.6 mAh g^{-1} at the 500th cycle, which is ascribed to a long-term activation process associated with the formation of a stable SEI layer and the typical nanoporous structure during the repeated lithiation and delithiation processes [41, 175]. Similarly, carbon materials with good electrical conductivity could also function as an efficient buffer matrix to maintain the structural integrity and suppress the aggregation of porous Fe_3O_4 during cycling,

finally enhancing the electrochemical activity and reversibility [176, 177]. Other successful examples within this scope include octahedral Mn_3O_4 [178], Mn_3O_4 octahedra@graphene [179], $Mn_3O_4/Ag@graphene$ [180], MnO_x microspheres [181], Co_3O_4 nanosheets [182], and Co_3O_4/Ag composites [183]. Apart from conversion-based metal oxide anodes, TiO_2 is a well-investigated intercalation/deintercalation anode material that exists in several polymorphs. During the lithiation process, the phase transformation could considerably affect the electrical and ionic conductivity [184]. Indeed, dealloyed TiO_2 from an Al–Ti binary alloy shows a 3D amorphous network structure with enhanced performance [185].

Bimetallic oxides are composed of one transition metal and another electrochemically active/inactive metal. Their conversion storage mechanism is slightly different from that of metal oxide anodes with a single component [186]. Benefitting from the complementary properties and synergetic activities arising from the substituted element, bimetallic oxides usually perform much better than simple oxides. A good example is cobalt-based bimetallic oxides with other low-cost transition metals such as Mn and Fe. Micro/nanostructured $MnCoO_x$ and $CoFe_2O_4$ nanoplates can be fabricated by dealloying the respective ternary alloys [187, 188]. EDX and XRD analyses prove the existence of mixed valence in the as-prepared samples. As expected, the $MnCoO_x$ microspheres and $CoFe_2O_4$ nanoplates deliver much better electrochemical performance than their corresponding pure metal oxides, since the novel nanostructure could accelerate the diffusion of electrolyte and offer extra space for conversion reactions. The fabrication of bimetallic oxides is greatly dependent on the atomic ratio between the different transition metal elements in the alloy precursors.

It is noted that the dealloyed product essentially retains the elemental proportion of the alloy precursors. Thus, it is easy to obtain desired compositions of oxide anodes simply by tuning the precursors. Owing to this advantage, the assembly of complex metal oxides has been achieved by dealloying multi-element alloy precursors. Nonetheless, it is difficult to accurately predict whether the dealloyed products will be a single phase or a composite. Additional caution should be used when designing alloy precursors to avoid the generation of bimetallic/trimetallic oxides with a pure phase. Other dealloying parameters such as etching conditions also have a critical effect on the structures and compositions of the final products. A common strategy to fabricate such nanocomposite anodes is the employment of ternary alloys with one active element. Hao et al. [189] reported a Co_3O_4/CuO nanocomposite with a controllable component by directly dealloying a $Co_{13}Cu_2Al_{85}$ precursor in NaOH solutions. The as-prepared sample exhibits a porous flower-like microstructure with abundant interconnected nanosheets.

The Co_3O_4/CuO nanocomposite displays high capacities along with excellent cycling stability owing to the innovative hierarchical architecture and the synergistic effect of two active electrode materials. A similar concept has been extended to other mixed metal oxide systems, including binary and even ternary mixed metal oxides [190–197].

Table 2 summaries the specific synthetic approach, morphology and electrochemical performance of selected dealloyed metal oxides. Most single-metal oxides with porous structure exhibit good electrochemical performance with a high utilization of theoretical capacity. With the incorporation of carbon buffers or metal matrixes, the rate capacity is greatly improved due to the enhanced electrical conductivity and structural integrity. Nanosheet-like metal oxides usually possess a better comprehensive performance than that of polyhedron-like metal oxides since their large specific surface area and interconnected porous structure facilitate electrolyte transfer and accelerate the ion diffusion kinetics. Besides, complex oxides composed of multiple metal ions demonstrate much better comprehensive Li storage properties compared to their single-metal counterparts. These good results are usually attributed to both componential and structural improvement. Indeed, diverse metallic ions show synergistic effects on electron and charge transport as well as structural stability. Further tailoring should focus on the incorporation of the conductive metal/carbon matrix to enhance rate performance.

3.1.1.4 Nanoporous metal sulfides (NPMSs) Compared to metal oxides, their sulfide counterparts usually possess higher electrical conductivity, enhanced interface stability, and more rapid ion diffusion kinetics during charge/discharge reactions [186, 198]. Meanwhile, they also have other advantages including low cost, low redox potential vs. Li/Li$^+$, and high theoretical capacity. Thus, metal sulfide anodes have attracted much attention as promising conversion-type electrodes in recent years. Wang et al. [199] synthesized a CuS nanowire-on-nanoplate network by a modified dealloying route. Specifically, a $Ti_{40}Cu_{60}$ ingot is sequentially etched in high-concentration H_2SO_4 solutions at 90 and 10 °C. The initial process at high temperature produces the CuS nanoplate matrix, while the following low-temperature treatment generates CuS nanowires on the nanoplates. With a hierarchical nanostructure and enhanced electrical conductivity, the obtained CuS anode displays an exceptional performance toward Li storage. It's expected that this simple processing strategy can be applied to the fabrication of different morphology and structures, such as mixed metal sulfides [200]. For example, Fe_3S_4/Co_9S_8 sulfide composites are fabricated through the hydrothermal sulfurization procedure. Compared with Fe_2O_3/CoO electrodes, the Fe_3S_4/Co_9S_8 sulfides exhibit much higher reversible capacity, superior cycling performance, and bet-

Table 2 Synthetic approach, morphology and electrochemical performance of selected dealloyed metal oxides. (Each box section includes two example studies. Left and right images correspond to the top and bottom studies in each box, respectively)
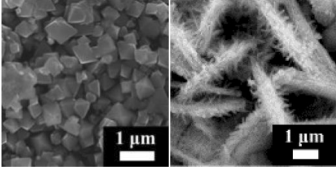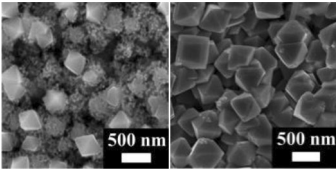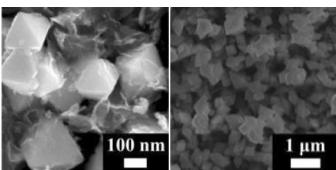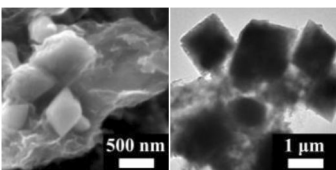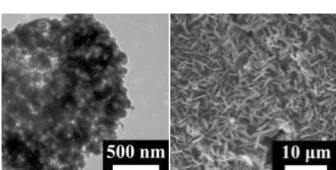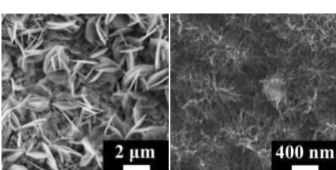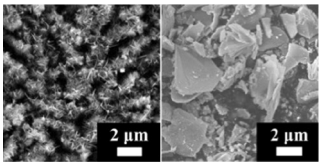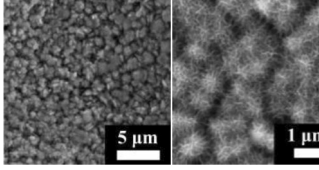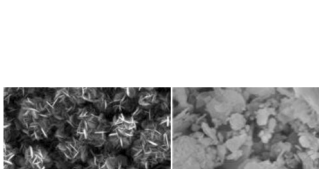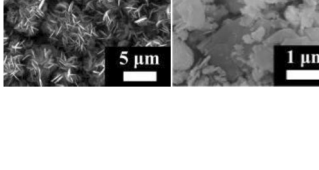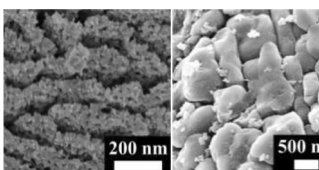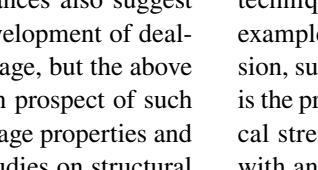
Mater.	Synthesis	Morphology	ICE	Cyclability (mAh g^{-1})	Rate (mAh g^{-1})	Ref.
Fe$_3$O$_4$ octahedra	Fe$_{15}$Al$_{85}$ alloy in NaOH		68.0%	365 at 50 mA g^{-1} after 38 cycles	–	[172]
Fe$_3$O$_4$/Ag material	Fe$_{12}$Ag$_3$Al$_{85}$ alloy in NaOH		72.6%	613.2 at 1000 mA g^{-1} after 500 cycles	310 at 3 A g^{-1}	[173]
Fe$_3$O$_4$/Cu nanocomposites	Fe$_{12}$Cu$_4$Al$_{84}$ alloy in NaOH		–	512.6 at 1000 mA g^{-1} after 500 cycles	505.8 at 1 A g^{-1}	[174]
Fe$_3$O$_4$ octahedra @ graphene	Fe$_{10}$Al$_{90}$ alloy in NaOH and GO		65.0%	523.2 at 1000 mA g^{-1} after 300 cycles	350.5 at 2 A g^{-1}	[176]
Fe$_3$O$_4$/Cu @graphene	Fe$_{12}$Cu$_3$Al$_{85}$ alloy in NaOH and GO		56%	442.6 at 2000 mA g^{-1} after 800 cycles	~350 at 3 A g^{-1}	[177]
Mn$_3$O$_4$ octahedra	Mn$_{15}$Al$_{85}$ alloy in NaOH		57.3%	638 at 300 mA g^{-1} after 500 cycles	240 at 1.5 A g^{-1}	[178]
Mn$_3$O$_4$ @graphene	Mn$_{10}$Al$_{90}$ alloy in NaOH and GO		52.0%	625.3 at 1000 mA g^{-1} after 200 cycles	430 at 3 A g^{-1}	[179]
Mn$_3$O$_4$/Ag @graphene	Mn$_9$Ag$_1$Al$_{90}$ alloy in NaOH and GO		62.1%	763.5 at 1000 mA g^{-1} after 200 cycles	522 at 3 A g^{-1}	[180]
Porous MnO$_x$ microspheres	Mn$_5$Al$_{95}$ alloy in H$_2$O$_2$–NaOH		68.0%	757 at 500 mA g^{-1} after 100 cycles	420 at 1 A g^{-1}	[181]
Co$_3$O$_4$ nanosheets	Co$_{15}$Al$_{85}$ alloy in NaOH		–	630 at 600 mA g^{-1} after 50 cycles	470 at 1 A g^{-1}	[182]
Co$_3$O$_4$/Ag nanosheets	Co$_{12}$Ag$_3$Al$_{85}$ alloy in NaOH		79.7%	467.3 at 1000 mA g^{-1} after 1000 cycles	390 at 3 A g^{-1}	[183]
TiO$_2$ nanowires	Ti$_{15}$Al$_{85}$ alloy in NaOH		72.0%	215 at 500 mA g^{-1} after 500 cycles	175 at 1 A g^{-1}	[185]

Table 2 (continued)

Mater.	Synthesis	Morphology	ICE	Cyclability (mAh g^{-1})	Rate (mAh g^{-1})	Ref.
Co$_3$O$_4$/CuO composites	Co$_{13}$Cu$_2$Al$_{85}$ alloy in NaOH		75.6%	~ 600 at 1000 mA g^{-1} after 400 cycles	500 at 2.5 A g^{-1}	[189]
TiO$_2$/Fe$_2$O$_3$ composites	Fe$_4$Ti$_2$Al$_{94}$ alloy in NaOH		60.4%	838.8 at 200 mA g^{-1} after 400 cycles	339 at 2 A g^{-1}	[190]
TiO$_2$/Co$_3$O$_4$ composites	Ti$_7$Co$_3$Al$_{90}$ alloy in NaOH		50.2%	180 at 300 mA g^{-1} after 500 cycles	152 at 1 A g^{-1}	[191]
TiO$_2$/MoO$_x$ composites	Ti$_{10.5}$Mo$_{4.5}$Al$_{85}$ alloy in NaOH		47.3%	321.6 at 300 mA g^{-1} after 500 cycles	167 at 1 A g^{-1}	[192]
Mn$_3$O$_4$/Fe$_3$O$_4$ composites	Mn$_5$Fe$_5$Al$_{90}$ alloy in NaOH		66.2%	1040 at 300 mA g^{-1} after 200 cycles	321 at 1.5 A g^{-1}	[193]
Fe$_3$O$_4$/NiFe$_2$O$_4$ composites	Fe$_{12}$Ni$_2$Al$_{86}$ alloy in NaOH		–	~ 500 at 200 mA g^{-1} after 750 cycles	–	[194]
GeO$_2$/Cu/Cu$_2$O composites	Cu$_{17}$Ge$_{1.3}$Al$_{81.7}$ alloy in NaOH		83.5%	504 at 1600 mA g^{-1} after 150 cycles	552 at 3.2 A g^{-1}	[195]
CoNi/CoO/NiO composites	Ni$_{13.4}$Co$_{14.6}$Al$_{72}$ alloy in NaOH		73.0%	578 at 200 mA g^{-1} after 600 cycles	260 at 2 A g^{-1}	[196]

ter rate capability. The lower EIS resistances also suggest enhanced electrical conductivity. The development of dealloyed metal sulfides is still on the early stage, but the above results highlight the attractive application prospect of such anode candidates with unique energy storage properties and facile fabrication procedures. In-depth studies on structural and compositional optimization should be implemented to further promote the applications of the dealloyed metal sulfides in future.

In summary, nanostructured alloy and oxide/sulfide anodes in LIBs could promote electrochemical performance by efficiently accommodating volume variation during cycling. The practical behaviors of such anodes are highly correlated to the design of the morphology, structures, and compositions. The most prominent merit of nanoporous materials is the rich selectivity of precursors and the highly tunable dealloying process, which provide a reliable technique to design products with desired electrodes. For example, for certain anodes with enormous volume expansion, such as Si and Ge, the fabrication of sufficient porosity is the primary task. In terms of Sn anodes that have mechanical strength problems, the design of reinforced structures with an extra matrix seems to be more important to inhibit the rapid capacity fading. The incorporation of binary or more complicated metals in nanostructured alloy/oxide anodes is challenging for conventional synthetic routes. However, this issue can be easily solved by rational design through the dealloying method. Furthermore, post-treatments including carbon decoration as a conductive coating or a buffer matrix (graphene, carbon fibers, or amorphous carbon) can be readily achieved with dealloyed samples as well, which ensures that dealloying is a very competitive technology to fabricate high-energy anodes for LIBs.
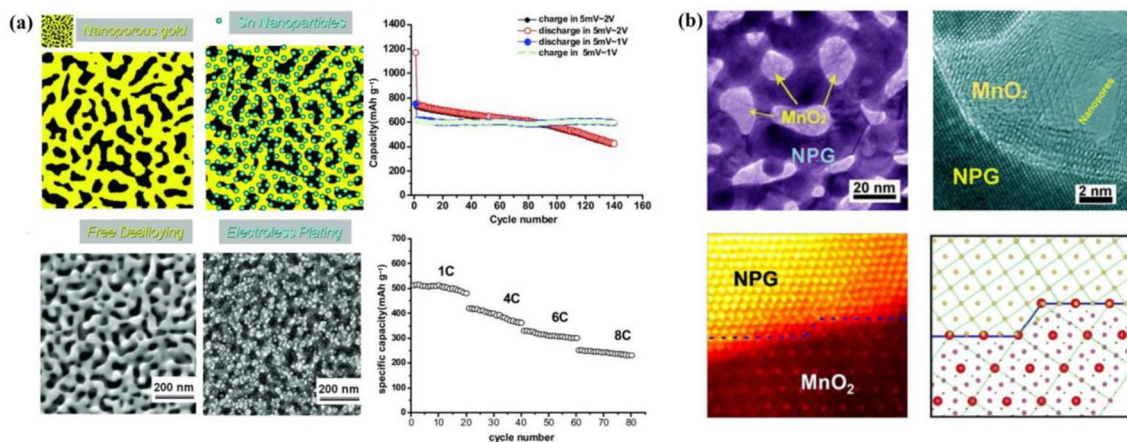
Fig. 5 a Synthetic scheme and corresponding SEM images of an NPG substrate and supported nanocrystalline Sn; cycling performance at 0.1 C with different voltage windows; rate capacity between 0.005 and 1.0 V. Reproduced with permission from Ref. [90]. Copyright 2011, Wiley–VCH. **b** TEM and HRTEM images of an NPG/ MnO$_2$ composite; high-angle annular dark-field scanning transmission electron microscopy (HAADF-STEM) images of the gold/MnO$_2$ interface; the atomic model of the NPG/MnO$_2$ interface. Reproduced with permission from Ref [203]. Copyright 2015, Royal Society of Chemistry
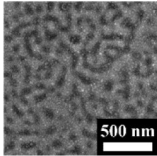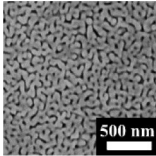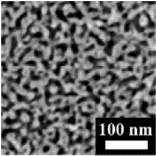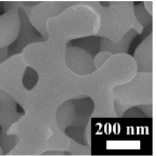
3.1.2 Nanoporous scaffolds

In consideration of their high electrical conductivity and 3D bicontinuous structure, dealloyed materials can also function as novel scaffolds to anchor electrochemically active species including metals, alloys, metal compounds, and even insertion materials. During the charge/discharge process, scaffolds accelerate electron/charge transfer and accommodate volume expansion to enhance the Li storage

properties of the composite electrodes. In this section, we introduce the application of dealloyed nanoporous materials as scaffolds/substrates in LIBs.

3.1.2.1 Nanoporous gold (NPG) As the most studied model, NPG has high electrical conductivity, robust mechanical rigidity, high corrosion resistance, and rich surface chemistry for further functionalization. NPG has been widely used in the energy storage and conversion fields, such as hetero-

Table 3 Synthetic approach, morphology, and electrochemical performance of selected NPG-based composites (all the capacity values have had the Au contributions subtracted)

Materials	3D NPG-supported nanocrystalline Sn	3D bicontinuous Au/amorphous–Ge thin films	NPG/MnO$_2$ composites	NPG/TiO$_2$ core/shell samples
Synthesis approach	Chemically dealloying and chemical reduction	Chemically dealloying and thermal evaporation technique	Chemically dealloying and potential dynamic electroplating method	Chemically dealloying and atomic layer deposition
Morphology				
Au content	20%	60%	20%	–
Theoretical specific capacity (mAh g^{-1})	992	1600	1230	335
Voltage window (V)	0.005–1.0	0.005–1.2	0.25–3.2	1.0–3.0
ICE	82%	70%	63%	73.2%
Cyclability (mAh g^{-1})	620 at 100 mA g^{-1} after 140 cycles	1066 at 320 mA g^{-1} after 100 cycles	650 at 50 mA g^{-1} after 240 cycles	~175 at 1680 mA g^{-1} after 500 cycles
Rate capability (mAh g^{-1})	260 at 8 A g^{-1}	360 at 96 A g^{-1}	400 at 1.5 A g^{-1}	~125 at 8.4 A g^{-1}
Reference	[48]	[114]	[115]	[116]

geneous catalysis, electrocatalysis, and fuel cell applications [2, 8, 201]. It has also been introduced in LIBs as a novel scaffold to support high-capacity active materials such as metal/alloys and metal oxides.

Yu et al. [90] first reported NPG-supported Sn-based nanocomposites as high-performance anodes for LIBs (Fig. 5a). Sn nanoparticles are plated on the NPG surface to fabricate the Sn/NPC composite. When cycled in the optimum voltage window of 0.005–1.0 V, the as-prepared anode exhibits high reversible capacities and good rate performance. The superior performance is ascribed to the innovative Sn/NPG nanostructures, which offer adequate void space to tolerate significant volume variations and enable a large contact area between the electrode and the electrolyte to accelerate electron/charge transfer. A similar concept was also applied to Ge on an NPG matrix for high-performance LIB anode [202], where Ge overlayers are deposited onto NPG substrates by thermal evaporation.

The decoration of metal oxides onto the surface of NPG can be achieved by electroplating followed by an annealing treatment. Guo et al. [203] fabricated NPG/MnO_2 hybrid anodes by such a route, where MnO_2 nanocrystals are grown epitaxially on the Au ligament surface and uniformly distributed within the network without changing the nanoporosity (Fig. 5b). Ye et al. [204] designed 3D NPG/TiO_2 core/shell electrodes and systematically studied the effects of their length scale on the electrochemical performance. It is found that a thinner TiO_2 coating could reduce the Li^+ diffusion pathway, enhance the Li^+ solid solubility, and minimize the voltage drop across the electrode/electrolyte interface. The optimized electrode shows supercapacitive power density and high energy densities.

Table 3 summarizes the synthetic approach, morphology, and electrochemical performance of these NPG-based composites. Because gold is electrochemically very stable, its modification by active materials is readily manageable, such as by chemical reduction, thermal evaporation, electroplating, and atomic layer deposition (ALD). In most cases, the bicontinuous structure of NPG can be well-maintained after the decoration treatment. Owing to the excellent electron transfer kinetics of NPG, the composite anodes tend to exhibit nearly perfect capacity as well as improved rate performance if only active materials are counted. Moreover, rigid NPG skeletons with sufficient nanoporosity accelerate ion diffusion and accommodate volume expansion. Thus, the multifunctional NPG is an ideal model substrate for high-capacity alloy/oxide anodes in LIBs. The only concern for its practical application is the high cost of Au. Nonetheless, NPG is a powerful and reliable material to study the structure-performance correlation considering the well-defined and elegant network topology, or can be used for high-performance on-chip micro-batteries.

3.1.2.2 Nanoporous copper (NPC) As mentioned above, the high price undoubtedly restricts the commercial applications of NPG. Thus, low-cost NPC substrates with similar physical and chemical properties have been developed as an alternative. Among the commonly used, cost-effective metals, copper has excellent ductility and electrical conductivity, which makes it feasible to fabricate nanoporous substrates for LIBs. Here, we introduce the fabrication of NPC-based electrodes and their electrochemical performance in LIBs. Metal-coated NPC, mainly Sn-coated NPC, is first discussed based on different NPC fabrication methods,
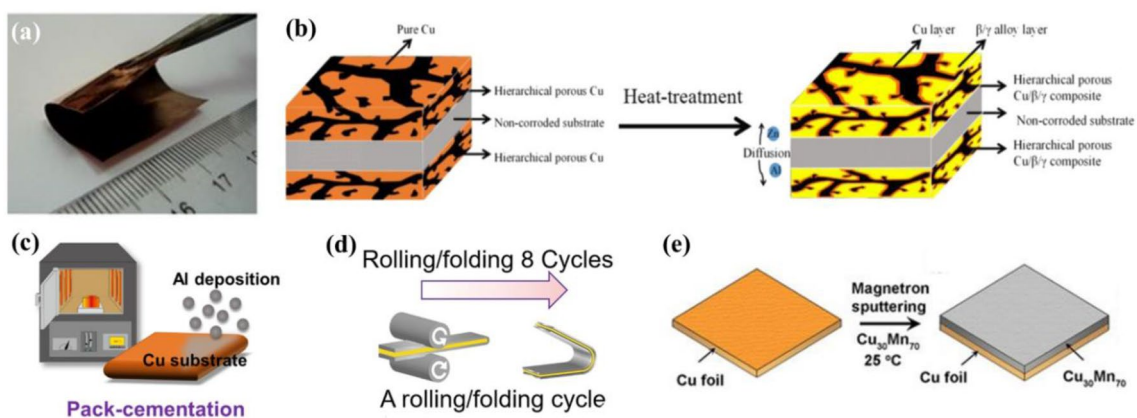
Fig. 6 Self-supporting NPC-based composites with high mechanical strength. **a** Photograph of a flexible NPG/MnO_2 hybrid bulk electrode (2 cm × 3 cm). Reproduced with permission from Ref. [211]. Copyright 2013, Nature Publishing Group. Schematic diagrams of the proposed novel synthesis methods to create self-supporting NPC. **b** Partial dealloying and heat treatment method; reproduced with permission from Ref. [209]. Copyright 2018, American Chemical Society. **c** Pack-cementation method; reproduced with permission from Ref. [210]. Copyright 2019, Elsevier. **d** Rolling/folding method; Reproduced with permission from Ref [212]. Copyright 2019, Elsevier. **e** Magnetron sputtering method. Reproduced with permission from Ref. [211]. Copyright 2013, Nature Publishing Group

including structural and componental optimization. Then, a series of NPC-supported copper oxides and several other metal oxides are also discussed to show the unique functions of NPC scaffolds.

Upon structure optimization, NPC could accelerate the ion transport, enhance the electronic conductivity, and alleviate large mechanical strains, thus enhancing the cycling stability of Sn anodes. Zhang et al. [91] first prepared NPC by a simple one-step dealloying of Al–Cu in NaOH solutions. Based on the Al–Cu phase diagram and experimental results, it is speculated the $CuAl_2$ phase first crystallizes into an island-like structure, and then the mixed Al and $CuAl_2$ phases precipitate together into a lamella-like structure. When Al is completely etched out, several island-like structures are uniformly distributed in the periodic structure of alternating channels and walls. After the electroless plating of Sn on the NPC, no morphology variation is evident. Compared with Sn-coated planar Cu foil (Sn@CF), the obtained Sn@NPC anode exhibits higher capacity retention and better CE after the initial several cycles. Similarly, Liu et al. [205] reported monodispersed Sn nanoparticles upon monolithic 3D NPC by dealloying Al–Cu binary alloy sheets in HCl solution and a subsequent low-temperature electroless plating technique. To further alleviate the serious volume expansion of Sn during the lithiation process, ultrafine Sn–Ni alloy nanoparticles could be deposited on the NPC by chemical dealloying of the as-cast Al–Cu alloy in HCl followed by pulsed electrodeposition [206]. The obtained electrode possesses a large porous skeleton similar to that of the NPC substrate. Moreover, Ni and Sn are uniformly distributed throughout the whole 3D NPC substrate, which further prevents cracking or detaching of active materials from the current collector during long-term cycling.
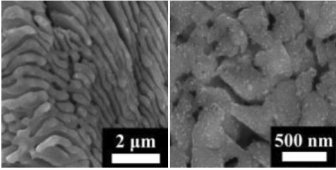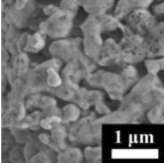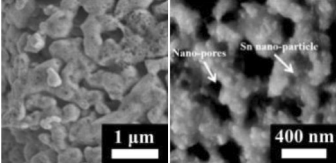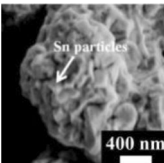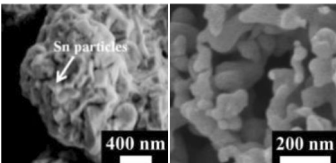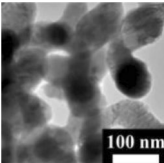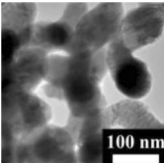
Although the hierarchical nanoporous structure can partially accommodate volume expansion, pure NPC is brittle as a free-standing substrate in LIBs. Meanwhile, it would possibly result in the generation of cracks and the collapse of the porous structure upon cycling. To further enhance the practicability and cycling stability, it is necessary to construct robust substrates with higher ligament hardness by component optimization (Fig. 6a). For example, a 3D NPC-supported Sn thin film with a sandwich-type structure was prepared by the partial chemical dealloying of an Al–Cu alloy [207]. By controlling the dealloying time, a uniform porous layer with complete Al removal could be formed on the outmost surface, while the central alloy layer with the Al–Cu phase is retained, thus resulting in a tri-layer microstructure composed of alternating porous and alloy layers. After electroless plating, a uniform and smooth Sn layer covers the surface and the interior of the bilateral porous structure. Meanwhile, the sandwich-type morphology with an open bicontinuous nanoporous network could be well-preserved in the resulting anode. Luo et al. [208] fabricated

NPC layers by a molten-metal infiltration method using spherical SiO_2 as space holder and subsequent dealloying in HCl. Next, particle-like Sn was uniformly deposited on the surface of the resulting 3D bimodal porous NPC substrate by electroless plating. Considering that a Cu–Zn–Al ternary alloy in the β or γ phase possesses a satisfactory conductivity and a higher hardness than pure Cu, Luo et al. [209] also fabricated a hierarchical porous Cu-based composite consisting of a layer of nanocrystalline Cu, β-(CuZn), and γ-(CuAl) phases by further heat treatment after chemical dealloying of Cu–Zn–Al (Fig. 6b). Through the electroless plating of Sn, particle-like Sn is uniformly distributed on the surface of porous Cu. In order to improve the mechanical properties of NPC, Han et al. [210] reported the innovative pack-cementation process for the precursor preparation to avoid the formation of metal powders after dealloying (Fig. 6c). Specifically, a Cu–Al alloy precursor could be obtained through the coating of a uniform thin Al layer onto the as-prepared Cu foil using a pack-cementation method and NPC could be obtained by leaching Al. After Sn coating, the resulting integrated anode exhibits a four-fold higher capacity than that of traditional graphite and better cycle stability during the charging/discharging process.

It is known that Cu has little activity with lithium to form Li–Cu alloys, but its oxides including Cu_2O and CuO have been extensively studied as high-capacity anodes [156]. The preparation of CuO@NPC is straightforward by thermal treatment of NPC in the presence of oxygen. Liu et al. [79] first reported 3D NPC-supported copper oxide ($Cu_2O@$NPC) composites. During the in situ thermal oxidation process, uniform Cu_2O layers are formed on the NPC surface. Nanoporous CuO/Cu hybrid electrodes are obtained either by ball milling NPC in water or by electrochemical oxidation [213, 214]. With the improved electrical conductivity, they exhibit stable cycling performance and good rate capability. By combining rolling/folding technology with the dealloying (Fig. 6d), Liu et al. [212] fabricated a novel NPC substrate with high mechanical stability. After single-side oxidation and dehydration, nanostructured CuO nanoflake arrays with a highly open microstructure on the NPC substrate are obtained. The above examples suggest that $Cu_2O/$CuO coating on NPC can be readily achieved by in situ oxidation, during which the high adhesive force between CuO and the NPC substrate maintains the structural stability and enhances the electrical conductivity at the interface.

Depending on the specific preparation process, the as-made CuO electrodes usually display different morphologies, such as uniform layer coating and nanoflake array distribution. Both structures effectively tolerate strain and stress during cycles, and the NPC skeleton provides excellent Li-ion and electron transfer pathways. Considering the low-cost fabrication, notable structural stability, and enhanced charge transfer processes, CuO/NPC hybrid anodes with

Table 4 Synthetic approach, morphology, and electrochemical performance of selected NPC-based composites (Each box section includes two example studies. Left and right images correspond to the top and bottom studies in each box, respectively)

Mater.	Synthesis	Morphology	ICE	Cyclability (mAh g^{-1})	Ref.
Sn-film coated on NPC	Dealloying Al–Cu alloy in NaOH solutions and electroless plating		~70%	~0.62 at 150 mA g^{-1} after 50 cycles	[91]
Sn nanoparticles on NPC	Dealloying Al–Cu alloy in HCl solutions and electroless plating		–	0.254 at 0.1 mA cm^{-2} after 500 cycles	[205]
Sn–Ni particles on NPC	Dealloying Al–Cu alloy in HCl solutions and pulse electrodeposition		51%	0.25 at 0.1 mA cm^{-2} after 200 cycles	[206]
Sn on NPC with sphere channels	Dealloying Cu–Al–Mn by in HCl solutions and electroless plating		75.2%	1.29 at 500 mA cm^{-2} after 100 cycles	[208]
Sn on NPC with Cu/β/γ phases	Dealloying Cu–Zn–Al in HCl solutions and electroless plating		~85%	0.93 at 0.1 mA cm^{-2} after 100 cycles	[209]
Sn-coated hierarchical Cu	Dealloying Cu–Al alloy by pack-cementation in HCl and electroless plating		77.3%	7.4 at 1000 mA cm^{-2} after 20 cycles	[210]
3D NPC@Cu$_2$O	Dealloying Al–Cu in NaOH and in situ thermal oxidation		69%	1.45 at 0.175 mA cm^{-2} after 120 cycles	[79]

superior electrochemical performance hold great promise for advanced LIBs.

Magnetron sputtering is also a promising technology to fabricate alloy precursors (Fig. 6e). After removing the active phase, the as-dealloyed NPC is seamlessly integrated with the robust solid Cu matrix, showing typical nanoporous morphology and excellent free-standing properties. Other metal oxides such as MnO_2 and SnO_2 can be deposited on NPC scaffolds to fabricate composite electrodes [211]. Both of them can deliver high energy at ultrahigh rates with superior stability. Qualitative analyses of CV curves at different scan rates show that capacitance contribution plays an important role in the high-rate capacity. Meanwhile, the innovative integration of solid and nanoporous hybrid architecture could effectively reduce the primary resistance, and density functional theory (DFT) calculations demonstrate that the strong binding energy between Cu/SnO_2 coherent interfaces greatly enhances the electron transfer. Moreover, $Li_4Ti_5O_{12}$ has been encapsulated as a zero-strain insertion

anode into interdigitated NPC by chemical deposition and annealing treatment [215]. The bicontinuous Cu/$Li_4Ti_5O_{12}$ nanocomposite exhibits significantly promoted rate capability. The procedures to fabricate heterogeneous NPC anodes are relatively complicated. However, the highly conductive NPC network offers great opportunity for high-capacity anodes compared with conventional Cu current collectors. It is one of the most promising nanoporous candidates to be utilized in practical Li-ion cells.

Table 4 summaries the synthetic approach, morphology and electrochemical performance of NPC-based composites. In general, Sn is the most used active material that can be readily incorporated with NPC substrates by electroless plating or electrodeposition. These NPC/Sn electrodes show much promoted electrochemical performance, indicating a more affordable NPC is a good alternative to NPG. Nonetheless, the brittle ligaments of pure NPC usually fail to endure large stress from volume expansion on long-term cycling. Some progress has been made to solve this issue by
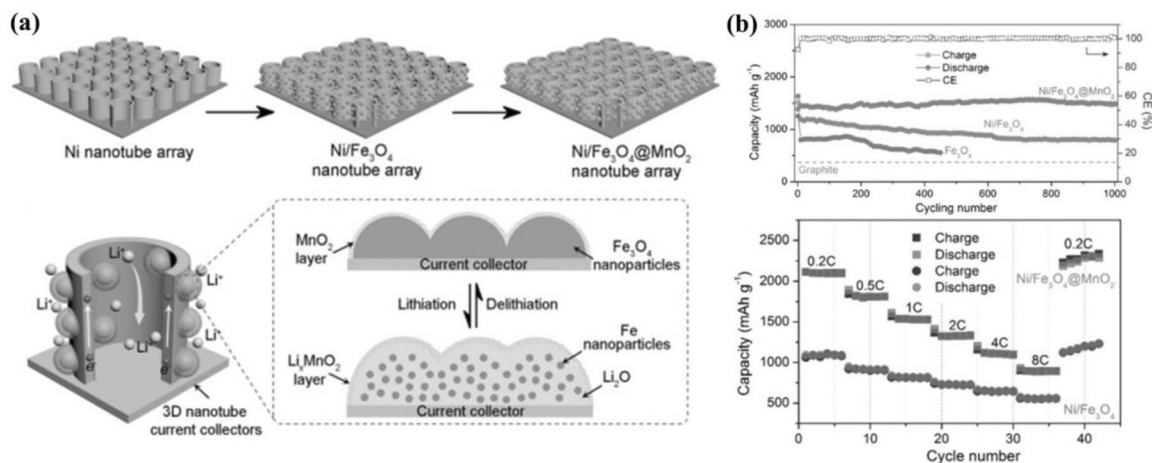
Fig. 7 a Schematics of the fabrication process and the lithiation/delithiation process of a Ni/Fe$_3$O$_4$@MnO$_2$ NTA hybrid electrode. **b** Capacity retention and CE of a Ni/Fe$_3$O$_4$@MnO$_2$ NTA electrode in a long-term cycling test at 1 A g^{-1}; comparison of rate capabilities from 0.2 to 8 C. Reproduced with permission from Ref [217]. Copyright 2017, Wiley–VCH

implementing novel electrode structural designs or introducing alloy phases to reinforce the structures [121, 122, 125].

3.1.2.3 Nanoporous nickel (NPN) Nanoporous nickel (NPN) is another alternative to the NPG scaffold, because of its similar physical and chemical properties to those of copper. Typically, NPN could be obtained by dealloying Ni–Al alloys in NaOH solutions, a standard Raney catalyst processing. The NiO layer was in situ formed on the surface of NPN upon exposure to air and water, thus generating a core/shell Ni/NiO nanoporous structure [216]. When used as an anode in LIBs, it shows excellent Li storage performance during the initial several cycles, but severe capacity deterioration to a negligible level after 150 cycles. The poor cycling performance is ascribed to the detachment of the active components from current collectors and the unstable SEI generation on the electrode surface. The former leads to the mechanical and conductive failure of electrodes, and the latter not only consumes the electrolyte but also impedes ion/electron transport.

To tackle the durability problem, Li et al. [217] reported Li-ion breathable hybrid electrodes with a unique 3D architecture (Fig. 7a). Cu-Ni alloy films are first electrodeposited on Ni foil and then the Cu component is electrochemically dealloyed in the same electrolyte to fabricate Ni nanotube arrays (NTAs). Subsequently, Fe$_3$O$_4$ nanoparticles encapsulated by the birnessite-type MnO$_2$ (δ-MnO$_2$) film are uniformly anchored onto the NTAs through the consecutive electroreduction of Fe^{3+} and Mn^{7+}. SEM characterization shows that high-density tube-like NTAs are vertically aligned on the Ni foil. Fe$_3$O$_4$ nanoparticles uniformly grow along internal and external walls of the nanotubes and are then further coated by δ-MnO$_2$ layers with much smoother surface. Structural and compositional characterizations

including HRTEM, XRD and X-ray photoelectron spectroscopy (XPS) further confirm the successful fabrication of hybrid electrodes. The Ni/Fe$_3$O$_4$@MnO$_2$ anode in LIBs exhibits a reversible capacity 1450 mAh g^{-1} at 1 A g^{-1} after 1000 cycles and a high-rate performance of 890 mAh g^{-1} at 8 A g^{-1} (Fig. 7b). The excellent electrochemical durability is also evidenced by the similar electrode morphologies before and after cycling.

Compared to NPC, studies on NPN are still in the very early stage. It is generally accepted that Ni has more environmental issues than Cu during the electrode fabrication process. More importantly, the high reactivity of Ni at moderate potentials might limit its applications as anode current collectors. Nevertheless, Ni-based porous substrates including Ni foam have been widely used in laboratory research. The simple fabrication process and the tunable porous architectures make NPN highly competitive among various porous Ni substrates.

3.1.2.4 Nanoporous graphene (NPGR) Most metallic porous frameworks have a notable electron transfer capability, but their high mass density results in substantial compromise in the energy density of the overall electrodes. In contrast, lightweight carbonaceous materials are promising candidates from the viewpoint of practical applications, especially those highly conductive carbons such as graphene. Graphene has been extensively explored in energy storage devices, owing to its high electrical conductivity, intrinsic electrochemical activity, low mass density, and excellent mechanical flexibility. NPGR can also be fabricated by CVD using dealloyed NPMs as scaffolds. For example, NPN obtained by etching a Ni–Mn alloy is utilized as a both catalyst and porous template for the CVD growth of graphene with pyridine as the precursor. After dissolving
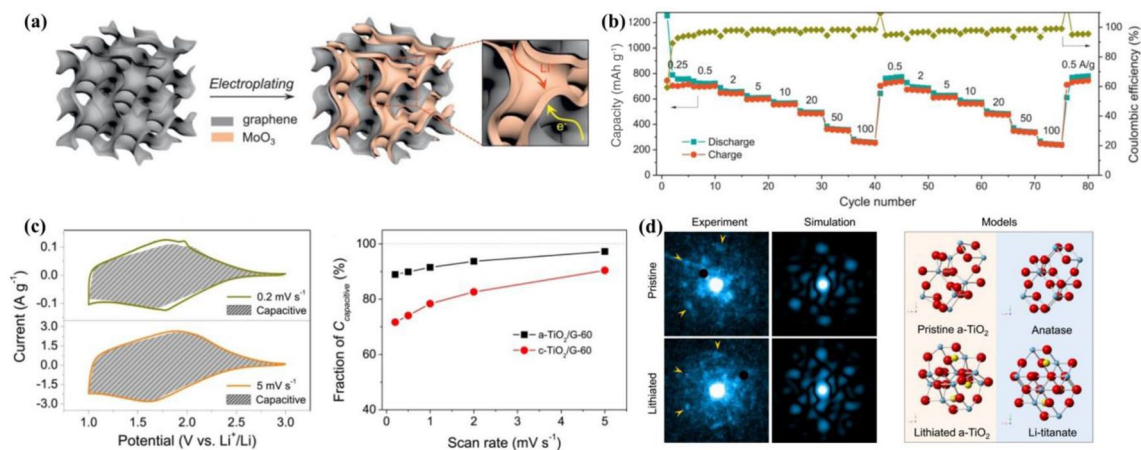
Fig. 8 **a** Fabrication of the bilayer MoO_3/graphene composite. **b** Rate performance of the nanoporous MoO_3/graphene electrode. Reproduced with permission from Ref. [218]. Copyright 2018, Elsevier. **c** CV curves collected at 0.2 and 5 mV s^{-1} with hatched portions showing the capacitive contributions and capacitive contribution analysis with a-TiO$_2$ and c-TiO$_2$. **d** Representative experimental ABED and simulated ABED patterns for pristine and lithiated a-TiO$_2$; local structure models of pristine and lithiated a-TiO$_2$ and c-TiO$_2$. Reproduced with permission from Ref. [219]. Copyright 2018, Elsevier

the NPN substrates in HCl, 3D bicontinuous NPGR sheets are fabricated, possessing inverse porous features of the dealloyed NPMs [84, 85].

Han et al. [218] fabricated 3D bilayer electrodes in LIBs by electrochemically plating thin molybdenum oxide (MoO_3) stacking films on the NPGR. Figure 8a shows the preparation procedure and porous architecture. After pulsed voltage deposition, a uniform and quasi-continuous MoO_3 film is formed on the internal surface of the NPGR with well-preserved 3D nanoporosity. By controlling the MoO_3 content based on the cycle number of pulsed voltage deposition, the optimized anode exhibits excellent rate performance (Fig. 8b). The cycling life and rate behaviors are comparable to those of electrochemical supercapacitors, but the capacity is over ten times higher than that of conventional supercapacitors. This exceptional performance is most likely attributable to the novel bilayer structure of the 3D nanoporous MoO_3/graphene composite, which could retain the active material in a thin-film structure tightly bonded with the highly conductive graphene, even at a high loading level.

Similarly, amorphous titanium dioxide (a-TiO$_2$) was fabricated by ALD to grow on the surface of dealloyed NPGR [219]. The obtained a-TiO$_2$@NPGR could also deliver a large capacity at high rates by the intercalation pseudocapacitive mechanism (Fig. 8c). Further studies reveal anatase-like local structures in a-TiO$_2$ are truly functional for Li-intercalation by local phase transformation. Extended X-ray absorption fine structure (EXAFS) analysis confirms a-TiO$_2$ had a similar lithiation-induced phase transformation as crystalline-TiO$_2$ (c-TiO$_2$). The local ordering in both pristine and lithiated a-TiO$_2$ is also verified by the distinct

symmetric spots, and the Angstrom-beam electron diffraction (ABED) patterns match well with the simulated ones (Fig. 8d). Thus, a-TiO$_2$ and c-TiO$_2$ have similar Li storage mechanisms at the unit-cell level, while the local structure variation in a-TiO$_2$ with pseudocapacitive behaviors could not cause much constraint on the overall charge storage kinetics. In general, crystalline or amorphous metal oxides based on dealloyed 3D bicontinuous NPGR substrates can deliver high energy and power densities. Compared with 2D graphene, 3D NPGR with its preserved large specific surface area and high electric conductivity allows sufficient ion and current delivery for rapid electrode reactions. These investigations show that NPGR could be an efficient scaffold for other active materials to realize high-performance graphene-based porous electrodes in LIBs.

3.2 Applications in LMBs

Large demand for future energy storage urges on-going scientific and technological breakthroughs beyond LIBs. Among various alternatives, lithium metal batteries (LMBs) based on lithium metal anodes have attracted much attention. Lithium metal is a high-energy anode with ultrahigh capacity (3860 mAh g^{-1}) and the most negative electrochemical potential (− 3.04 V versus standard hydrogen electrode) [220]. Combined with high-capacity oxygen or sulfur cathodes, the Li–O$_2$ and Li–S batteries are of great interests due to their high theoretical energy densities, low costs and high availability. In the past decade, great progress has been achieved with these new systems [221, 222], but several issues still exist before their

commercialization. For LOBs, the high thermodynamic stability and the intrinsic insulating character of discharge products could cause the low round-trip efficiency and the surge of polarization during cycles. In terms of Li–S batteries, large sulfur volume expansion and the serious polysulfide shuttle significantly affect the cycling and rate performance. At the anode side, Li metal faces crucial challenges of progressive corrosion and dendrite morphology on cycling. Nanoporous materials have been successfully applied to both oxygen/sulfide cathodes and lithium anodes, with the aim to solve the above issues. In this context, such substrates are first discussed to prepare advanced LOB and Li–S cathodes. Next, the fabrication of nanoporous current collectors, especially NPC-based materials, is summarized with respect to the newly emerging research area of Li-metal anode protection.

3.2.1 Nanoporous substrates for oxygen cathodes in LOBs

LOBs hold promise as a high-energy system owing to their large theoretical and estimated energy densities. The dominant cathode reactions [$2Li^+ + 2e^- + O_2 \leftrightarrow Li_2O_2$ ($E_0 = 2.96$ V vs. Li/Li$^+$)] are based on the formation/

decomposition of Li_2O_2 upon the discharge/charge process [222–224]. Typical configurations of aprotic LOBs include the air-breathing cathode, the non-aqueous electrolyte, and the Li-metal anode [225–227]. Tremendous efforts have been devoted to exploring new cathode materials with great success. Critical challenges include high discharge/charge overpotentials and severe capacity loss in the course of cycling, which mainly result from cathode degradation [228]. A durable substrate against electrolytes and external corrosion is vital for long-term cycling of LOBs. Other fundamental properties of a good substrate include high electrical conductivity and high surface area to maximize catalytic activities and hence the conversion kinetics of oxygen in the cathodes. Dealloyed NPMs including NPG, NPN, and Ti (NPT) have attracted increasing attention as promising air-breathing cathodes, owing to the following advantages. First, 3D NPMs with natural chemical affinity for oxides can dramatically enhance the electron transfer of insulating oxides in composite electrodes. Second, their intrinsic high catalytic efficiency and electrochemical/mechanical stability facilitate the reversible formation/decomposition of the Li_2O_2 product. Third, the open framework structures can accelerate electrolyte penetration, assure the arrival of

Fig. 9 DEMS of the NPG cathode during **a** discharge and **b** charge in 0.1 M LiClO$_4$-DMSO. Linear potential scans at 0.1 mV s^{-1} (corresponding to a low discharge/charge rate) between 2.3 and 4.0 V were used. Reproduced with permission from Ref. [229]. Copyright 2012, American Association for the Advancement of Science
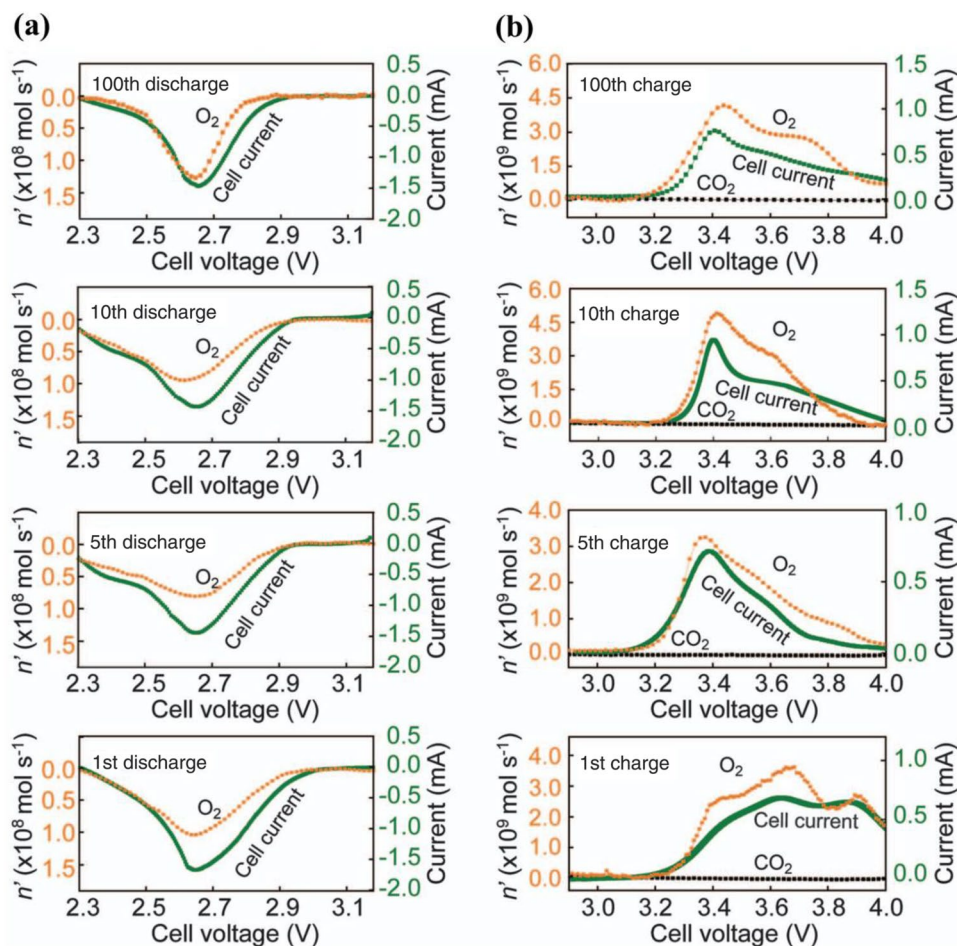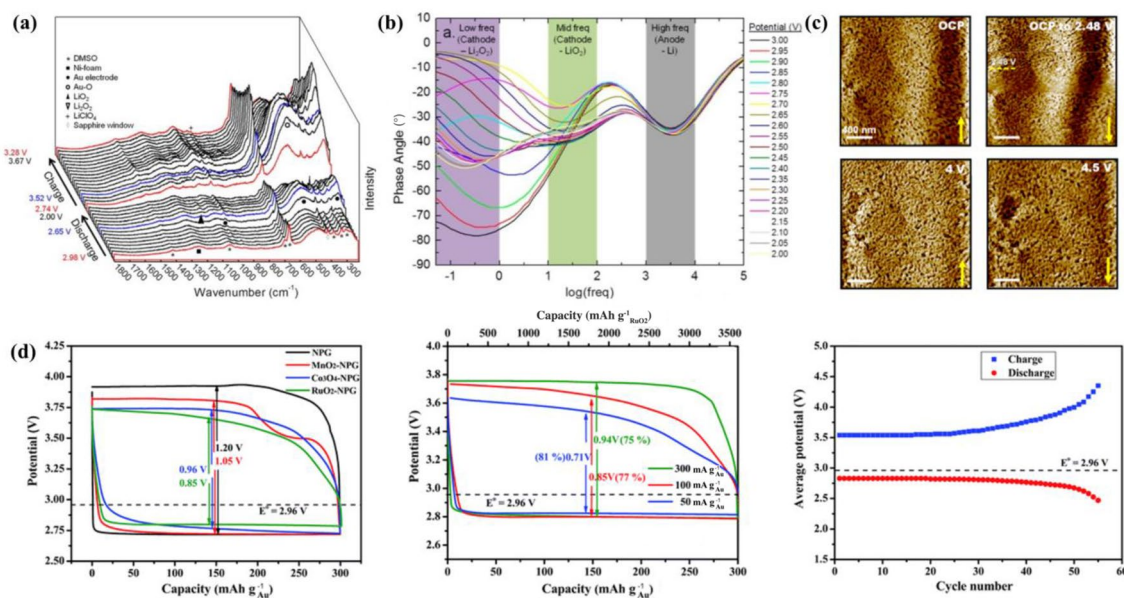
Fig. 10 a Operando Raman spectra of an Au–Ni foam electrode with a DMSO-based electrolyte during the first discharge and charge cycle (front to back). **b** Representative phase angle versus log(freq) of in situ EIS spectra. Reproduced with permission from Ref. [231]. Copyright 2014, American Chemical Society. **c** In situ AFM topography images of an NPG electrode upon ORR and OER in a Li–O$_2$ cell.

Reproduced with permission from Ref. [232]. Copyright 2014, Royal Society of Chemistry. **d** Galvanostatic discharge/charge curves of different cathodes in LOBs; rate dependence and cycling performance of RuO$_2$-NPG-based batteries. Reproduced with permission from Ref. [233]. Copyright 2015, Royal Society of Chemistry

active species, and provide enough space for the storage of discharge products such as Li$_2$O$_2$.

Among these NPMs, NPG as an active catalyst itself or an substrate (core/shell metal oxides/NPG composites) has been well-studied as cathodes in LOBs. Peng et al. [229] first reported pure NPG as a cathode in LOBs, which was made by dealloying the Ag–Au leaf. Coupled with a novel LiClO$_4$-dimethyl sulfoxide (DMSO) electrolyte system, the NPG-based cell exhibits much improved stability over 100 cycles compared with a carbon configuration. By normalizing the capacity value to the Au mass, the NPG cathode can deliver a moderate capacity of 300 mAh g^{-1}. Differential electrochemical mass spectrometry (DEMS) measurement shows that the charge-to-mass ratio on the discharge/charge process is determined to be 2e$^-$/O$_2$, confirming that the reversible formation and decomposition of Li$_2$O$_2$ on the NPG surface are the dominant reactions during cell operation (Fig. 9). The discharge products on the 100th cycle have a high purity of Li$_2$O$_2$ (more than 99%) and nearly all of them could be reversibly decomposed upon charging. Moreover, the NPG electrode itself exhibits considerable catalytic kinetics toward Li$_2$O$_2$ decomposition, with a decomposition rate of nearly 100% below 4 V and 50% below 3.3 V, which is ~ 10 times faster than that with carbon materials. The excellent electrochemical performance could be ascribed to their intrinsic catalytic activity and unique nanoporous structure. However, the poor charge transfer between the

Li$_2$O$_2$ particles and the solid electrode surface results in serious voltage polarization during the charging processes. The charge potential is still high (up to 4.0 V), even with a low charge plateau at 3.3 V, which is a serious problem in aprotic LOBs. To solve this issue, Chen et al. [230] further introduced a redox mediator of tetrathiafulvalene (TTF) into the DMSO electrolyte and NPG cathodes. Even under a high current density of 1 mA cm^{-2}, the cell with the TTF additive could still function well for 100 cycles, assisted by the excellent electrical conduction of the NPG cathode substrate.

Several operando characterizations have been conducted to study the NPG interface in LOBs [231, 232]. For example, Gittleson et al. [231] monitored the Au electrode surface by operando surface-enhanced Raman spectroscopy and electrochemical impedance spectroscopy (EIS) during typical discharge and charge processes to explore the formation and evolution process of the discharge product in practical LOBs. Raman signals from the electrode itself, discharge products, and the electrolyte could be clearly distinguished to offer insight into the stoichiometry, product flux, and proximity to the catalyst surface (Fig. 10a). In contrast to several investigations that suggest Li superoxide (LiO$_2$) is a mere intermediate in the formation of Li$_2$O$_2$, the stable and reversible precipitation of LiO$_2$ is observed, which is consistent with the reduced overpotentials during discharge. Then, Li$_2$O$_2$ reduced by LiO$_2$ produces an insulating layer that passivates the Au electrode. In turn, a superficial oxidized coating

generated at low charging overpotentials (< 0.6 V) renders residual products in poor contact with the electrode surface. In situ EIS measurements have been utilized to distinguish LiO_2 and Li_2O_2 products by analyzing the frequency- and potential-dependent real resistance, and correlate the reduction and oxidation potentials to the formation mechanism of Li_2O_2 (Fig. 10b). In addition, in situ electrochemical atomic force microscopy (AFM) has been carried out to observe the nucleation, growth, and decomposition of discharge products on NPG substrates in LOBs (Fig. 10c) [232]. It is found that the strong interaction between discharge products and NPG could greatly minimize side reactions and stabilize the reaction system. These operando investigations confirm the critical role of NPG substrates in the reversible conversion of the discharge product Li_2O_2.

In addition to electrolyte optimization, several other strategies on the architecture and composition design of NPG-based cathodes in LOBs have also been exploited to further improve the electrochemical performance and develop their potential applications [93, 233, 234]. For example, NPG with higher porosity affords more Li_2O_2 for higher capacity, and the larger accessible surface area accelerates the reaction kinetics of Li_2O_2 formation and decomposition during cycling. Guo et al. [93] designed a hierarchical NPG with secondary nanopores in the ligaments by a two-step dealloying approach. In the first step, Ag residual of ~ 70 at.% is retained in the Au–Ag precursor with an average pore size of ~ 20 nm. Subsequently, an annealing treatment in air is conducted to coarsen the structure with pore and ligament sizes of 80–100 nm. Finally, Ag in the coarsened product is further etched by a second dealloying step, thus generating hierarchical NPG with a high porosity of 80–82 vol% and large effective surface area of ~ 82.9 $m^2 g^{-1}$. With the addition of the redox mediator TTF, the as-prepared NPG cathode in LOBs exhibits a greatly enhanced reversible capacity and long cycling stability with low charge/discharge overpotentials.

Another optimization strategy is to introduce low-cost metal oxides to construct hybrid NPG electrodes. Compared with noble metal-based electrodes, metal oxides also exhibit great oxygen reduction reaction (ORR) and hydrogen evolution reaction (OER) activity, and have been extensively studied as potential cathode materials in LOBs. NPG can be utilized as an efficient scaffold to support metal oxide electrocatalysts as advanced composite cathodes, which demonstrate high electrical conductivity, excellent electrochemical/mechanical stability, and strong chemical affinity between NPG and oxides [233]. The preparation process usually involves chemical dealloying, electrochemical plating, and subsequent heat treatment. A series of metal oxide/NPG hybrid catalysts are fabricated through such a process including RuO_2/NPG, MnO_2/NPG, and Co_3O_4/NPG. Bright-field TEM characterization demonstrates that RuO_2 is uniformly distributed on the NPG surface, generating a 3D core/shell nanostructure. The 3–5 nm oxide coating is well-bonded to the NPG substrate. MnO_2/NPG and Co_3O_4/NPG composites also have similar microstructures. When processed in LOBs, these metal oxide/NPG hybrid catalysts exhibit synergetic performance of the highly conductive NPG scaffold and catalytically active metal oxides. The voltage profiles (Fig. 10d) show lower average charge potential (3.6–3.8 V) for the composite anodes as compared to pure NPG (approximately 3.9 V), suggesting the efficiently enhanced decomposition kinetics of Li_2O_2. Meanwhile, the average discharge potentials of these metal oxide-deposited cathodes are close to 2.8 V, slightly higher than that of bare NPG. The charge and discharge overpotentials are strongly associated with the metal oxides, among which RuO_2/NPG electrode displays the best rate and cycling performance. In addition, electrochemical synthesis of NPG thin films (< 100 nm) on various low-cost substrates is a feasible method to improve the economic applicability of NPG [234]. Specifically, NPG on a glassy carbon substrate shows good cycling stability with significantly reduced voltage hysteresis.

In spite of the high cost, NPG frameworks provide new insights into the exploration of reaction mechanisms in LOBs. The well-defined porosity, elegant network topology, and highly stable nature are key advantages of NPG substrates. In a lab-scale model system, NPG-based carbon-free cathodes demonstrate great opportunity to precisely understand catalyst-electrolyte interfacial phenomena and describe the chemical and electrochemical reactions during cycles. In addition, new technologies have shown great potential to reduce its use level in oxygen cathodes, which is critical for the practical development of NPG.

The dealloying method has been exploited to prepare low-cost transition metal substrates such as NPN and NPT. Similar to NPG, these dealloyed substrates exhibit abundant porosity, large specific surface area, and high electrical conductivity. However, the poor electrochemical stability of these nanoporous transition metals upon charging limits their direct application in LOBs. To overcome this issue, Gao et al. [235] employed atomic-level N-doped graphene coatings to enhance the electrochemical stability of NPN in LOBs. The NPN prepared by chemical dealloying shows a typical bicontinuous open structure, which serves as both the template and catalyst for graphene growth through CVD. N-doped graphene is uniformly coated on NPN ligaments under a mixed atmosphere of H_2 and Ar gas, with pyridine as the carbon and nitrogen source. With a cut-off capacity of 280 mAh cm^{-2} (55% of the maximum discharge capacity), the free-standing N-doped graphene@NPN cathode exhibits excellent cycling performance of 100 cycles with the charge potential of < 4.30 V. Moreover, the charge potential gradually decreases upon cycling, whereas the discharge potential does not change evidently. The rate dependence is also

studied based on the cut-off capacity of 155 mAh cm^{-2}. As the current density is increased from 0.03 to 0.2 mA cm^{-2}, the average discharge potential continuously decreases from 2.57 to 2.45 V, and the average charge potential is slightly increased from 4.10 to 4.30 V. These results reveal that the composite cathode preserves the merits of low charge/discharge overpotentials and high conductivity of NPMs as well as the high electrochemical stability of carbon materials.

To reduce the consumption of noble metals, a novel configuration employing low-cost metals to support noble metal catalysts has been proposed for the cathode design of LOBs. Zhao et al. [236] first prepared vertically aligned Ti nanowire arrays on Ti foam by a facile dealloying method of a Ti–Mo alloy and then deposited Au nanoparticles on the Ti matrix by cool spurting. The free-standing Ti@Au nanowire matrix provides abundant active sites to facilitate electrochemical reactions. Meanwhile, the absence of conductive carbon and the polymer binder in cathodes effectively inhibits side reactions and promote long cycle stability. Electrochemical measurements demonstrate that the Ti@Au nanowire cathode could achieve a high capacity of 5000 mAh g^{-1} at 1 A g^{-1}. The good stability and high conductivity of the Ti nanowire array endow the batteries with excellent durability of more than 640 cycles within a capacity limitation of 1000 mAh g^{-1} at a current density of 5 A g^{-1}. Apart from the traditional chemical dealloying method, Zhao et al. [237] also fabricated porous Ti foam via a liquid metal dealloying approach with Mg as the molten medium. After coating the surface with Au nanoparticles, this self-supported cathode also exhibits a good cycling life in LOBs (118 cycles at 2 A g^{-1} with a capacity limitation of 1000 mAh g^{-1}). These results suggest that cost-effective NPN/NPT cathodes can be promising alternatives to NPG by employing rational design for LOBs.

To date, carbon-based materials with considerable catalytic performance have been widely studied in LOBs, but these cathodes are usually unstable at high oxidation potentials, owing to electrolyte decomposition and irreversible side reactions [238]. Recent works suggest that 3D NPGR could show exceptionally high electrochemical stability as a cathode substrate for high-capacity LOBs [239–241]. However, it would also cause poor wettability with electrolytes and weak interaction with the discharged product of Li$_2$O$_2$. Moreover, the charge overpotentials are considerably high in NPGR-based LOBs, giving rise to low energy efficiency. An efficient strategy to solve these issues is the introduction of heteroatoms with precise atomic control. By optimizing the surface wettability and electronic conductivity, they can greatly facilitate the charge transfer and accelerate electrode/electrolyte interactions. Han et al. [242] synthesized 3D nanoporous nondoped/N-doped/S-doped graphene based on the NPM-based CVD method with benzene/pyridine/thiophene as the carbon/nitrogen/sulfur sources. These three samples exhibit similar micro-morphology with nanopore channels and interconnected tubular graphene ligaments, but the heteroatom-doped graphene samples have larger specific surface areas and more lattice defects. The subsequent electrochemical evaluation reveals that N-doping could effectively enhance the ORR kinetics to deliver an extremely high discharge capacity of 10400 mAh g^{-1}, whereas S-doping is beneficial to promote Li$_2$O$_2$ oxidation, inhibits accumulation of side products, and finally sustains a longer cycling behavior of 300 cycles at 1000 mAh g^{-1} (Fig. 11a).

Another modification strategy is the incorporation of an appropriate redox-active molecule in electrolytes to lower the critical impact of the electrode-Li$_2$O$_2$ interface and efficiently reduce charge potentials [243]. Han et al. [244] integrated a dealloyed NPGR cathode with a compatible TTF redox additive in a DMSO-based aprotic electrolyte. The NPGR substrate provides abundant reaction sites and efficient pathways for both oxygen reduction and oxygen diffusion in the nanochannels. XPS spectra after cycling (Fig. 11b) manifest that the amounts of alkylcarbonate and Li$_2$CO$_3$ are significantly reduced with the TTF additive in the nanoporous graphene cathode. Combining the TTF-induced catalyzed effect to lower the charge potential, the NPGR cathodes exhibit attractive comprehensive performance including large reversible capacities of 2000 mAh g^{-1} at 2000 mA g^{-1} and a long lifespan over 100 cycles. Of particular note is that this work first demonstrates that a TTF additive could function well with carbonaceous cathodes. Thus, further structural tailoring with dealloyed nanoporous carbons may produce more practical performance in LOBs by exploring suitable electrolyte mediators in future studies.

The incorporation of noble metal or metal oxide nanoparticles with high catalytic performance has also been proposed to enhance the reaction kinetics of graphene electrodes [223]. However, the weak bonding between nanostructured catalysts and the carbon surface could induce coarsening and agglomeration of the active components. To solve this issue, Guo et al. [245] fabricated N-doped NPGR with encapsulated RuO$_2$ nanoparticles. Figure 11c shows a schematic illustration of the preparation process. N-doped NPGR/RuO$_2$ is initially prepared by chemically plating RuO$_2$ into the channels of dealloyed N-doped NPGR. The sample is then treated by the CVD process, during which RuO$_2$ nanoparticles are homogeneously encapsulated by atomic coating of N-doped graphene layers. HRTEM images confirm the elaborate structures of 3–5 nm RuO$_2$ particles encapsulated by two or three layers of graphene. The as-made composite cathodes exhibit superiorstability toward Li$_2$O$_2$ formation and decomposition owing to the additional graphene protection.

In summary, both NPMs and NPGR can serve as cathodes themselves or as scaffolds to load other high-performance catalysts in LOBs. Compared with conventional powder
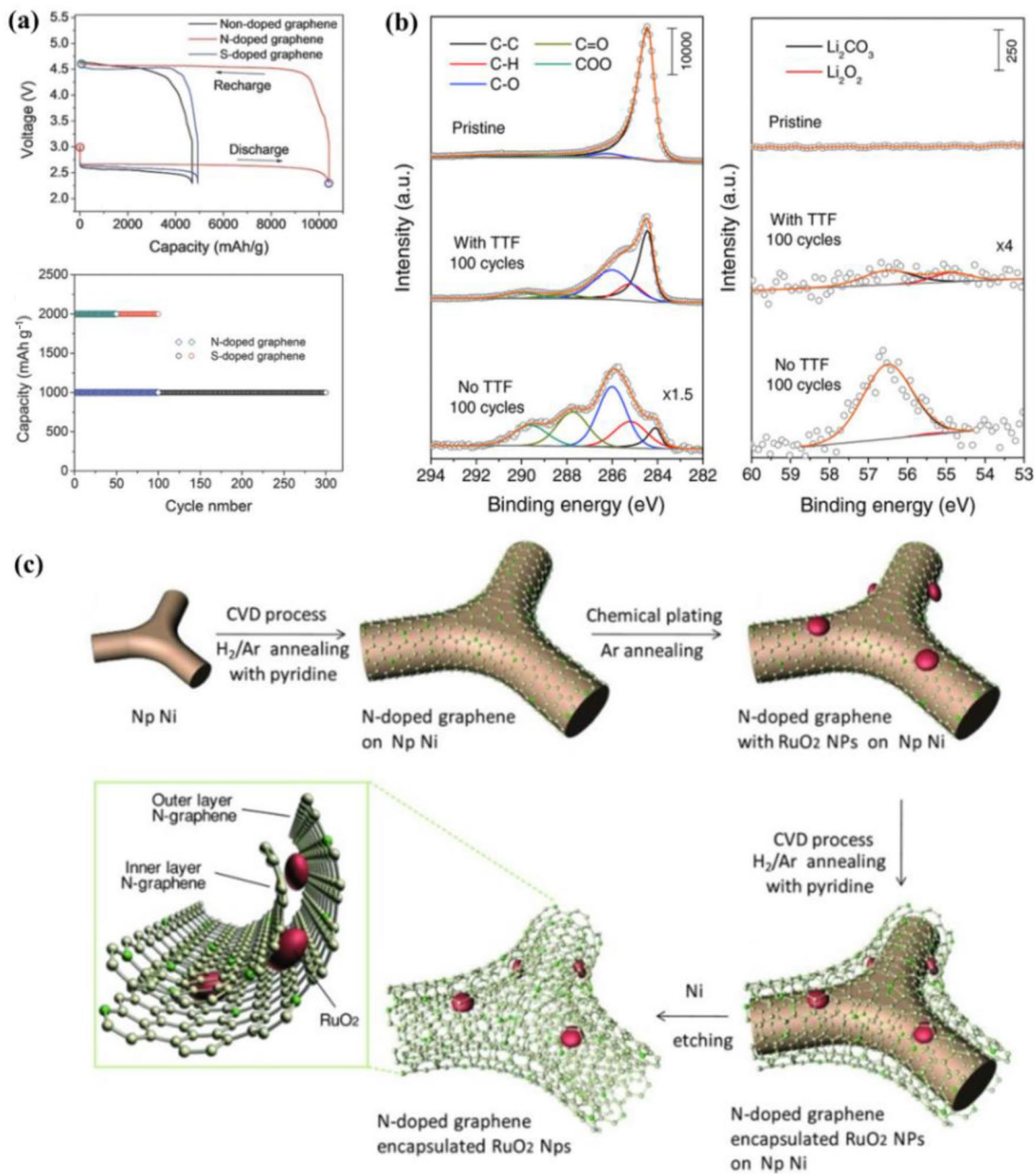
Fig. 11 a Galvanostatic discharge–charge profiles of LOBs with nanoporous graphene cathodes at 200 mA g^{-1}; cycling stability of nanoporous N- and S-doped graphene LOBs. Reproduced with permission from Ref. [242]. Copyright 2016, Wiley–VCH. **b** C 1s and Li 1s XPS spectra of pristine nanoporous graphene and graphene cathodes after 100 cycles (1000 mAh g^{-1} and 1000 mA g^{-1}) with and without TTF in the electrolyte. Reproduced with permission from Ref. [244]. Copyright 2017, Wiley–VCH. **c** Schematic of the preparation process of nanoporous N-doped graphene with encapsulated RuO$_2$ nanoparticles from Ref. [245]. Copyright 2015, Wiley–VCH

cathodes, the continuity and integrity of nanoporous membranes provide remarkable improvement in electron and ion transfers, which are two critical factors for large capacities, good rate performance, and extended cycling lives. For stable electrodes such as NPG, the optimized cell configurations achieved by employing novel electrolyte systems demonstrate very promising long-term stability. Even with low-cost

materials including Ti-, Ni-, and C-based nanoporous substrates, appropriate modifications of structures and compositions could result in significant advances in performance, indicating that dealloying technology holds a unique place in the rational design of oxygen cathodes. This is actually not surprising considering the successful applications of nanoporous materials in proton exchange membrane (PEM)

fuel cells [246–248], where the design principles of membrane electrodes are comparable to those of oxygen cathodes for LOBs in many aspects. Thus, it is highly possible that more valuable experience derived from PEM fuel cells can be extended to the LOB system by employing nanoporous materials as suitable media.

3.2.2 Nanoporous substrates for sulfur cathodes in Li–S batteries

Li–S batteries represent another promising alternative to LIBs due to their high theoretical capacity of 1672 mAh g^{-1} and energy densities of 3500 Wh kg^{-1}. Sulfur is also a low-cost, environmentally benign and naturally abundant element, which is suitable for large-scale engineering production [249–251]. Despite these promising merits, sulfur cathodes suffer from several critical challenges that hinder the practical development of Li–S batteries, including the electric and ionic insulating character of sulfur, large volume expansion upon discharge(up to 80%), and the serious polysulfide shuttle effect on cycling. Nanostructure engineering and composition regulation are effective to address these issues [252]. Typically, the introduction of porous carbon (low density, high conductivity, high specific surface area and chemical stability) to form porous carbon/sulfur composite electrodes can not only enhance the conductivity and sulfur utilization, but also trap the soluble polysulfides in the porous matrix by physical confinement [253]. Besides, polar metal oxides as additives or complexes in sulfur cathodes possess strong chemical interaction with polysulfides, which can further prevent polysulfides shuttle [254]. Dealloying is a versatile technology to fabricate porous metals, compounds and even carbon materials. When functioned as a sulfur host, these dealloyed nanoporous materials could endow considerably enhanced capacities and long-term stability even at a high sulfur loading.

A good example is NPGR that exhibits unique porous structure, interconnected conductive pathways and abundant free space. Based on chemically dealloying and modified CVD methods, Lu et al. [255] fabricated 3D interconnected NPGR after etching NPN templates. NPGR layer and pore structures could be readily adjusted, and macroscopic foams are also achieved by carefully controlling the processing conditions. Benefiting from the topological structure and enhanced electrical conductivity, the NPGR-sulfur composites with optimized tubular pores of 50 nm deliver 520 mAh g^{-1} after 260 cycles. It has been demonstrated that physical adsorption between nonpolar carbon hosts and polar lithium polysulfides can only slow down the sulfur loss for a short term. The introduction of the heteroatoms (N or P) offers stronger adsorption of polysulfides by weak chemical interactions [256, 257]. By utilizing an analogous dealloying method (MgO as sacrificial materials), Shi et al. [258]

proposed N-doped graphene skin on the 3D NPGR framework as anchoring sites to inhibit polysulfide shuttle in Li–S batteries. Different from the routine N-doping with bulk distribution, such N-doped graphene skin could still maintain high electrical conductivity. After incorporating sulfur via a shearing dispersion-filtration method, the NPGR-S composite electrode delivers 667 mAh g^{-1} after 400 cycles at 1 C.

Polysulfide confinement by reinforced chemical binding could also be achieved with certain metal oxides [221]. As discussed above, various NPMO can be straightforwardly fabricated by chemical dealloying in alkaline solutions, which has been demonstrated as nonconductive interlayers for high-loading Li–S batteries. For example, a hierarchically porous TiO_2 matrix is fabricated by etching the $Ti_{10}Al_{90}$ (at.%) alloy in 2 M NaOH solutions for 72 h [259]. As a classic polysulfide reservoir, the dealloyed TiO_2 with an interconnected porous structure and large surface area offers efficient contact between sulfur and host material, which helps trap the polysulfide species and relieves the shuttle effect. Nevertheless, metal oxides generally show poor electrical conductivity, thus it is inevitable to regulate the cell configuration by combining the carbon host to achieve high sulfur loading. Based on this assumption, Wu et al. [260] utilized a similar chemical dealloying method to prepare porous CeO_2 as an interlayer and commercial Ketjen black as the sulfur host. Compared with the pristine sulfur/Ketjen black cathodes, the incorporation of nanoporous CeO_2 greatly enhances cell cyclability for 120 cycles even with a high sulfur loading of 6 mg cm^{-2}. It is demonstrated that the proper redox potential of the Ce^{3+}/Ce^{4+} couple could effectively catalyze polysulfides on the particle surface of CeO_2. Moreover, Mn_3O_4 octahedral microparticles with strong adsorption capabilities to soluble polysulfides are also fabricated by chemical dealloying [261]. In Li–S batteries, the obtained S/Mn_3O_4 cathodes can deliver a capacity of 679 mAh g^{-1} after 150 cycles due to the strong catalytic properties of Mn-based oxides.

Unlike the wide applications in LOBs, there are so far only a few studies on dealloyed materials in Li–S batteries. Nonetheless, it is demonstrated either dealloyed carbon or metal compound could effectively enhance cell performance by providing a conductive porous matrix for sulfur to solve the volume expansion and electron transfer problems. On the other hand, the fabrication of nonconductive interlayer is another promising strategy to maintain active materials at the cathode side.

3.2.3 Nanoporous materials for Li-metal anode protection

The Li-metal anode is featured by its high specific capacity (3800 mAh g^{-1}), lowest redox potential (-3.04 V vs. standard hydrogen electrode), and low mass density (0.53 g cm^{-3}). The implementation of Li-metal anodes is

critically important to achieve high-energy-density LOBs. Moreover, it is the source of Li ions to enable the cells to operate properly with Li-free oxygen and sulfur cathodes. The practical application of Li-metal anodes is hindered by dendrite-associated issues, which cause severe performance degradation over cycling as well as safety concerns. In a Li–O_2 cell, the Li anode faces external contamination owing to the special operation atmosphere, which further complicates Li protection. Several strategies have been introduced to address the Li anode issues, particularly for the inhibition of dendrite growth [262]. For example, studies from different groups have suggested a close correlation between plating/stripping currents and dendritic morphology in Li anodes, which can be explained by the well-known Sand's time theory [263–265]. Porous frameworks with high surface area can effectively reduce the actual current densities in electrodes and accommodate the significant volume expansion/contraction of anodes upon Li plating/stripping. Therefore, Li-composite anodes and current collectors with 3D porous architectures have been extensively investigated for Li protection. Modifications of commercial Cu foil current collectors have been implemented by different research groups, usually with complex procedures [262]. In contrast, the essential advantages of dealloying technology afford

accurate design of desired nanoporous structures in a simple and controllable manner. In this section, we discuss the application of dealloyed NPC current collectors for Li-metal anode protection based on different preparation methods.

Brass is a commercially available alloy composed of copper and zinc, with a typical Cu/Zn ratio of 3:2. Yun et al. [266] first produced NPC current collectors by selectively etching Zn from brass foils. The resulting copper has a typical 3D microstructure and the interconnected pore size in the Cu skeleton could be easily controlled by adjusting the dealloying time. Compared with 2D planar Cu, the optimized 3D Cu frameworks provide abundant space for Li deposition upon cycling and reduce the practical electrode current to suppress dendrite formation. The Li/Li@Cu cell assembled with such NPC current collectors demonstrates excellent cycling stability with very high CE of > 97% over 250 cycles at 0.5 mA cm^{-2}, or a long lifespan up to 1000 h at 0.2 mA cm^{-2} with observably reduced polarization. When paired with a LiFePO$_4$ cathode, the prototype full cell exhibits increased capacity of 136 mAh g^{-1} with high retention of 89.7% after 300 cycles. To achieve better control of nanoporous structures, Zhao et al. [267] developed a linear sweep voltammetry method to electrochemically fabricate compact 3D Cu current collectors from brass (Fig. 12a). The robust
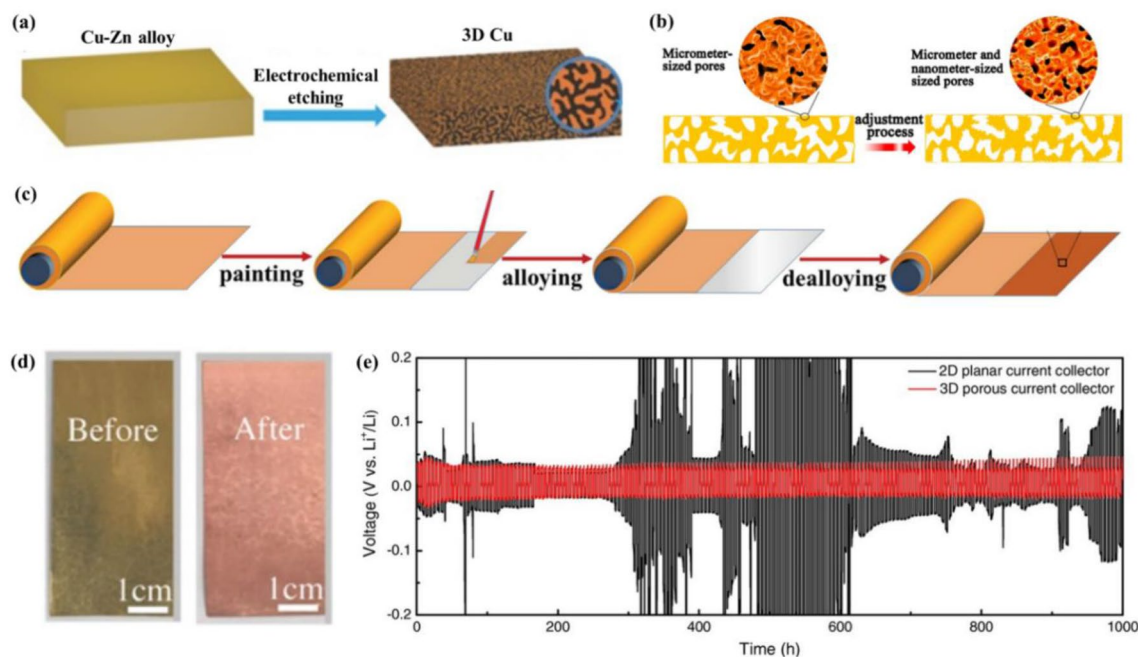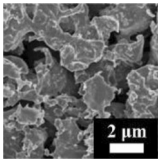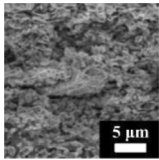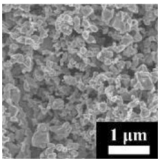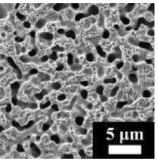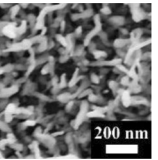
Fig. 12 Schematic of different dealloying methods to fabricate the 3D Cu current collectors: **a** an electrochemical etching method; reproduced with permission from Ref [267]. Copyright 2018, Wiley–VCH. **b** Vacuum distillation dealloying method; reproduced with permission from Ref. [269]. Copyright 2019, Elsevier. **c** Liquid metal dealloying method. Reproduced with permission from Ref. [270]. Copyright 2019, Royal Society of Chemistry. **d** Photo images of Cu–Zn alloy tape and the as-prepared 3D Cu current collector. Reproduced with permission from Ref. [267]. Copyright 2018, Wiley–VCH. **e** Typical cycling performances of Li‖Li@Cu cells using 2D and 3D Cu current collectors with an Li plating/stripping for 1 h at a current density of 1 mA cm^{-2}. Reproduced with permission from Ref. [266]. Copyright 2016, Wiley–VCH

Electrochemical Energy Reviews (2020) 3:541–580

Table 5 Synthetic methods, morphology characterization, and electrochemical performance of selected dealloyed porous Cu current collectors for Li-metal anode protection

Materials	Nanoporous Cu	3D porous Cu	3D porous Cu	Nanoporous/macroporous Cu	3D porous Cu
Precursor alloy	$Cu_{64}Zn_{36}$		Cu–Ga alloy	$Cu_{30}Zn_{70}$	$Cu_{75}Zn_{25}$
Synthetic methods	Chemical dealloying	Electrochemical dealloying	Liquid metal dealloying	Vacuum distillation dealloying	
Morphology	(SEM, scale bar 2 μm)	(SEM, scale bar 5 μm)	(SEM, scale bar 1 μm)	(SEM, scale bar 5 μm)	(SEM, scale bar 200 nm)
Cycling performance of the symmetric battery	250 cycles at 0.5 mA cm^{-2} for 1 mAh cm^{-2}	200 cycles at 1 mA cm^{-2} for 1 mAh cm^{-2}	300 cycles at 1 mA cm^{-2} for 0.5 mAh cm^{-2}	After 200 cycles at 0.5 mA cm^{-2} for 0.5 mAh cm^{-2}	After 800 cycles at 0.52 mA cm^{-2} for 0.26 mAh cm^{-2}
Full battery cathode	$LiFePO_4$				$Li(NiCoMn)O_2$
Cycling performance of the full battery	136 mAh g^{-1} at 90 mA g^{-1} after 300 cycles	127.5 mAh g^{-1} at 180 mA g^{-1} after 350 cycles	~110 mAh g^{-1} at 90 mA g^{-1} after 150 cycles	~150 mAh g^{-1} at 90 mA g^{-1} after 50 cycles	128.8 mAh g^{-1} at 50 mA g^{-1} after 300 cycles
Reference	[266]	[267]	[270]	[269]	[268]

ligaments and homogeneously porous structures induce smooth and stable SEI formation, which is a key factor to suppress dendritic growth and dead Li.

It is worth noting that Zn has a relatively low boiling point of 907 °C. Based on this characteristic, An et al. [268] produced a 3D porous Cu current collector by a one-step vacuum distillation method to avoid the time-consuming and complex manufacturing process. By regulating the distillation temperature and time, the optimized Cu current collector with proper voids could restrain the growth of Li dendrite and accommodate the huge volume expansion of the Li anode during cycling, thereby ensuring a stable SEI layer and electrode structure. Subsequently, Liu et al. [269] also fabricated a porous conductive Cu current collector by utilizing a similar vacuum dealloying approach (Fig. 12b). To further increase the specific surface area and pore volume, a subsequent chemical etching process is conducted, resulting in 3D nanoporous/macroporous structures. The microscale pores and skeletons are functionalized as "cages/hosts" for Li plating/stripping, and nanopores well-distributed in Cu skeletons effectively facilitate Li nucleation under a low overpotential to induce flat Li growth morphology in the sprouting stage.

In addition, Shi et al. [270] proposed a novel liquid metal dealloying strategy to fabricate a self-supported porous Cu current collector (Fig. 12c). At the elevated temperature of 80 °C, liquid Ga can be homogeneously painted onto the surface of a commercial Cu foil to form a $CuGa_2$ intermetallic phase. After dealloying in a mixed acid solution of HNO_3 and HF, both metallic Ga and $CuGa_2$ alloy are selectively etched away, during which Cu atoms undergo rearrangement to form the nanoporous structure, which effectively reduces polarization and enhances electrochemical performance during cycling.

Table 5 summarizes the synthetic methods, morphology characterization, and electrochemical performance of these dealloyed porous Cu current collectors for Li-metal anode protection. Despite the different preparation techniques, they all show typical nanoporous morphology with strong mechanical flexibility as of the pristine brass tape (Fig. 12d). Compared with 2D planar Cu, these 3D porous Cu current collectors afford greatly enhanced cycling stability in both symmetric batteries and full batteries (Fig. 12e), which is mainly ascribed to the interconnected network with large surface area to effectively reduce the current densities. The abundant porosity and tunable structures provide the necessary space for electrode volume expansion upon Li plating, and thus dendritic morphology can be suppressed by physically confining Li deposition within the nanopores. It should be noted that nanostructured Li-composite anodes have been extensively studied based on similar design principles. In our opinion, the modification of current collectors is a more attractive strategy in terms of maintaining the high capacities of the overall anodes. Additionally, the excellent conductivity of metal foils such as copper is also a key advantage over carbon-based frameworks when applied in full cells coupled with high-loading cathodes. Nonetheless, it is still challenging to fabricate robust current collectors with desired porous structures for practical applications. For example, a large areal capacity of > 3 mAh cm^{-2} is necessary for the practical

🖉 Springer

development of Li–O$_2$ batteries, which require the abundant porosity of 3D current collectors for plated lithium. However, the fabrication of such nanoporous frameworks with good flexibility and mechanical strength is yet to be proved for non-noble metals such as copper. Future studies may focus on the rational design of alloy current collectors that have more rigid ligaments to afford structural integrity upon the dealloying treatment.

4 Conclusions and prospects

Dealloying is a versatile technique to prepare a wide variety of nanoporous electrodes including metals (NPG, NPC, NPSN, NPN, and NPT), semiconductors (NPSI and NPGE), compounds (NPMO and NPMS), and even carbons (NPGR). The dealloyed materials possess typical open networks with nanoscale ligaments, tunable pore sizes, and rich surface chemistry, all of which make these materials very promising candidates for utilization in energy storage/conversion devices. This review has comprehensively presented the fabrication and modification of dealloyed nanoporous materials and their applications in rechargeable lithium batteries. Specifically, we introduced typical preparation and modification techniques to regulate the structures and functions to satisfy the special requirements in lithium batteries. Furthermore, recent advances in the applications of rationally designed electrodes in LIBs and LMBs are summarized.

Based on their electrochemical activities, nanoporous materials have been extensively studied as high-capacity anodes in LIBs. A large group of metals/alloys/compounds exhibit highly reversible capacities stemming from the alloying or conversion reaction mechanisms. However, the large volume variation of these anodes results in severe particle pulverization and hence capacity degradation upon cycling. Nanoporous materials are ideal candidates to solve this problem by providing abundant space to accommodate the volume expansion. Furthermore, certain nanoporous materials without electrochemical activity can serve as 3D scaffolds to load desired active components. This strategy has also been extended to the fabrication of oxygen cathodes in LOBs, in which both NPMs and NPGR can be functionalized as cathodes themselves or as scaffolds to load other high-performance catalysts for the delivery of high specific capacity with superior cycling stability. Benefiting from the abundant porosity and facile composition regulation, NPGR and NPMO as porous substrates for sulfur cathodes also effectively mitigate serious shuttle effect and volume variation in Li–S batteries. As for Li-metal anode protection, we propose the application of NPC as current collectors prepared by different preparation methods. Based on the multifunctionality of 3D porous Cu, the obtained LMBs exhibit much better cycling stability with high energy and power densities.

Generally, the superior electrochemical performance of nanoporous materials mainly originates from several intrinsic structural features: (1) 3D open architectures offer high surface areas that are readily accessible by carrier charges and electrolytes; (2) the interconnected nanopores and ligaments efficiently reduce the ion diffusion pathways between the electrolyte and the electrode, and promote the internal permeation of active substances; (3) the high porosity with considerable residual space in the electrode greatly alleviates the large volume expansion during cycling.

In spite of the promising progress, the practical development of nanoporous materials in rechargeable lithium batteries remains immature and several technical challenges need to be resolved: (1) the traditional etching process with corrosive acid/alkali is not environmentally benign; (2) the limited types of reported systems still cannot meet the comprehensive requirements of designated composite designs; (3) the high cost of noble NPMs, especially for NPG, is a major obstacle to their commercialization and limits their scope of appropriate applications to lab-scale model systems; (4) additional complex optimization procedures increase the manufacturing cost; (5) the large specific surface area and low packing density usually lead to relatively low ICE and inferior volumetric energy density; (6) synergistic effects must be considered to promote the comprehensive performance of batteries. For example, electrolytes as an essential component of battery construction should be fully regulated to modify the SEI generation on electrode surfaces. In LOBs, the incorporation of a TTF mediator in DMSO solvent can allow for both lower charge/discharge overpotentials and longer cycling lifespans in NPG-based LOBs [230].

Considering the above challenges, we propose the following potential directions and perspectives for further development of dealloyed materials. (1) It is urgent to explore more alloy precursors. To date, most studies have focused on binary alloy precursors. Considering rich alloy systems, the fabrication of complex alloys may lead to more controllable compositions and structures. For example, the use of NPM-based scaffolds must be carefully controlled because high mass density can decrease the overall energy density of composite electrodes. This is particularly important in the design of nanoporous current collectors for Li-metal anodes. (2) In spite of versatile dealloying techniques, it is still difficult to prepare alkali and alkaline-earth metals due to their high reactivity. Thus, more efficient dealloying routes should be developed for the preparation of these commonly used metals in rechargeable batteries. (3) In terms of physical structure, it is particularly desirable to acquire large dimension, free-standing membranes with sufficient porosity and controlled thickness, especially for electroactive, economically affordable transition metals. (4) More indepth studies including high space and time resolution characterization and theoretical calculations are recommended

to better seek suitable nanoporous functional materials and thoroughly understand the corresponding electrochemical behaviors. (5) Based on similar functional figurations and operation mechanisms, valuable experience from dealloyed technologies can be readily extended to other alkali-metal systems including Na- and K-ion batteries. The exploration of intrinsic correlations between structures and performance is necessary for the design of such electrodes to promote their performance in next-generation batteries.

References

1. Ding, Y., Kim, Y.J., Erlebacher, J.: Nanoporous gold leaf: "ancient technology"/advanced material. Adv. Mater. **16**, 1897–1900 (2004). https://doi.org/10.1002/adma.200400792

2. Chen, Q., Ding, Y., Chen, M.: Nanoporous metal by dealloying for electrochemical energy conversion and storage. MRS Bull. **43**, 43–48 (2018). https://doi.org/10.1557/mrs.2017.300

3. Li, R., Sieradzki, K.: Ductile-brittle transition in random porous Au. Phys. Rev. Lett. **68**, 1168–1171 (1992). https://doi.org/10.1103/PhysRevLett.68.1168

4. Qian, L.H., Chen, M.W.: Ultrafine nanoporous gold by low-temperature dealloying and kinetics of nanopore formation. Appl. Phys. Lett. **91**, 083105 (2007). https://doi.org/10.1063/1.2773757

5. Qi, Z., Weissmüller, J.: Hierarchical nested-network nanostructure by dealloying. ACS Nano **7**, 5948–5954 (2013). https://doi.org/10.1021/nn4021345

6. Ding, Y., Erlebacher, J.: Nanoporous metals with controlled multimodal pore size distribution. J. Am. Chem. Soc. **125**, 7772–7773 (2003). https://doi.org/10.1021/ja035318g

7. Lang, X., Hirata, A., Fujita, T., et al.: Nanoporous metal/oxide hybrid electrodes for electrochemical supercapacitors. Nat. Nanotechnol. **6**, 232–236 (2011). https://doi.org/10.1038/nnano.2011.13

8. Ding, Y., Chen, M.: Nanoporous metals for catalytic and optical applications. MRS Bull. **34**, 569–576 (2011). https://doi.org/10.1557/mrs2009.156

9. Snyder, J., Asanithi, P., Dalton, A.B., et al.: Stabilized nanoporous metals by dealloying ternary alloy precursors. Adv. Mater. **20**, 4883–4886 (2008). https://doi.org/10.1002/adma.200702760

10. Zhang, J., Li, C.M.: Nanoporous metals: fabrication strategies and advanced electrochemical applications in catalysis, sensing and energy systems. Chem. Soc. Rev. **41**, 7016–7031 (2012). https://doi.org/10.1039/C2CS35210A

11. Guo, D.J., Ding, Y.: Porous nanostructured metals for electrocatalysis. Electroanalysis **24**, 2035–2043 (2012). https://doi.org/10.1002/elan.201200450

12. Jin, H.J., Wang, X.L., Parida, S., et al.: Nanoporous Au–Pt alloys as large strain electrochemical actuators. Nano Lett. **10**, 187–194 (2010). https://doi.org/10.1021/nl903262b

13. Detsi, E., Sellès, M.S., Onck, P.R., et al.: Nanoporous silver as electrochemical actuator. Scripta Mater. **69**, 195–198 (2013). https://doi.org/10.1016/j.scriptamat.2013.04.003

14. Biener, J., Wittstock, A., Zepeda-Ruiz, L.A., et al.: Surface-chemistry-driven actuation in nanoporous gold. Nat. Mater. **8**, 47–51 (2009). https://doi.org/10.1038/nmat2335

15. Wittstock, A., Biener, J., Bäumer, M.: Nanoporous gold: a new material for catalytic and sensor applications. Phys. Chem. Chem. Phys. **12**, 12919–12930 (2010). https://doi.org/10.1039/C0CP00757A

16. Zhang, L., Chang, H., Hirata, A., et al.: Nanoporous gold based optical sensor for sub-ppt detection of mercury ions. ACS Nano **7**, 4595–4600 (2013). https://doi.org/10.1021/nn4013737

17. Wang, J., Gao, H., Sun, F., et al.: Nanoporous PtAu alloy as an electrochemical sensor for glucose and hydrogen peroxide. Sensors Actuators B Chem. **191**, 612–618 (2014). https://doi.org/10.1016/j.snb.2013.10.034

18. Oh, J., Deutsch, T.G., Yuan, H.-C., et al.: Nanoporous black silicon photocathode for H_2 production by photoelectrochemical water splitting. Energy Environ. Sci. **4**, 1690–1694 (2011). https://doi.org/10.1039/C1EE01124C

19. Bak, C.H., Kim, K., Jung, K., et al.: Efficient photoelectrochemical water splitting of nanostructured hematite on a three-dimensional nanoporous metal electrode. J. Mater. Chem. A **2**, 17249–17252 (2014). https://doi.org/10.1039/C4TA03578J

20. Yang, Y., Ruan, G., Xiang, C., et al.: Flexible three-dimensional nanoporous metal-based energy devices. J. Am. Chem. Soc. **136**, 6187–6190 (2014). https://doi.org/10.1021/ja501247f

21. Polat, O., Seker, E.: Halide-gated molecular release from nanoporous gold thin films. J. Phys. Chem. C **119**, 24812–24818 (2015). https://doi.org/10.1021/acs.jpcc.5b06959

22. Garcia-Gradilla, V., Sattayasamitsathit, S., Soto, F., et al.: Ultrasound-propelled nanoporous gold wire for efficient drug loading and release. Small **10**, 4154–4159 (2014). https://doi.org/10.1002/smll.201401013

23. Seker, E., Berdichevsky, Y., Staley, K.J., et al.: Microfabrication-compatible nanoporous gold foams as biomaterials for drug delivery. Adv. Healthc. Mater. **1**, 172–176 (2012). https://doi.org/10.1002/adhm.201200002

24. Zhang, Z., Wang, Y., Qi, Z., et al.: Generalized fabrication of nanoporous metals (Au, Pd, Pt, Ag, and Cu) through chemical dealloying. J. Phys. Chem. C **113**, 12629–12636 (2009). https://doi.org/10.1021/jp811445a

25. Rebbecchi, T.A., Chen, Y.: Template-based fabrication of nanoporous metals. J. Mater. Res. **33**, 2–15 (2017). https://doi.org/10.1557/jmr.2017.383

26. Nishio, K., Masuda, H.: Anodization of gold in oxalate solution to form a nanoporous black film. Angew. Chem. Int. Ed. **50**, 1603–1607 (2011). https://doi.org/10.1002/anie.201005700

27. Näth, O., Stephen, A., Rösler, J., et al.: Structuring of nanoporous nickel-based superalloy membranes via laser etching. J. Mater. Process. Technol. **209**, 4739–4743 (2009). https://doi.org/10.1016/j.jmatprotec.2008.11.042

28. Kazanskiy, N.L., Murzin, S.P., Osetrov, Y.L., et al.: Synthesis of nanoporous structures in metallic materials under laser action. Opt. Laser. Eng. **49**, 1264–1267 (2011). https://doi.org/10.1016/j.optlaseng.2011.07.001

29. Tappan, B.C., Steiner III, S.A., Luther, E.P.: Nanoporous metal foams. Angew. Chem. Int. Ed. **49**, 4544–4565 (2010). https://doi.org/10.1002/anie.200902994

30. Tappan, B.C., Huynh, M.H., Hiskey, M.A., et al.: Ultralow-density nanostructured metal foams: combustion synthesis, morphology, and composition. J. Am. Chem. Soc. **128**, 6589–6594 (2006). https://doi.org/10.1021/ja056550k

31. Avisar-Levy, M., Levy, O., Ascarelli, O., et al.: Fractal structures of highly-porous metals and alloys at the nanoscale. J.

Alloys Compd. **635**, 48–54 (2015). https://doi.org/10.1016/j.jallcom.2015.02.073

32. Zhang, X., Guan, P., Malic, L., et al.: Nanoporous twinned PtPd with highly catalytic activity and stability. J. Mater. Chem. A **3**, 2050–2056 (2015). https://doi.org/10.1039/C4TA06250G

33. Ding, Y., Zhang, Z.: Formation and microstructural regulation of nanoporous metals. In: Nanoporous Metals for Advanced Energy Technologies, pp. 37–81. Springer, Cham (2016)

34. Huber, G.W., Shabaker, J.W., Dumesic, J.A.: Raney Ni-Sn catalyst for H_2 production from biomass-derived hydrocarbons. Science **300**, 2075–2077 (2003). https://doi.org/10.1126/science.1085597

35. Raney nickel catalyst market report 2019-global and Chinese market report, share & trends analysis, by manufacturers, products, applications. IOP Publishing PhysicsWeb. https://www.prof-research.com/index.phproute=product/product&product_id=81238(2020). Accessed 13 Jan 2020

36. Weissmüller, J., Sieradzki, K.: Dealloyed nanoporous materials with interface-controlled behavior. MRS Bull. **43**, 14–19 (2018). https://doi.org/10.1557/mrs.2017.299

37. Kunduraci, M.: Dealloying technique in the synthesis of lithium-ion battery anode materials. J. Solid State Electrochem. **20**, 2105–2111 (2016). https://doi.org/10.1007/s10008-016-3226-3

38. Song, T., Yan, M., Qian, M.: The enabling role of dealloying in the creation of specific hierarchical porous metal structures—a review. Corros. Sci. **134**, 78–98 (2018). https://doi.org/10.1016/j.corsci.2018.02.013

39. Hu, Y.-S., Guo, Y.G., Sigle, W., et al.: Electrochemical lithiation synthesis of nanoporous materials with superior catalytic and capacitive activity. Nat. Mater. **5**, 713–717 (2006). https://doi.org/10.1038/nmat1709

40. Liu, X.H., Huang, S., Picraux, S.T., et al.: Reversible Nanopore formation in Ge nanowires during lithiation–delithiation cycling: an in Situ transmission electron microscopy study. Nano Lett. **11**, 3991–3997 (2011). https://doi.org/10.1021/nl2024118

41. Chen, Q., Sieradzki, K.: Spontaneous evolution of bicontinuous nanostructures in dealloyed Li-based systems. Nat. Mater. **12**, 1102–1106 (2013). https://doi.org/10.1038/nmat3741

42. Tavassol, H., Cason, M.W., Nuzzo, R.G., et al.: Influence of oxides on the stress evolution and reversibility during SnO_x conversion and Li-Sn alloying reactions. Adv. Energy Mater. **5**, 1400317 (2015). https://doi.org/10.1002/aenm.201400317

43. Xia, H., Lai, M.O., Lu, L.: Nanoporous MnO_x thin-film electrodes synthesized by electrochemical lithiation/delithiation for supercapacitors. J. Power Sources **196**, 2398–2402 (2011). https://doi.org/10.1016/j.jpowsour.2010.09.032

44. Nishio, K., Yoshida, M., Masuda, H.: Fabrication of nanoporous Pt by electrochemical alloying and dealloying with Li. ECS Electrochem. Lett. **2**, C43–C45 (2013). https://doi.org/10.1149/2.007311eel

45. Hu, Y., Zhang, T., Cheng, F.: Recycling application of Li–MnO_2 batteries as rechargeable lithium-air batteries. Angew. Chem. Int. Ed. **54**, 4338–4343 (2015). https://doi.org/10.1002/anie.201411626

46. Kennedy, T., Mullane, E., Geaney, H., et al.: High-performance Germanium nanowire-based lithium-ion battery anodes extending over 1000 cycles through in Situ formation of a continuous porous network. Nano Lett. **14**, 716–723 (2014). https://doi.org/10.1021/nl403979s

47. Lian, Q., Zhou, G., Liu, J., et al.: Extrinsic pseudocapacitve Li-ion storage of SnS anode via lithiation-induced structural optimization on cycling. J. Power Sources **366**, 1–8 (2017). https://doi.org/10.1016/j.jpowsour.2017.09.009

48. Cao, B., Liu, Z., Xu, C., et al.: High-rate-induced capacity evolution of mesoporous C@SnO_2@C hollow nanospheres for ultra-long cycle lithium-ion batteries. J. Power Sources **414**, 233–241 (2019). https://doi.org/10.1016/j.jpowsour.2019.01.001

49. Juarez, T., Biener, J., Weissmüller, J., et al.: Nanoporous metals with structural hierarchy: areview. Adv. Energy. Mater. **19**, 1700389 (2017). https://doi.org/10.1002/adem.201700389

50. Hakamada, M., Mabuchi, M.: Fabrication, microstructure, and properties of nanoporous Pd, Ni, and their alloys by dealloying. Crit. Rev. Solid State Mater. Sci. **38**, 262–285 (2013). https://doi.org/10.1080/10408436.2012.674985

51. McCue, I., Benn, E., Gaskey, B., et al.: Dealloying and dealloyed materials. Annu. Rev. Mater. Res. **46**, 263–286 (2016). https://doi.org/10.1146/annurev-matsci-070115-031739

52. Meng, F., Ding, Y.: Sub-micrometer-thick all-solid-state supercapacitors with high power and energy densities. Adv. Mater. **23**, 4098–4102 (2011). https://doi.org/10.1002/adma.201101678

53. Qian, L., Ding, Y., Fujita, T., et al.: Synthesis and optical properties of three-dimensional porous core-shell nanoarchitectures. Langmuir **24**, 4426–4429 (2008). https://doi.org/10.1021/la703621c

54. Ding, Y., Zhang, Z.: Nanoporous metals for supercapacitor applications. In: Nanoporous Metals for Advanced Energy Technologies, pp. 137–173. Springer, Cham (2016)

55. Liu, L., Lyu, J., Zhao, T., et al.: Preparations and properties of porous copper materials for lithium-ion battery applications. Chem. Eng. Commun. **203**, 707–713 (2016). https://doi.org/10.1080/00986445.2015.1104504

56. Erlebacher, J., Aziz, M.J., Karma, A., et al.: Evolution of nanoporosity in dealloying. Nature **410**, 450–453 (2001). https://doi.org/10.1038/35068529

57. Weissmüller, J., Newman, R.C., Jin, H.J., et al.: Nanoporous metals by alloy corrosion: formation and mechanical properties. MRS Bull. **34**, 577–586 (2011). https://doi.org/10.1557/mrs2009.157

58. McCue, I., Benn, E., Gaskey, B., et al.: Dealloying and dealloyed materials. Ann Rev Mater Res **46**, 263–286 (2016). https://doi.org/10.1146/annurev-matsci-070115-031739

59. Xu, C., Su, J., Xu, X., et al.: Low temperature CO oxidation over unsupported nanoporous gold. J. Am. Chem. Soc. **129**, 42–43 (2007). https://doi.org/10.1021/ja0675503

60. Fujita, T., Qian, L.H., Inoke, K., et al.: Three-dimensional morphology of nanoporous gold. Appl. Phys. Lett. **92**, 251902 (2008). https://doi.org/10.1063/1.2948902

61. Wada, T., Yubuta, K., Inoue, A., et al.: Dealloying by metallic melt. Mater. Lett. **65**, 1076–1078 (2011). https://doi.org/10.1016/j.matlet.2011.01.054

62. Gaskey, B., McCue, I., Chuang, A., et al.: Self-assembled porous metal-intermetallic nanocomposites via liquid metal dealloying. Acta Mater. **164**, 293–300 (2019). https://doi.org/10.1016/j.actamat.2018.10.057

63. Wada, T., Yamada, J., Kato, H.: Preparation of three-dimensional nanoporous Si using dealloying by metallic melt and application as a lithium-ion rechargeable battery negative electrode. J. Power Sources **306**, 8–16 (2016). https://doi.org/10.1016/j.jpowsour.2015.11.079

64. Sun, Y., Ren, Y.: New preparation method of porous copper powder through vacuum dealloying. Vacuum **122**, 215–217 (2015). https://doi.org/10.1016/j.vacuum.2015.09.031

65. Sun, Y., Ren, Y., Yang, K.: New preparation method of micron porous copper through physical vacuum dealloying of Cu–Zn alloys. Mater. Lett. **165**, 1–4 (2016). https://doi.org/10.1016/j.matlet.2015.11.102

66. Parida, S., Kramer, D., Volkert, C.A., et al.: Volume change during the formation of nanoporous gold by dealloying. Phys. Rev. Lett. **97**, 035504 (2006). https://doi.org/10.1103/PhysRevLett.97.035504

67. Yu, J., Ding, Y., Xu, C., et al.: Nanoporous metals by dealloying multicomponent metallic glasses. Chem. Mater. **20**, 4548–4550 (2008). https://doi.org/10.1021/cm8009644

68. Renner, F.U., Stierle, A., Dosch, H., et al.: Initial corrosion observed on the atomic scale. Nature **439**, 707–710 (2006). https://doi.org/10.1038/nature04465

69. Yeh, F.H., Tai, C.C., Huang, J.F., et al.: Formation of porous silver by electrochemical alloying/dealloying in a water-insensitive zinc chloride-1-ethyl-3-methyl imidazolium chloride ionic liquid. J. Phys. Chem. B **110**, 5215–5222 (2006). https://doi.org/10.1021/jp0552527

70. Xu, J., Zhang, C., Wang, X., et al.: Fabrication of bi-modal nanoporous bimetallic Pt–Au alloy with excellent electrocatalytic performance towards formic acid oxidation. Green Chem. **13**, 1914–1922 (2011). https://doi.org/10.1039/C1GC15208D

71. Gan, L., Heggen, M., O'Malley, R., et al.: Understanding and controlling nanoporosity formation for improving the stability of bimetallic fuel cell catalysts. Nano Lett. **13**, 1131–1138 (2013). https://doi.org/10.1021/nl304488q

72. Zhang, H., Wang, Z., Yang, M., et al.: The effect of an external magnetic field on the dealloying process of the Ni–Al alloy in alkaline solution. Phys. Chem. Chem. Phys. **19**, 18167–18171 (2017). https://doi.org/10.1039/C7CP03363J

73. Xu, H., Shen, K., Liu, S., et al.: Micromorphology and phase composition manipulation of nanoporous gold with high methanol electro-oxidation catalytic activity through adding a magnetic field in the dealloying process. J. Phys. Chem. C **122**, 3371–3385 (2018). https://doi.org/10.1021/acs.jpcc.7b10475

74. Cheng, I.C., Hodge, A.M.: High temperature morphology and stability of nanoporous Ag foams. J. Porous Mater. **21**, 467–474 (2014). https://doi.org/10.1007/s10934-014-9793-8

75. Kertis, F., Snyder, J., Govada, L., et al.: Structure/processing relationships in the fabrication of nanoporous gold. JOM **62**, 50–56 (2010). https://doi.org/10.1007/s11837-010-0087-6

76. Chen-Wiegart, Y.C.K., Wang, S., Chu, Y.S., et al.: Structural evolution of nanoporous gold during thermal coarsening. Acta Mater. **60**, 4972–4981 (2012). https://doi.org/10.1016/j.actamat.2012.05.012

77. Shui, J.L., Zhang, J.W., Li, J.C.M.: Making Pt-shell $Pt_{30}Ni_{70}$ nanowires by mild dealloying and heat treatments with little Ni loss. J. Mater. Chem. **21**, 6225–6229 (2011). https://doi.org/10.1039/C1JM10216H

78. Vega, A.A., Newman, R.C.: Beneficial effects of adsorbate-induced surface segregation of Pt in nanoporous metals fabricated by dealloying of Ag–Au–Pt alloys. J. Electrochem. Soc. **161**, C11–C19 (2014). https://doi.org/10.1149/2.014401jes

79. Liu, D., Yang, Z., Wang, P., et al.: Preparation of 3D nanoporous copper-supported cuprous oxide for high-performance lithium ion battery anodes. Nanoscale **5**, 1917–1921 (2013). https://doi.org/10.1039/C2NR33383J

80. Xu, Z.L., Liu, X., Luo, Y., et al.: Nanosilicon anodes for high performance rechargeable batteries. Prog. Mater. Sci. **90**, 1–44 (2017). https://doi.org/10.1016/j.pmatsci.2017.07.003

81. Ellis, B.L., Nazar, L.F.: Sodium and sodium-ion energy storage batteries. Curr. Opin. Solid State Mater. Sci. **16**, 168–177 (2012). https://doi.org/10.1016/j.cossms.2012.04.002

82. Wu, X., Xing, Z., Zhao, Y., et al.: Insert Zn nanoparticles into the 3D porous carbon ultrathin films as a superior anode material for lithium ion battery. Part. Part. Syst. Char. **35**, 1700355 (2018). https://doi.org/10.1002/ppsc.201700355

83. Wu, X., Zhao, W., Wang, H., et al.: Enhanced capacity of chemically bonded phosphorus/carbon composite as an anode material for potassium-ion batteries. J. Power Sources **378**, 460–467 (2018). https://doi.org/10.1016/j.jpowsour.2017.12.077

84. Ito, Y., Qiu, H.-J., Fujita, T., et al.: Bicontinuous nanoporous N-doped graphene for the oxygen reduction reaction.

85. Adv. Mater. **26**, 4145–4150 (2014). https://doi.org/10.1002/adma.201400570

86. Ito, Y., Tanabe, Y., Qiu, H.J., et al.: High-quality three-dimensional nanoporous graphene. Angew. Chem. Int. Ed. **53**, 4822–4826 (2014). https://doi.org/10.1002/anie.201402662

86. Fan, W., Liu, X., Wang, Z., et al.: Synergetic enhancement of the electronic/ionic conductivity of a Li-ion battery by fabrication of a carbon-coated nanoporous SnO_xSb alloy anode. Nanoscale **10**, 7605–7611 (2018). https://doi.org/10.1039/C8NR00550H

87. Chen, Z., Ye, J., Qin, R., et al.: Carbon particles modified macroporous Si/Ni composite as an advanced anode material for lithium ion batteries. Int. J. Hydrogen Energy **44**, 1078–1087 (2019). https://doi.org/10.1016/j.ijhydene.2018.11.065

88. Feng, J., Zhang, Z., Ci, L., et al.: Chemical dealloying synthesis of porous silicon anchored by in situ generated graphene sheets as anode material for lithium-ion batteries. J. Power Sources **287**, 177–183 (2015). https://doi.org/10.1016/j.jpowsour.2015.04.051

89. Huang, K., Xing, Z., Wang, L., et al.: Direct synthesis of 3D hierarchically porous carbon/Sn composites via in situ generated NaCl crystals as templates for potassium-ion batteries anode. J. Mater. Chem. A **6**, 434–442 (2018). https://doi.org/10.1039/C7TA08171E

90. Yu, Y., Gu, L., Lang, X., et al.: Li storage in 3D nanoporous Au-supported nanocrystalline tin. Adv. Mater. **23**, 2443–2447 (2011). https://doi.org/10.1002/adma.201004331

91. Zhang, S., Xing, Y., Jiang, T., et al.: A three-dimensional tin-coated nanoporous copper for lithium-ion battery anodes. J. Power Sources **196**, 6915–6919 (2011). https://doi.org/10.1016/j.jpowsour.2010.12.021

92. Hao, Q., Hou, J., Ye, J., et al.: Hierarchical macroporous Si/Sn composite: easy preparation and optimized performances towards lithium storage. Electrochim. Acta **306**, 427–436 (2019). https://doi.org/10.1016/j.electacta.2019.03.163

93. Guo, X., Han, J., Liu, P., et al.: Hierarchical nanoporosity enhanced reversible capacity of bicontinuous nanoporous metal based Li–O_2 battery. Sci. Rep. **6**, 33466 (2016). https://doi.org/10.1038/srep33466

94. Lu, L., Han, X., Li, J., et al.: A review on the key issues for lithium-ion battery management in electric vehicles. J. Power Sources **226**, 272–288 (2013). https://doi.org/10.1016/j.jpowsour.2012.10.060

95. Etacheri, V., Marom, R., Elazari, R., et al.: Challenges in the development of advanced Li-ion batteries: a review. Energy Environ. Sci. **4**, 3243–3262 (2011). https://doi.org/10.1039/C1EE01598B

96. Poizot, P., Laruelle, S., Grugeon, S., et al.: Nano-sized transition-metal oxides as negative-electrode materials for lithium-ion batteries. Nature **407**, 496–499 (2000). https://doi.org/10.1038/35035045

97. Zhang, W.J.: A review of the electrochemical performance of alloy anodes for lithium-ion batteries. J. Power Sources **196**, 13–24 (2011). https://doi.org/10.1016/j.jpowsour.2010.07.020

98. Obrovac, M.N., Chevrier, V.L.: Alloy negative electrodes for Li-ion batteries. Chem. Rev. **114**, 11444–11502 (2014). https://doi.org/10.1021/cr500207g

99. Kasavajjula, U., Wang, C., Appleby, A.J.: Nano- and bulk-silicon-based insertion anodes for lithium-ion secondary cells. J. Power Sources **163**, 1003–1039 (2007). https://doi.org/10.1016/j.jpowsour.2006.09.084

100. Szczech, J.R., Jin, S.: Nanostructured silicon for high capacity lithium battery anodes. Energy Environ. Sci. **4**, 56–72 (2011). https://doi.org/10.1039/C0EE00281J

101. Chae, S., Choi, S.-H., Kim, N., et al.: Integration of graphite and silicon anodes for the commercialization of high-energy

lithium-ion batteries. Angew. Chem. Int. Ed. **59**, 110–135 (2020). https://doi.org/10.1002/anie.201902085

102. Sharma, R.A., Seefurth, R.N.: Thermodynamic properties of the lithium-silicon system. J. Electrochem. Soc. **123**, 1763–1768 (1976). https://doi.org/10.1149/1.2132692

103. Soto, F.A., Ma, Y., Martinez de la Hoz, J.M., et al.: Formation and growth mechanisms of solid-electrolyte interphase layers in rechargeable batteries. Chem. Mater. **27**, 7990–8000 (2015). https://doi.org/10.1021/acs.chemmater.5b03358

104. Su, X., Wu, Q., Li, J., et al.: Silicon-based nanomaterials for lithium-ion batteries: a review. Adv. Energy Mater. **4**, 1300882 (2014). https://doi.org/10.1002/aenm.201300882

105. He, W., Tian, H., Xin, F., et al.: Scalable fabrication of micro-sized bulk porous Si from Fe–Si alloy as a high performance anode for lithium-ion batteries. J. Mater. Chem. A **3**, 17956–17962 (2015). https://doi.org/10.1039/C5TA04857E

106. Liang, J., Li, X., Hou, Z., et al.: Nanoporous silicon prepared through air-oxidation demagnesiation of Mg$_2$Si and properties of its lithium ion batteries. Chem. Commun. **51**, 7230–7233 (2015). https://doi.org/10.1039/C5CC01659B

107. Sohn, M., Lee, D.G., Park, H.I., et al.: Microstructure controlled porous silicon particles as a high capacity lithium storage material via dual step pore engineering. Adv. Funct. Mater. **28**, 1800855 (2018). https://doi.org/10.1002/adfm.201800855

108. Terranova, M.L., Orlanducci, S., Tamburri, E., et al.: Si/C hybrid nanostructures for Li-ion anodes: an overview. J. Power Sources **246**, 167–177 (2014). https://doi.org/10.1016/j.jpowsour.2013.07.065

109. Rahman, M.A., Song, G., Bhatt, A.I., et al.: Nanostructured silicon anodes for high-performance lithium-ion batteries. Adv. Funct. Mater. **26**, 647–678 (2016). https://doi.org/10.1002/adfm.201502959

110. Zhang, L., Liu, X., Zhao, Q., et al.: Si-containing precursors for Si-based anode materials of Li-batteries: a review. Energy Storage Mater. **4**, 92–102 (2016). https://doi.org/10.1016/j.ensm.2016.01.011

111. Yin, Y., Wan, L., Guo, Y.: Silicon-based nanomaterials for lithium-ion batteries. Chin. Sci. Bull. **57**, 4104–4110 (2012). https://doi.org/10.1007/s11434-012-5017-2

112. Zuo, X., Zhu, J., Müller-Buschbaum, P., et al.: Silicon based lithium-ion battery anodes: a chronicle perspective review. Nano Energy **31**, 113–143 (2017). https://doi.org/10.1016/j.nanoen.2016.11.013

113. An, Y., Fei, H., Zeng, G., et al.: Green, scalable, and controllable fabrication of nanoporous silicon from commercial alloy precursors for high-energy lithium-ion batteries. ACS Nano **12**, 4993–5002 (2018). https://doi.org/10.1021/acsnano.8b02219

114. Wada, T., Ichitsubo, T., Yubuta, K., et al.: Bulk-nanoporous-silicon negative electrode with extremely high cyclability for lithium-ion batteries prepared using a top-down process. Nano Lett. **14**, 4505–4510 (2014). https://doi.org/10.1021/nl501500g

115. Saager, S., Scheffel, B., Zywitzki, O., et al.: Porous silicon thin films as anodes for lithium ion batteries deposited by co-evaporation of silicon and zinc. Surf. Coat. Technol. **358**, 586–593 (2019). https://doi.org/10.1016/j.surfcoat.2018.11.064

116. Zhao, C., Wada, T., De Andrade, V., et al.: Imaging of 3D morphological evolution of nanoporous silicon anode in lithium ion battery by X-ray nano-tomography. Nano Energy **52**, 381–390 (2018). https://doi.org/10.1016/j.nanoen.2018.08.009

117. Jiang, Z., Li, C., Hao, S., et al.: An easy way for preparing high performance porous silicon powder by acid etching Al–Si alloy powder for lithium ion battery. Electrochim. Acta **115**, 393–398 (2014). https://doi.org/10.1016/j.electacta.2013.08.123

118. Profatilova, I.A., Stock, C., Schmitz, A., et al.: Enhanced thermal stability of a lithiated nano-silicon electrode by fluoroethylene carbonate and vinylene carbonate. J. Power Sources **222**, 140–149 (2013). https://doi.org/10.1016/j.jpowsour.2012.08.066

119. Jiang, T., Zhang, R., Yin, Q., et al.: Morphology, composition and electrochemistry of a nano-porous silicon versus bulk silicon anode for lithium-ion batteries. J. Mater. Sci. **52**, 3670–3677 (2017). https://doi.org/10.1007/s10853-016-0599-8

120. Hwang, G., Kim, J.M., Hong, D., et al.: Multifunctional natural agarose as an alternative material for high-performance rechargeable lithium-ion batteries. Green Chem. **18**, 2710–2716 (2016). https://doi.org/10.1039/C5GC02654G

121. Wu, X., Chen, Y., Xing, Z., et al.: Advanced carbon-based anodes for potassium-ion batteries. Adv. Energy Mater. **9**, 1900343 (2019). https://doi.org/10.1002/aenm.201900343

122. Lv, X., Wei, W., Huang, B., et al.: Achieving high energy density for lithium-ion battery anodes by Si/C nanostructure design. J. Mater. Chem. A **7**, 2165–2171 (2019). https://doi.org/10.1039/C8TA10936B

123. Park, H.I., Sohn, M., Kim, D.S., et al.: Carbon nanofiber/3D nanoporous silicon hybrids as high capacity lithium storage materials. ChemSusChem **9**, 834–840 (2016). https://doi.org/10.1002/cssc.201501633

124. Jia, H., Zheng, J., Song, J., et al.: A novel approach to synthesize micrometer-sized porous silicon as a high performance anode for lithium-ion batteries. Nano Energy **50**, 589–597 (2018). https://doi.org/10.1016/j.nanoen.2018.05.048

125. Zhou, W., Jiang, T., Zhou, H., et al.: The nanostructure of the Si–Al eutectic and its use in lithium batteries. MRS Commun. **3**, 119–121 (2013). https://doi.org/10.1557/mrc.2013.20

126. Nguyen, H.T., Zamfir, M.R., Duong, L.D., et al.: Alumina-coated silicon-based nanowire arrays for high quality Li-ion battery anodes. J. Mater. Chem. **22**, 24618–24626 (2012). https://doi.org/10.1039/C2JM35125K

127. He, Y., Yu, X., Wang, Y., et al.: Alumina-coated patterned amorphous silicon as the anode for a lithium-ion battery with high coulombic efficiency. Adv. Mater. **23**, 4938–4941 (2011). https://doi.org/10.1002/adma.201102568

128. Hwang, G., Park, H., Bok, T., et al.: A high-performance nanoporous Si/Al$_2$O$_3$ foam lithium-ion battery anode fabricated by selective chemical etching of the Al–Si alloy and subsequent thermal oxidation. Chem. Commun. **51**, 4429–4432 (2015). https://doi.org/10.1039/C4CC09956G

129. Hao, Q., Zhao, D., Duan, H., et al.: Si/Ag composite with bimodal micro-nano porous structure as a high-performance anode for Li-ion batteries. Nanoscale **7**, 5320–5327 (2015). https://doi.org/10.1039/C4NR07384C

130. Xu, C., Hao, Q., Zhao, D.: Facile fabrication of a nanoporous Si/Cu composite and its application as a high-performance anode in lithium-ion batteries. Nano Res. **9**, 908–916 (2016). https://doi.org/10.1007/s12274-015-0973-x

131. Ma, W., Liu, X., Wang, X., et al.: Crystalline Cu-silicide stabilizes the performance of a high capacity Si-based Li-ion battery anode. J. Mater. Chem. A **4**, 19140–19146 (2016). https://doi.org/10.1039/C6TA08740J

132. Wang, J., Du, N., Zhang, H., et al.: Cu-Si$_{1-x}$Ge$_x$ core-shell nanowire arrays as three-dimensional electrodes for high-rate capability lithium-ion batteries. J. Power Sources **208**, 434–439 (2012). https://doi.org/10.1016/j.jpowsour.2012.02.039

133. Kim, D., Li, N., Sheehan, C.J., et al.: Degradation of Si/Ge core/shell nanowire heterostructures during lithiation and delithiation at 0.8 and 20 A g^{-1}. Nanoscale **10**, 7343–7351 (2018). https://doi.org/10.1039/C8NR00865E

134. Lin, N., Wang, L., Zhou, J., et al.: A Si/Ge nanocomposite prepared by a one-step solid-state metathesis reaction and its enhanced electrochemical performance. J. Mater. Chem. A **3**, 11199–11202 (2015). https://doi.org/10.1039/C5TA02216A
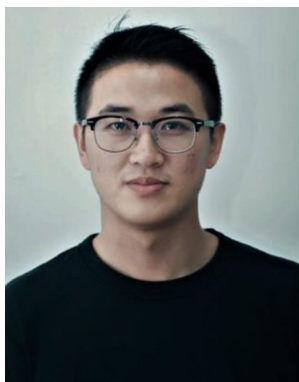
135. Luo, W., Shen, D., Zhang, R., et al.: Germanium nanograin decoration on carbon shell: boosting lithium-storage properties of silicon nanoparticles. Adv. Funct. Mater. **26**, 7800–7806 (2016). https://doi.org/10.1002/adfm.201603335

136. Wu, S., Han, C., Iocozzia, J., et al.: Germanium-based nanomaterials for rechargeable batteries. Angew. Chem. Int. Ed. **55**, 7898–7922 (2016). https://doi.org/10.1002/anie.201509651

137. Yang, Y., Liu, S., Bian, X., et al.: Morphology- and porosity-tunable synthesis of 3D nanoporous SiGe alloy as a high-performance lithium-ion battery anode. ACS Nano **12**, 2900–2908 (2018). https://doi.org/10.1021/acsnano.8b00426

138. Ye, J., Chen, Z., Hao, Q., et al.: One-step mild fabrication of porous core-shelled Si@TiO$_2$ nanocomposite as high performance anode for Li-ion batteries. J. Colloid Interface Sci. **536**, 171–179 (2019). https://doi.org/10.1016/j.jcis.2018.10.029

139. Tian, H., Tan, X., Xin, F., et al.: Micro-sized nano-porous Si/C anodes for lithium ion batteries. Nano Energy **11**, 490–499 (2015). https://doi.org/10.1016/j.nanoen.2014.11.031

140. Wang, J., Meng, X., Fan, X., et al.: Scalable synthesis of defect abundant Si nanorods for high-performance Li-ion battery anodes. ACS Nano **9**, 6576–6586 (2015). https://doi.org/10.1021/acsnano.5b02565

141. Jiang, H., Zhou, X., Liu, G., et al.: Free-standing Si/Graphene paper using Si nanoparticles synthesized by acid-etching Al–Si Alloy powder for high-stability Li-ion battery anodes. Electrochim. Acta **188**, 777–784 (2016). https://doi.org/10.1016/j.electacta.2015.12.023

142. Zhang, S., Zheng, Y., Huang, X., et al.: Structural engineering of hierarchical micro-nanostructured Ge-C framework by controlling the nucleation for ultralong-life Li storage. Adv. Energy Mater. **9**, 1900081 (2019). https://doi.org/10.1002/aenm.201900081

143. Wang, B., Jin, J., Rui, K., et al.: Scalable synthesis of hierarchical porous Ge/rGO microspheres with an ultra-long cycling life for lithium storage. J. Power Sources **396**, 124–133 (2018). https://doi.org/10.1016/j.jpowsour.2018.06.024

144. Cui, G., Gu, L., Zhi, L., et al.: A Germanium-carbon nanocomposite material for lithium batteries. Adv. Mater. **20**, 3079–3083 (2008). https://doi.org/10.1002/adma.200800586

145. Yang, H., Huang, S., Huang, X., et al.: Orientation-dependent interfacial mobility governs the anisotropic swelling in lithiated silicon nanowires. Nano Lett. **12**, 1953–1958 (2012). https://doi.org/10.1021/nl204437t

146. Han, J., Li, C., Lu, Z., et al.: Vapor phase dealloying: a versatile approach for fabricating 3D porous materials. Acta Mater. **163**, 161–172 (2019). https://doi.org/10.1016/j.actamat.2018.10.012

147. Liu, S., Feng, J., Bian, X., et al.: Nanoporous germanium as high-capacity lithium-ion battery anode. Nano Energy **13**, 651–657 (2015). https://doi.org/10.1016/j.nanoen.2015.03.039

148. Hao, Q., Liu, Q., Zhang, Y., et al.: Easy preparation of nanoporous Ge/Cu$_3$Ge composite and its high performances towards lithium storage. J. Colloid Interface Sci. **539**, 665–671 (2019). https://doi.org/10.1016/j.jcis.2018.12.104

149. Hu, R.Z., Zhang, L., Liu, X., et al.: Investigation of immiscible alloy system of Al–Sn thin films as anodes for lithium ion batteries. Electrochem. Commun. **10**, 1109–1112 (2008). https://doi.org/10.1016/j.elecom.2008.05.012

150. Chen, L.B., Xie, J.Y., Yu, H.C., et al.: Si–Al thin film anode material with superior cycle performance and rate capability for lithium ion batteries. Electrochim. Acta **53**, 8149–8153 (2008). https://doi.org/10.1016/j.electacta.2008.06.025

151. Wang, M., Zhang, F., Lee, C.S., et al.: Low-cost metallic anode materials for high performance rechargeable batteries. Adv. Energy Mater. **7**, 1700536 (2017). https://doi.org/10.1002/aenm.201700536

152. Ma, W., Wang, Y., Yang, Y., et al.: Temperature-dependent Li storage performance in nanoporous Cu–Ge–Al alloy. ACS Appl. Mater. Interfaces **11**, 9073–9082 (2019). https://doi.org/10.1021/acsami.8b20654

153. Cook, J.B., Detsi, E., Liu, Y., et al.: Nanoporous tin with a granular hierarchical ligament morphology as a highly stable Li-ion battery anode. ACS Appl. Mater. Interfaces **9**, 293–303 (2017). https://doi.org/10.1021/acsami.6b09014

154. Cook, J.B., Lin, T.C., Detsi, E., et al.: Using X-ray microscopy to understand how nanoporous materials can be used to reduce the large volume change in alloy anodes. Nano Lett. **17**, 870–877 (2017). https://doi.org/10.1021/acs.nanolett.6b04181

155. Song, T., Yan, M., Qian, M.: A dealloying approach to synthesizing micro-sized porous tin (Sn) from immiscible alloy systems for potential lithium-ion battery anode applications. J. Porous Mater. **22**, 713–719 (2015). https://doi.org/10.1007/s10934-015-9944-6

156. Reddy, M.V., Subba Rao, G.V., Chowdari, B.V.R.: Metal oxides and oxysalts as anode materials for Li ion batteries. Chem. Rev. **113**, 5364–5457 (2013). https://doi.org/10.1021/cr3001884

157. Liu, J., Wen, Y., van Aken, P.A., et al.: Facile synthesis of highly porous Ni–Sn intermetallic microcages with excellent electrochemical performance for lithium and sodium storage. Nano Lett. **14**, 6387–6392 (2014). https://doi.org/10.1021/nl5028606

158. Liu, X., Zhang, R., Yu, W., et al.: Three-dimensional electrode with conductive Cu framework for stable and fast Li-ion storage. Energy Storage Mater. **11**, 83–90 (2018). https://doi.org/10.1016/j.ensm.2017.09.008

159. Xing, Y., Wang, S., Fang, B., et al.: Three-dimensional nanoporous Cu$_6$Sn$_5$/Cu composite from dealloying as anode for lithium ion batteries. Microporous Mesoporous Mater. **261**, 237–243 (2018). https://doi.org/10.1016/j.micromeso.2016.11.036

160. He, M., Walter, M., Kravchyk, K.V., et al.: Monodisperse SnSb nanocrystals for Li-ion and Na-ion battery anodes: synergy and dissonance between Sn and Sb. Nanoscale **7**, 455–459 (2015). https://doi.org/10.1039/C4NR05604C

161. Antitomaso, P., Fraisse, B., Sougrati, M.T., et al.: Ultra-fast dry microwave preparation of SnSb used as negative electrode material for Li-ion batteries. J. Power Sources **325**, 346–350 (2016). https://doi.org/10.1016/j.jpowsour.2016.06.010

162. Zhang, J., Wang, Z., Hong, Y., et al.: Electrochemical fabrication of porous Sn/SnSb negative electrodes from mixed SnO$_2$–Sb$_2$O$_3$. Electrochem. Commun. **38**, 36–39 (2014). https://doi.org/10.1016/j.elecom.2013.10.030

163. Ding, Y., Li, Z.F., Timofeeva, E.V., et al.: In Situ EXAFS-derived mechanism of highly reversible tin phosphide/graphite composite anode for Li-ion batteries. Adv. Energy Mater. **8**, 1702134 (2018). https://doi.org/10.1002/aenm.201702134

164. Xia, Y., Han, S., Zhu, Y., et al.: Stable cycling of mesoporous Sn$_4$P$_3$/SnO$_2$@C nanosphere anode with high initial coulombic efficiency for Li-ion batteries. Energy Storage Mater. **18**, 125–132 (2019). https://doi.org/10.1016/j.ensm.2019.01.021

165. Wang, X., Kim, H.M., Xiao, Y., et al.: Nanostructured metal phosphide-based materials for electrochemical energy storage. J. Mater. Chem. A **4**, 14915–14931 (2016). https://doi.org/10.1039/C6TA06705K

166. Liu, Q., Ye, J., Chen, Z., et al.: Double conductivity-improved porous Sn/Sn$_4$P$_3$@carbon nanocomposite as high performance anode in lithium-ion batteries. J. Colloid Interface Sci. **537**, 588–596 (2019). https://doi.org/10.1016/j.jcis.2018.11.060

167. Xing, Z., Ju, Z., Yang, J., et al.: One-step hydrothermal synthesis of ZnFe$_2$O$_4$ nano-octahedrons as a high capacity anode material for Li-ion batteries. Nano Res. **5**, 477–485 (2012). https://doi.org/10.1007/s12274-012-0233-2

168. Xing, Z., Ji, X., Zhao, Y., et al.: Co$_{2+x}$Ti$_{1-x}$O$_4$ nano-octahedra as high performance anodes for lithium-ion batteries. J. Mater.

Chem. A **5**, 8714–8724 (2017). https://doi.org/10.1039/C7TA01152K

169. Tan, C., Cao, J., Khattak, A.M., et al.: High-performance tin oxide-nitrogen doped graphene aerogel hybrids as anode materials for lithium-ion batteries. J. Power Sources **270**, 28–33 (2014). https://doi.org/10.1016/j.jpowsour.2014.07.059

170. Mei, J., Liao, T., Kou, L., et al.: Two-dimensional metal oxide nanomaterials for next-generation rechargeable batteries. Adv. Mater. **29**, 1700176 (2017). https://doi.org/10.1002/adma.201700176

171. Xu, C., Wang, R., Zhang, Y., et al.: A general corrosion route to nanostructured metal oxides. Nanoscale **2**, 906–909 (2010). https://doi.org/10.1039/B9NR00351G

172. Jia, S., Song, T., Zhao, B., et al.: Dealloyed Fe₃O₄ octahedra as anode material for lithium-ion batteries with stable and high electrochemical performance. J. Alloys Compd. **617**, 787–791 (2014). https://doi.org/10.1016/j.jallcom.2014.08.081

173. Hao, Q., Wang, Z., Ye, J., et al.: Fe₃O₄/Ag microsheets assembled by interlaced nanothorns as high performance anode materials for lithium storage. Int. J. Hydrogen Energy **42**, 10072–10080 (2017). https://doi.org/10.1016/j.ijhydene.2017.01.079

174. Ye, J., Wang, Z., Hao, Q., et al.: Facile fabrication of Fe₃O₄ octahedra/nanoporous copper network composite for high-performance anode in Li-ion batteries. J. Colloid Interface Sci. **493**, 171–180 (2017). https://doi.org/10.1016/j.jcis.2017.01.036

175. Li, X., Huang, X., Liu, D., et al.: Synthesis of 3D hierarchical Fe₃O₄/graphene composites with high lithium storage capacity and for controlled drug delivery. J. Phys. Chem. C **115**, 21567–21573 (2011). https://doi.org/10.1021/jp204502n

176. Ye, J., Hao, Q., Liu, B., et al.: Facile preparation of graphene nanosheets encapsulated Fe₃O₄ octahedra composite and its high lithium storage performances. Chem. Eng. J. **315**, 115–123 (2017). https://doi.org/10.1016/j.cej.2017.01.023

177. Hao, Q., Ye, J., Xu, C.: Facile fabrication of Fe₃O₄ octahedra with bimodal conductive network of nanoporous Cu and graphene nanosheets for high-performance anode in Li-ion batteries. J. Alloys Compd. **727**, 34–42 (2017). https://doi.org/10.1016/j.jallcom.2017.08.139

178. Hao, Q., Wang, J., Xu, C.: Facile preparation of Mn₃O₄ octahedra and their long-term cycle life as an anode material for Li-ion batteries. J. Mater. Chem. A **2**, 87–93 (2014). https://doi.org/10.1039/C3TA13510A

179. Hao, Q., Liu, B., Ye, J., et al.: Well encapsulated Mn₃O₄ octahedra in graphene nanosheets with much enhanced Li-storage performances. J. Colloid Interface Sci. **504**, 603–610 (2017). https://doi.org/10.1016/j.jcis.2017.05.079

180. Liu, B., Qi, L., Ye, J., et al.: Facile fabrication of graphene-encapsulated Mn₃O₄ octahedra cross-linked with a silver network as a high-capacity anode material for lithium ion batteries. New J. Chem. **41**, 13454–13461 (2017). https://doi.org/10.1039/C7NJ03498A

181. Jiang, X., Wang, Y., Yang, L., et al.: Dealloying to porous hybrid manganese oxides microspheres for high performance anodes in lithium ion batteries. J. Power Sources **274**, 862–868 (2015). https://doi.org/10.1016/j.jpowsour.2014.10.088

182. Hao, Q., Li, M., Jia, S., et al.: Controllable preparation of Co₃O₄ nanosheets and their electrochemical performance for Li-ion batteries. RSC Adv. **3**, 7850–7854 (2013). https://doi.org/10.1039/C3RA23448G

183. Hao, Q., Yu, Y., Zhao, D., et al.: Composited Co₃O₄/Ag with flower-like nanosheets anchored on a porous substrate as a high-performance anode for Li-ion batteries. J. Mater. Chem. A **3**, 15944–15950 (2015). https://doi.org/10.1039/C5TA03658E

184. Liang, C., Gao, M., Pan, H., et al.: Lithium alloys and metal oxides as high-capacity anode materials for lithium-ion batteries. J. Alloys Compd. **575**, 246–256 (2013). https://doi.org/10.1016/j.jallcom.2013.04.001

185. Hao, Q., Chen, L., Xu, C.: Facile fabrication of a three-dimensional cross-linking TiO₂ nanowire network and its long-term cycling life for lithium storage. ACS Appl. Mater. Interfaces **6**, 10107–10112 (2014). https://doi.org/10.1021/am5010305

186. Zhao, Y., Wang, L.P., Sougrati, M.T., et al.: A review on design strategies for carbon based metal oxides and sulfides nanocomposites for high performance Li and Na ion battery anodes. Adv. Energy Mater. **7**, 1601424 (2017). https://doi.org/10.1002/aenm.201601424

187. Ye, J., Zhao, D., Hao, Q., et al.: Facile fabrication of hierarchical manganese-cobalt mixed oxide microspheres as high-performance anode material for lithium storage. Electrochim. Acta **222**, 1402–1409 (2016). https://doi.org/10.1016/j.electacta.2016.11.117

188. Wang, Z., Fei, P., Xiong, H., et al.: CoFe₂O₄ nanoplates synthesized by dealloying method as high performance Li-ion battery anodes. Electrochim. Acta **252**, 295–305 (2017). https://doi.org/10.1016/j.electacta.2017.08.189

189. Hao, Q., Zhao, D., Duan, H., et al.: Porous Co₃O₄/CuO composite assembled from nanosheets as high-performance anodes for lithium-ion batteries. ChemSusChem **8**, 1435–1441 (2015). https://doi.org/10.1002/cssc.201403420

190. Zhao, W., Fei, P., Zhang, X., et al.: Porous TiO₂/Fe₂O₃ nanoplate composites prepared by de-alloying method for Li-ion batteries. Mater. Lett. **211**, 254–257 (2018). https://doi.org/10.1016/j.matlet.2017.10.019

191. Zhao, D., Hao, Q., Xu, C.: Nanoporous TiO₂/Co₃O₄ composite as an anode material for lithium-ion batteries. Electrochim. Acta **211**, 83–91 (2016). https://doi.org/10.1016/j.electacta.2016.06.043

192. Ye, J., Hao, Q., Xu, C.: Facile preparation of nanoporous TiO₂/MoOₓ composite and its high lithium storage performances as an anode material. Int. J. Hydrogen Energy **42**, 6820–6828 (2017). https://doi.org/10.1016/j.ijhydene.2016.12.077

193. Zhao, D., Hao, Q., Xu, C.: Facile fabrication of composited Mn₃O₄/Fe₃O₄ nanoflowers with high electrochemical performance as anode material for lithium ion batteries. Electrochim. Acta **180**, 493–500 (2015). https://doi.org/10.1016/j.electacta.2015.08.146

194. Xu, H., Wang, X., Liu, H., et al.: Facile synthesis of Fe₃O₄/NiFe₂O₄ nanosheets with enhanced lithium-ion storage by one-step chemical dealloying. J. Mater. Sci. **53**, 15631–15642 (2018). https://doi.org/10.1007/s10853-018-2729-y

195. Wang, Z., Zhang, X., Yan, Y., et al.: Nanoporous GeO₂/Cu/Cu₂O network synthesized by dealloying method for stable Li-ion storage. Electrochim. Acta **300**, 363–372 (2019). https://doi.org/10.1016/j.electacta.2019.01.127

196. Liu, H., Wang, X., Wang, J., et al.: Hierarchical porous CoNi/CoO/NiO composites derived from dealloyed quasicrystals as advanced anodes for lithium-ion batteries. Scripta Mater. **139**, 30–33 (2017). https://doi.org/10.1016/j.scriptamat.2017.06.011

197. Liu, H., Wang, X., Xu, H., et al.: Nanostructured CoO/NiO/CoNi anodes with tunable morphology for high performance lithium-ion batteries. Dalton Trans. **46**, 11031–11036 (2017). https://doi.org/10.1039/C7DT01904A

198. Zhang, R., Wang, Y., Jia, M., et al.: One-pot hydrothermal synthesis of ZnS quantum dots/graphene hybrids as a dual anode for sodium ion and lithium ion batteries. Appl. Surf. Sci. **437**, 375–383 (2018). https://doi.org/10.1016/j.apsusc.2017.12.110

199. Wang, Z., Zhang, X., Zhang, Y., et al.: Chemical dealloying synthesis of CuS nanowire-on-nanoplate network as anode

materials for Li-ion batteries. Metals **8**, 252–261 (2018). https://doi.org/10.3390/met8040252

200. Liu, Q., Chen, Z., Qin, R., et al.: Hierarchical mulberry-like Fe_3S_4/Co_9S_8 nanoparticles as highly reversible anode for lithium-ion batteries. Electrochim. Acta **304**, 405–414 (2019). https://doi.org/10.1016/j.electacta.2019.03.034

201. Zielasek, V., Jürgens, B., Schulz, C., et al.: Gold catalysts: nanoporous gold foams. Angew. Chem. Int. Ed. **45**, 8241–8244 (2006). https://doi.org/10.1002/anie.200602484

202. Yu, Y., Yan, C., Gu, L., et al.: Three-dimensional (3D) bicontinuous Au/amorphous-Ge thin films as fast and high-capacity anodes for lithium-ion batteries. Adv. Energy Mater. **3**, 281–285 (2013). https://doi.org/10.1002/aenm.201200496

203. Guo, X., Han, J., Zhang, L., et al.: A nanoporous metal recuperated MnO_2 anode for lithium ion batteries. Nanoscale **7**, 15111–15116 (2015). https://doi.org/10.1039/C5NR05011A

204. Ye, J., Baumgaertel, A.C., Wang, Y.M., et al.: Structural optimization of 3D porous electrodes for high-rate performance lithium ion batteries. ACS Nano **9**, 2194–2202 (2015). https://doi.org/10.1021/nn505490u

205. Liu, W., Chen, X., Xiang, P., et al.: Chemically monodisperse tin nanoparticles on monolithic 3D nanoporous copper for lithium ion battery anodes with ultralong cycle life and stable lithium storage properties. Nanoscale **11**, 4885–4894 (2019). https://doi.org/10.1039/C8NR09398A

206. Dong, X., Liu, W., Chen, X., et al.: Novel three dimensional hierarchical porous Sn–Ni alloys as anode for lithium ion batteries with long cycle life by pulse electrodeposition. Chem. Eng. J. **350**, 791–798 (2018). https://doi.org/10.1016/j.cej.2018.06.031

207. Liu, W., Zhang, S., Li, N., et al.: Preparation and characterization of sandwich-typed three-dimensional nanoporous copper-supported tin thin-film anode for lithium ion battery. Int. J. Electrochem. Sci. **8**, 347–358 (2013)

208. Luo, Z., Xu, J.C., Yuan, B., et al.: A novel 3D bimodal porous current collector with large interconnected spherical channels for improved capacity and cycling stability of Sn anode in Li-ion batteries. Mater. Lett. **213**, 189–192 (2018). https://doi.org/10.1016/j.matlet.2017.11.089

209. Luo, Z., Xu, J., Yuan, B., et al.: 3D hierarchical porous Cu-based composite current collector with enhanced ligaments for notably improved cycle stability of Sn anode in Li-ion batteries. ACS Appl. Mater. Interfaces **10**, 22050–22058 (2018). https://doi.org/10.1021/acsami.8b04049

210. Han, G., Um, J.H., Park, H., et al.: Hierarchically structured nanoporous copper for use as lithium-ion battery anode. Scripta Mater. **163**, 9–13 (2019). https://doi.org/10.1016/j.scriptamat.2018.12.030

211. Hou, C., Lang, X.Y., Han, G.F., et al.: Integrated solid/nanoporous copper/oxide hybrid bulk electrodes for high-performance lithium-ion batteries. Sci. Rep. **3**, 2878 (2013). https://doi.org/10.1038/srep02878

212. Liu, Y., Xiong, L., Li, P., et al.: Self-supported CuO nanoflake arrays on nanoporous Cu substrate as high-performance negative-electrodes for lithium-ion batteries. J. Power Sources **428**, 20–26 (2019). https://doi.org/10.1016/j.jpowsour.2019.04.102

213. Xu, X., Han, M., Ma, J., et al.: Preparation of a nanoporous CuO/Cu composite using a dealloy method for high performance lithium-ion batteries. RSC Adv. **5**, 71760–71764 (2015). https://doi.org/10.1039/C5RA14123K

214. Yang, W., Wang, J., Ma, W., et al.: Free-standing CuO nanoflake arrays coated Cu foam for advanced lithium ion battery anodes. J. Power Sources **333**, 88–98 (2016). https://doi.org/10.1016/j.jpowsour.2016.09.154

215. Wang, X., Liu, D., Weng, Q., et al.: $Cu/Li_4Ti_5O_{12}$ scaffolds as superior anodes for lithium-ion batteries. NPG Asia Mater. **7**, e171–e171 (2015). https://doi.org/10.1038/am.2015.23

216. Rahman, M.A., Zhu, X., Wen, C.: Fabrication of nanoporous Ni by chemical dealloying Al from Ni–Al alloys for lithium-ion batteries. Int. J. Electrochem. Sci. **10**, 3767–3783 (2015)

217. Li, Y.Q., Li, J.C., Lang, X.Y., et al.: Lithium ion breathable electrodes with 3D hierarchical architecture for ultrastable and high-capacity lithium storage. Adv. Funct. Mater. **27**, 1700447 (2017). https://doi.org/10.1002/adfm.201700447

218. Han, J., Liu, P., Ito, Y., et al.: Bilayered nanoporous graphene/molybdenum oxide for high rate lithium ion batteries. Nano Energy **45**, 273–279 (2018). https://doi.org/10.1016/j.nanoen.2018.01.006

219. Han, J., Hirata, A., Du, J., et al.: Intercalation pseudocapacitance of amorphous titanium dioxide@nanoporous graphene for high-rate and large-capacity energy storage. Nano Energy **49**, 354–362 (2018). https://doi.org/10.1016/j.nanoen.2018.04.063

220. Cheng, X.B., Zhao, C.Z., Yao, Y.X., et al.: Recent advances in energy chemistry between solid-state electrolyte and safe lithium-metal anodes. Chem **5**, 74–96 (2019). https://doi.org/10.1016/j.chempr.2018.12.002

221. Peng, H.J., Huang, J.Q., Cheng, X.B., et al.: Review on high-loading and high-energy lithium-sulfur batteries. Adv. Energy. Mater. **7**, 1700260 (2017). https://doi.org/10.1002/aenm.201700260

222. Lu, J., Li, L., Park, J.-B., et al.: Aprotic and aqueous $Li-O_2$ batteries. Chem. Rev. **114**, 5611–5640 (2014). https://doi.org/10.1021/cr400573b

223. Balaish, M., Jung, J.W., Kim, I.D., et al.: A critical review on functionalization of air-cathodes for nonaqueous $Li–O_2$ batteries. Adv. Funct. Mater. (2019). https://doi.org/10.1002/adfm.201808303

224. Armand, M., Tarascon, J.M.: Building better batteries. Nature **451**, 652–657 (2008). https://doi.org/10.1038/451652a

225. Liu, Y., Li, B., Kitaura, H., et al.: Fabrication and performance of all-solid-state Li-air battery with SWCNTs/LAGP cathode. ACS Appl. Mater. Interfaces **7**, 17307–17310 (2015). https://doi.org/10.1021/acsami.5b04409

226. Xia, C., Kwok, C.Y., Nazar, L.F.: A high-energy-density lithium-oxygen battery based on a reversible four-electron conversion to lithium oxide. Science **361**, 777–781 (2018). https://doi.org/10.1126/science.aas9343

227. Abraham, K.M., Jiang, Z.: A polymer electrolyt-based rechargeable lithium/oxygen battery. J. Electrochem. Soc. **143**, 1–5 (1996). https://doi.org/10.1149/1.1836378

228. Zhang, W., Huang, Y., Liu, Y., et al.: Strategies toward stable nonaqueous alkali metal-O_2 batteries. Adv. Energy Mater. **9**, 1900464 (2019). https://doi.org/10.1002/aenm.201900464

229. Peng, Z., Freunberger, S.A., Chen, Y., et al.: A reversible and higher-rate $Li-O_2$ battery. Science **337**, 563–566 (2012). https://doi.org/10.1126/science.1223985

230. Chen, Y., Freunberger, S.A., Peng, Z., et al.: Charging a $Li–O_2$ battery using a redox mediator. Nat. Chem. **5**, 489–494 (2013). https://doi.org/10.1038/nchem.1646

231. Gittleson, F.S., Ryu, W.H., Taylor, A.D.: Operando observation of the gold-electrolyte interface in $Li–O_2$ batteries. ACS Appl. Mater. Interfaces **6**, 19017–19025 (2014). https://doi.org/10.1021/am504900k

232. Wen, R., Byon, H.R.: In situ monitoring of the $Li–O_2$ electrochemical reaction on nanoporous gold using electrochemical AFM. Chem. Commun. **50**, 2628–2631 (2014). https://doi.org/10.1039/C3CC49625B

233. Chen, L.Y., Guo, X.W., Han, J.H., et al.: Nanoporous metal/oxide hybrid materials for rechargeable lithium-oxygen batteries. J. Mater. Chem. A **3**, 3620–3626 (2015). https://doi.org/10.1039/C4TA05738D

234. Yang, H., Xia, J., Bromberg, L., et al.: Electrochemically synthesized nanoporous gold as a cathode material for Li–O$_2$ batteries. J. Solid State Electrochem. **21**, 463–468 (2017). https://doi.org/10.1007/s10008-016-3374-5

235. Guo, X., Han, J., Liu, P., et al.: Graphene@nanoporous nickel cathode for Li–O$_2$ batteries. ChemNanoMat **2**, 176–181 (2016). https://doi.org/10.1002/cnma.201500214

236. Zhao, G., Zhang, L., Niu, Y., et al.: Enhanced durability of Li–O$_2$ batteries employing vertically standing Ti nanowire array supported cathodes. J. Mater. Chem. A **4**, 4009–4014 (2016). https://doi.org/10.1039/C6TA00318D

237. Zhao, G., Zhang, L., Niu, Y., et al.: A molten Mg corrosion method for preparing porous Ti foam as self-supported Li–O$_2$ battery cathodes. Electrochim. Acta **224**, 64–70 (2017). https://doi.org/10.1016/j.electacta.2016.12.033

238. Lim, H.D., Lee, B., Bae, Y., et al.: Reaction chemistry in rechargeable Li–O$_2$ batteries. Chem. Soc. Rev. **46**, 2873–2888 (2017). https://doi.org/10.1039/C6CS00929H

239. Surwade, S.P., Smirnov, S.N., Vlassiouk, I.V., et al.: Water desalination using nanoporous single-layer graphene. Nat. Nanotechnol. **10**, 459–464 (2015). https://doi.org/10.1038/nnano.2015.37

240. Ito, Y., Cong, W., Fujita, T., et al.: High catalytic activity of nitrogen and sulfur co-doped nanoporous graphene in the hydrogen evolution reaction. Angew. Chem. Int. Ed. **54**, 2131–2136 (2015). https://doi.org/10.1002/anie.201410050

241. Moreno, C., Vilas-Varela, M., Kretz, B., et al.: Bottom-up synthesis of multifunctional nanoporous graphene. Science **360**, 199–203 (2018). https://doi.org/10.1126/science.aar2009

242. Han, J., Guo, X., Ito, Y., et al.: Effect of chemical doping on cathodic performance of bicontinuous nanoporous graphene for Li–O$_2$ batteries. Adv. Energy Mater. **6**, 1501870 (2016). https://doi.org/10.1002/aenm.201501870

243. Park, J.B., Lee, S.H., Jung, H.G., et al.: Redox mediators for Li–O$_2$ batteries: status and perspectives. Adv. Mater. **30**, 1704162 (2018). https://doi.org/10.1002/adma.201704162

244. Han, J., Huang, G., Ito, Y., et al.: Full performance nanoporous graphene based Li–O$_2$ batteries through solution phase oxygen reduction and redox-additive mediated Li$_2$O$_2$ oxidation. Adv. Energy Mater. **7**, 1601933 (2017). https://doi.org/10.1002/aenm.201601933

245. Guo, X., Liu, P., Han, J., et al.: 3D nanoporous nitrogen-doped graphene with encapsulated RuO$_2$ nanoparticles for Li–O$_2$ batteries. Adv. Mater. **27**, 6137–6143 (2015). https://doi.org/10.1002/adma.201503182

246. Ding, Y., Chen, M., Erlebacher, J.: Metallic mesoporous nanocomposites for electrocatalysis. J. Am. Chem. Soc. **126**, 6876–6877 (2004). https://doi.org/10.1021/ja0320119

247. Wang, R., Wang, C., Cai, W.-B., et al.: Ultralow-platinum-loading high-performance nanoporous electrocatalysts with nanoengineered surface structures. Adv. Mater. **22**, 1845–1848 (2010). https://doi.org/10.1002/adma.200903548

248. Li, J., Yin, H.M., Li, X.B., et al.: Surface evolution of a Pt–Pd–Au electrocatalyst for stable oxygen reduction. Nat. Energy **2**, 1–9 (2017). https://doi.org/10.1038/nenergy.2017.111

249. Manthiram, A., Fu, Y., Su, Y.-S.: Challenges and prospects of lithiu-sulfur batteries. Acc. Chem. Res. **46**, 1125–1134 (2013). https://doi.org/10.1021/ar300179v

250. Ji, X., Nazar, L.F.: Advances in Li-S batteries. J. Mater. Chem. **20**, 9821–9826 (2010). https://doi.org/10.1039/B925751A

251. Ji, X., Lee, K.T., Nazar, L.F.: A highly ordered nanostructured carbon-sulphur cathode for lithium-sulphur batteries. Nat. Mater. **8**, 500–506 (2009). https://doi.org/10.1038/nmat2460

252. Seh, Z.W., Sun, Y., Zhang, Q., et al.: Designing high-energy lithium-sulfur batteries. Chem. Soc. Rev. **45**, 5605–5634 (2016). https://doi.org/10.1039/C5CS00410A

253. He, G., Ji, X., Nazar, L.: High "C" rate Li-S cathodes: sulfur imbibed bimodal porous carbons. Energy Environ. Sci. **4**, 2878–2883 (2011). https://doi.org/10.1039/C1EE01219C

254. He, J., Luo, L., Chen, Y., et al.: Yolk-shelled C@Fe$_3$O$_4$ nanoboxes as efficient sulfur hosts for high-performance lithium-sulfur batteries. Adv. Mater. **29**, 1702707 (2017). https://doi.org/10.1002/adma.201702707

255. Lu, L.Q., Schriever, N., De Hosson, J.T.M., et al.: Low-temperature solid-state growth of three-dimensional bicontinuous nanoporous graphene with tunable porosity for lithium-sulfur batteries. J. Mater. Chem. A **6**, 11405–11415 (2018). https://doi.org/10.1039/C8TA03488E

256. Gu, X., Tong, C.J., Lai, C., et al.: A porous nitrogen and phosphorous dual doped graphene blocking layer for high performance Li-S batteries. J. Mater. Chem. A **3**, 16670–16678 (2015). https://doi.org/10.1039/C5TA04255K

257. Zhou, G., Zhao, Y., Manthiram, A.: Dual-confined flexible sulfur cathodes encapsulated in nitrogen-doped double-shelled hollow carbon spheres and wrapped with graphene for Li-S batteries. Adv. Energy Mater. **5**, 1402263 (2015). https://doi.org/10.1002/aenm.201402263

258. Shi, J.L., Tang, C., Huang, J.Q., et al.: Effective exposure of nitrogen heteroatoms in 3D porous graphene framework for oxygen reduction reaction and lithium-sulfur batteries. J. Energy Chem. **27**, 167–175 (2018). https://doi.org/10.1016/j.jechem.2017.09.014

259. Liu, N., Wang, L., Zhao, Y., et al.: Hierarchically porous TiO$_2$ matrix encapsulated sulfur and polysulfides for high performance lithium/sulfur batteries. J. Alloys Compd. **769**, 678–685 (2018). https://doi.org/10.1016/j.jallcom.2018.08.027

260. Wu, L., Wang, Z., An, C., et al.: Chemical-dealloying to fabricate nonconductive interlayers for high-loading lithium sulfur batteries. J. Alloys Compd. **806**, 881–888 (2019). https://doi.org/10.1016/j.jallcom.2019.07.339

261. Zhao, Y., Tian, Y., Zhang, X., et al.: Mn$_3$O$_4$ octahedral microparticles prepared by facile dealloying process as efficient sulfur hosts for lithium/sulfur batteries. Metal **8**, 515–522 (2018). https://doi.org/10.3390/met8070515

262. Lin, D., Liu, Y., Cui, Y.: Reviving the lithium metal anode for high-energy batteries. Nat. Nanotechnol. **12**, 194–206 (2017). https://doi.org/10.1038/nnano.2017.16

263. Barai, P., Higa, K., Srinivasan, V.: Lithium dendrite growth mechanisms in polymer electrolytes and prevention strategies. Phys. Chem. Chem. Phys. **19**, 20493–20505 (2017). https://doi.org/10.1039/C7CP03304D

264. Jin, S., Jiang, Y., Ji, H., et al.: Advanced 3D current collectors for lithium-based batteries. Adv. Mater. **30**, 1802014 (2018). https://doi.org/10.1002/adma.201802014

265. Rosso, M., Brissot, C., Teyssot, A., et al.: Dendrite short-circuit and fuse effect on Li/polymer/Li cells. Electrochim. Acta **51**, 5334–5340 (2006). https://doi.org/10.1016/j.electacta.2006.02.004

266. Yun, Q., He, Y.B., Lv, W., et al.: Chemical dealloying derived 3D porous current collector for Li metal anodes. Adv. Mater. **28**, 6932–6939 (2016). https://doi.org/10.1002/adma.201601409

267. Zhao, H., Lei, D., He, Y.B., et al.: Compact 3D copper with uniform porous structure derived by electrochemical dealloying as dendrite-free lithium metal anode current collector. Adv. Energy Mater. **8**, 1800266 (2018). https://doi.org/10.1002/aenm.201800266

268. An, Y., Fei, H., Zeng, G., et al.: Vacuum distillation derived 3D porous current collector for stable lithium-metal batteries. Nano Energy **47**, 503–511 (2018). https://doi.org/10.1016/j.nanoen.2018.03.036

269. Liu, H., Wang, E., Zhang, Q., et al.: Unique 3D nanoporous/macroporous structure Cu current collector for dendrite-free lithium deposition. Energy Storage Mater. **17**, 253–259 (2019). https://doi.org/10.1016/j.ensm.2018.07.010

270. Shi, Y., Wang, Z., Gao, H., et al.: A self-supported, three-dimensional porous copper film as a current collector for advanced lithium metal batteries. J. Mater. Chem. A **7**, 1092–1098 (2019). https://doi.org/10.1039/C8TA09384A

Yi Ding received his B.S. and M.S. in Chemistry from the University of Science and Technology of China and his Ph.D. in Materials Science from Johns Hopkins University. Dr. Ding is currently a distinguished professor at the Institute for New Energy Materials and Low-Carbon Technologies, Tianjin University of Technology and his research is focused on the design and processing of dealloyed nanoporous metals for green catalysis and advanced energy technologies. Dr. Ding has also been granted 40 patents and published 120 journal articles with a total citation of over 13000 times and an H-index of 62.

Xuan Wu received his M.S. in the China University of Mining and Technology in 2018 and is currently a Ph.D. candidate at the Macau University of Science and Technology with joint training at the Tianjin University of Technology. Xuan Wu's research is focused on the synthesis of novel nanostructured materials for alkali-metal batteries.

Guang He received his Ph.D. in Chemistry from the University of Waterloo and subsequently worked as a postdoctoral fellow at the University of Texas at Austin and the University of Waterloo in 2013 and 2015, respectively. Currently, Dr. He is a professor at the Institute for New Energy Materials and Low-Carbon Technologies, Tianjin University of Technology, and his research is focused on novel materials and designs for electrochemical energy systems.